



Ayozie, Ikechukwu Ugochukwu (2016) *3D printing of capsule endoscopes for rapid testing*. [MSc]

<http://endeavour.gla.ac.uk/207/>

Copyright and moral rights for this work are retained by the author(s)

A copy can be downloaded for personal non-commercial research or study, without prior permission or charge

This work cannot be reproduced or quoted extensively from without first obtaining permission in writing from the author(s)

The content must not be changed in any way or sold commercially in any format or medium without the formal permission of the author

When referring to this work, full bibliographic details including the author, title, institution and date must be given

Enlighten Dissertations
<http://endeavour.gla.ac.uk/>
deposit@lib.gla.ac.uk



University of Glasgow | School of Engineering

3D Printing of Capsule Endoscopes for Rapid Testing

Ikechukwu Ugochukwu Ayozie



Supervised By **Prof. Sandy Cochran, Dr Vipin Seetohul**

A thesis submitted in partial fulfilment of the requirements for the degree of
Master of Science (MSc.) in Mechatronics

AUGUST 2016

ABSTRACT

3D printing has revolutionized the production of biomedical devices with ground-breaking rapid prototyping technologies. The Sonopill project attempts to exploit 3D printing for rapid production of capsule endoscope prototypes for clinical research targeted at the diagnosis of gastrointestinal diseases (GI) using ultrasound capsule endoscopy (USCE). The primary goal of this project is to create prototypes of ultrasound capsule endoscopes also known as pills with a 3D printing technique. In order to provide a stable means of actuating the capsule to target areas of the GI tract and for efficient supply of electricity and unaltered transmission of control signals in the capsule control system a tethered design was considered. The capsule design was achieved with the SolidWorks three-dimensional Computer-aided Design (3D CAD) software and stereolithography (SLA) rapid prototyping technique was utilised in the 3D printing of the capsules. For quality control measures, mechanical evaluation methods which include tensile test and 3-point bend test were applied to ensure that the tether qualifies clinically and mechanically for endoscopy operations. Adhesive bonding was also implemented to bond the tether to the pill. Results from the 3D printing and mechanical evaluations show that ultrasound capsule endoscopes can be rapidly produced efficiently with SLA if temporary support materials used in the printing process. The bond strength of the tether-to-pill integration was found to be strong enough to avoid a capsule retention in the gastrointestinal tract. Based on these findings, the Sonopill project will be advanced through rapid production of tethered ultrasound capsule endoscopes (TUSCE) as this will give the research team the opportunity to understand the technicalities of the TUSCE prototypes before USCE becomes an expedient medical imaging technology.

LIST OF OBJECTIVES

General Objectives

- ❖ Fabrication of simplified ultrasound capsule prototypes using 3D printing technology

Specific Objectives

1. Three-dimensional Computer-aided Design (3D CAD) of the pills according to stipulated design specifications for Sonopill prototypes and use of a 3D printer for rapid prototyping of the 3D models.
 - ❖ This was achieved through the use of SolidWorks 3D CAD modelling software and stereolithography (SLA) 3D printing technique.
2. The design of a tether integration system for the capsule prototypes.
 - ❖ This was achieved through the 3D CAD design and mechanical evaluation methods such as tensile strength tests and 3-point bend tests.
3. Microscopic and mechanical evaluation of the pills through measurements and tests.
 - ❖ This was accomplished through the use of mechanical instruments such as the microscope, weighing scale, vernier calliper and mechanical tests such as visual inspection and bond strength test.
4. Clinical evaluation of the fabricated pills such as biocompatibility (medical grading of materials and biodegradability of the pill).
 - ❖ This was accomplished through physical biocompatibility assessment such as assessing the type of tether material, adhesive material and the biodegradability of the pill in conformance to the ISO 13485.

These objectives were fulfilled in this project through intensive research and laboratory work.

ACKNOWLEDGMENTS

I want to express my gratitude to my project supervisor, Prof. Sandy Cochran, for giving me the rare opportunity of taking on a new and promising technology and for being part of the Sonopill project. Thanks for the challenges you fashioned that developed my skills.

Thanks to Dr Vipin Seetohul for guiding me as my immediate supervisor in this project. I also thank Dr. Gerard Cummins, Dr. Holly Lay (especially for the PCBs), Dr. Yongqiang Qiu (for the transducer) and Xiachoun, for their corrections and suggestions during the technical aspects and the Sonopill team for their support.

My gratitude goes to the CAD/Rapid Prototyping Office and the Materials Laboratory of the School of Engineering for their patience during the mechanical testing and fabrication work.

I express my gratitude to the National Information Technology Agency (NITDA) and the Federal Government of Nigeria for the privilege of studying at the University of Glasgow.

I thank Prof. Solomon Braide, Sir & Lady O. T. Elem, Ven. Basil Orah, Rev. Can. Sullivan S. B. Odike, Sir & Lady Charles Obunwo, Sir & Lady Ikechi Nwogu, Mr. Uzoma Akalabu and Mr. Martin Ayers for their encouragement and support.

Finally, I appreciate to my parents, Sir & Lady H. I. Ayozie for their guidance and moral education, my aunt Joy Ayozie, my siblings: Chinonye and her husband Clifford, Chukwudi, Chukwuka, Izuchukwu Ibeh and my extended family. You are all wonderful.

TABLE OF CONTENTS

ABSTRACT.....	I
LIST OF OBJECTIVES	II
ACKNOWLEDGMENTS.....	III
TABLE OF CONTENTS	IV
NOTATION	IX
CHAPTER 1 INTRODUCTION.....	1
1.1 Background.....	1
1.1.1 Medical Imaging of the Gastrointestinal (GI) Tract.....	1
1.1.2 Ultrasound Capsule Endoscopy	4
1.1.3 Sonopill	4
CHAPTER 2 LITERATURE REVIEW.....	7
2.1 Tethered Capsule Endoscopy (TCE).....	7
2.2 Tethered Capsule Endoscopes and Tether Systems.....	7
2.2.1 Tethered Endoscope	7
2.2.2 Cytosponge	8
2.2.3 Tethered Endoscope Endomicroscopy	9
2.3 Design Considerations in Capsule Endoscopy	10
2.2.1 Form factor.....	10
2.2.2 Power.....	10
2.2.3 Capsule Weight.....	10
2.2.4 Aiding the ingestion of the Capsule	10
2.4 3D Printing	11
2.4.1 Definition of 3D Printing.....	11
2.4.2 Additive Manufacturing	12
2.4.3 The 3D Printing Process.....	12
2.4.4 3D Printing Materials	15
2.4.5 Rapid Prototyping Technologies in 3D Printing.....	16
Stereolithography.....	16
The Stratasys Objet30 PolyJet 3D Printing Technology	17
2.4.6 Examples of 3D-Printed Capsule Endoscopes	18
Case Study 1: Endoscopic Submarine Capsules	18
Case Study 2: Magnetically Actuated Capsule Endoscopy for Obesity Treatment	19
2.5 Mechanical Evaluation of Materials for Tether Design	19
2.5.1 Micro coaxial Cables	19

2.5.2	Hook-up Cables.....	20
2.5.3	Mechanical Evaluation of Cables.....	20
	Ultimate Tensile Strength Test	20
	The “dogbone” shape of the specimen.....	23
	Ductility	23
2.5.4	Bending Tests	24
	Bend Radius	25
	Bending Test Procedure	25
	Case Study: National Aeronautics and Space Administration (NASA) Wire and Cable Cold Bending Test	25
	Mathematical evaluation of the bending force	26
	General Trend of Bending Force Curves.....	27
	Bending curve for a Teflon and Peek Insulated Wire.....	27
2.6	Biocompatibility	28
2.6.1	Standards used in the Evaluation of Medical Devices	28
2.6.2	Biocompatible Fluoropolymers used in Endoscopy.....	28
	PTFE	28
	PFA.....	29
	FEP.....	29
2.7	Adhesive Bonding	30
2.7.1	Silicone	30
2.7.2	Bond strength of adhesives	30
2.7.3	Elongation property of silicone adhesive	31
2.8	Maximum Pulling force for endoscopy	31
CHAPTER 3 MATERIALS, METHODS, AND RESULTS.....		32
3.1	Project Flowchart.....	32
3.2	Specification	33
3.3	Design Concept.....	34
3.4	Possible Strategies.....	34
3.5	Method: 3D Modelling of Pills	35
3.5.1.	Design of V 2-2.....	35
	Drawing the hemispherical end cap	35
	Base cap design and tether inlet (integration) design.....	36
	Smoothing edges with the “fillet” tool.....	36
	Pill cover design (cover cap)	37
3.5.2	Design of V 3-1.....	38
	Application of shelling	38
	Smoothing the edges with the “fillet” tool.....	38

Tether inlet (integration) design and pin hole design	39
Cover cap design	39
3.5.3 Results for 3D modelling of pills	41
Pill Assembly 3D Design	41
3.6 3D printing of the designed pills	47
3.6.1 Conversion to STL file format	47
3.6.2 3D printing machine	47
3.6.3 Post-processing.....	47
3.6.4 Results of 3D printing	48
STL File Format	48
3D-printed parts after post-processing	48
3.7 Mechanical Evaluation 3D-printed Pills	49
3.7.2 Measurement of the pill mass.....	49
3.7.4 Pill size	49
3.7.5 Microscopic evaluation of pills	50
3.7.6 Results of mechanical evaluation of pills	50
Evaluation of PCB slots and transducer holders.....	50
Measurement of the pill mass	51
Results for measurement of pill size.....	51
Results from the microscopic evaluation of the pills	52
3.8 Design of the tether	52
3.8.1 Measurement principle	53
3.8.2 Selection of cable samples	53
3.8.3 Material Test Machines	53
Zwick/Roell Z2.0 and Zwick/Roell Z250	53
Method.....	54
Precautions.....	55
3.8.2 Results of UTS test for micro-coaxial cable samples	56
Coax 1	56
Coax2	57
Coax3	58
Coax4	59
Coax5	61
PW1.....	62
PW2.....	64
3.8.3 Tether tests	65
Selection of micro-coaxial and power cables.....	65

Selection of Teflon Tube	65
Materials	66
Test Machine	66
Digital Multimeter	66
3.8.5 Test 1: Three-point Bend Test.....	66
Method.....	66
3.8.6 Results for 3-point Bend Test	68
Continuity test of cables	70
3.8.7 Test 2: Ultimate tensile strength test.....	70
Materials	70
Method.....	70
3.8.5 Results	71
3.9 Adhesive Bonding and Bond Strength Test	74
3.9.1 Materials.....	74
3.9.2 Method	74
3.9.3 Adhesive Bonding Strength Test	75
Material test Machine	75
3.9.4 Result.....	76
4.1 Biocompatibility	78
4.1.1 Results	78
The biocompatibility results are shown in table 22 below.....	78
4.2 Final Products	78
CHAPTER 5 DISCUSSION.....	79
5.1 Assembly of 3D Designed Pills.....	79
5.1.1 Results of 3D Printing.....	79
5.1.2 Microscopic Evaluation of Pills	79
5.1.3 Conversion to STL File Format.....	79
5.1.4 Comparison between mechanical measurements of the pills to the 3D CAD dimensions	80
5.1.5 Comparison of the TUSCEs to Commercial WCEs and TCEs	80
5.1.6 The pins and tether inlet	80
5.2 Tension tests.....	80
5.2.1 Variations in Test Time.....	80
5.2.2 Graphical Plotting	81
5.2.3 UTS test results of micro-coaxial cable samples.....	81
5.2.4 Deformation in specimens	82
5.2.5 Trend in re-tested specimens	82
5.2.6 Cable selection for tether design	82

5.3	Tether Design.....	83
5.3.1	Choice of Teflon	83
5.3.2	Bend test.....	83
5.3.3	UTS Test of the tether	83
5.4	Application.....	84
5.5	Adhesive Bonding and Bonding Strength Test.....	84
5.6	Final Product Description	84
5.6.1	V 2-2	84
5.6.2	V 3-1	85
5.6.3	Comparison between V 2-2 and V 3-1	85
5.6.4	The Tether.....	85
CHAPTER 7	CONCLUSIONS.....	86
CHAPTER 8	FUTURE CONSIDERATIONS.....	88
CHAPTER 9	REFERENCES.....	89
CHAPTER 10	APPENDIX	102
10.1	Appendix A.....	102
10.2	Appendix B.....	103
10.3	Appendix C	105
10.4	Appendix-CD	106

NOTATION

A_o = original area of cross-section

COF = co-efficient of friction

dB = decibel

dL = elongation or extension from a tensile test

F = bending force

F_{max} = maximum force obtained from a tensile test

Ft = feet

g = gram

Hz = hertz

ID = inner diameter

K = kelvin

m = mass

MHz = megahertz

MPa = megapascal

mm/min = millimetres per minute

N = newtons

OD = outer diameter

P = load applied in a tensile test

P_{max} = maximum load in a tensile test

psi = pounds per square inch

r = radius

RP = rapid prototyping

STL = standard tessellation language file

SLDPRT = SolidWorks part file

T = torque

TS = tensile strength

Δl = elongation or change in length

σ = engineering stress

CHAPTER 1 INTRODUCTION

1.1 Background

1.1.1 Medical Imaging of the Gastrointestinal (GI) Tract

Gastrointestinal (GI) diseases have caused high mortality rates worldwide. [1] There has been an increase in the incidence of most gastrointestinal diseases which have major implications for future healthcare needs. [1] According to a report on gastroenterology services in the United Kingdom (UK) commissioned by the British Society for Gastroenterology, it was observed that GI diseases account for a third of the overall deaths and the number one source of cancer death in the UK. [1] In the United States of America (USA) GI diseases caused significant morbidity with an estimated 60 to 70 million people affected annually. [2] In 2008, the International Agency for Research on Cancer (IARC) reported about 715,000 fresh cases of cancer [3] and 542,000 cancer deaths in Africa [4]. GI diseases refer to diseases of the GI tract which include Barret's oesophagus, Crohn's disease, and gastric ulcers. [5] The GI tract is a track of organs joined in a long, curling tube from the mouth to the anus. The organs of the GI tract are the mouth, oesophagus, stomach, small and large intestines, and rectum [6], and the digestive system organs (which include the liver, pancreas and gall bladder). Figure 1 below shows the parts of the gastrointestinal tract.

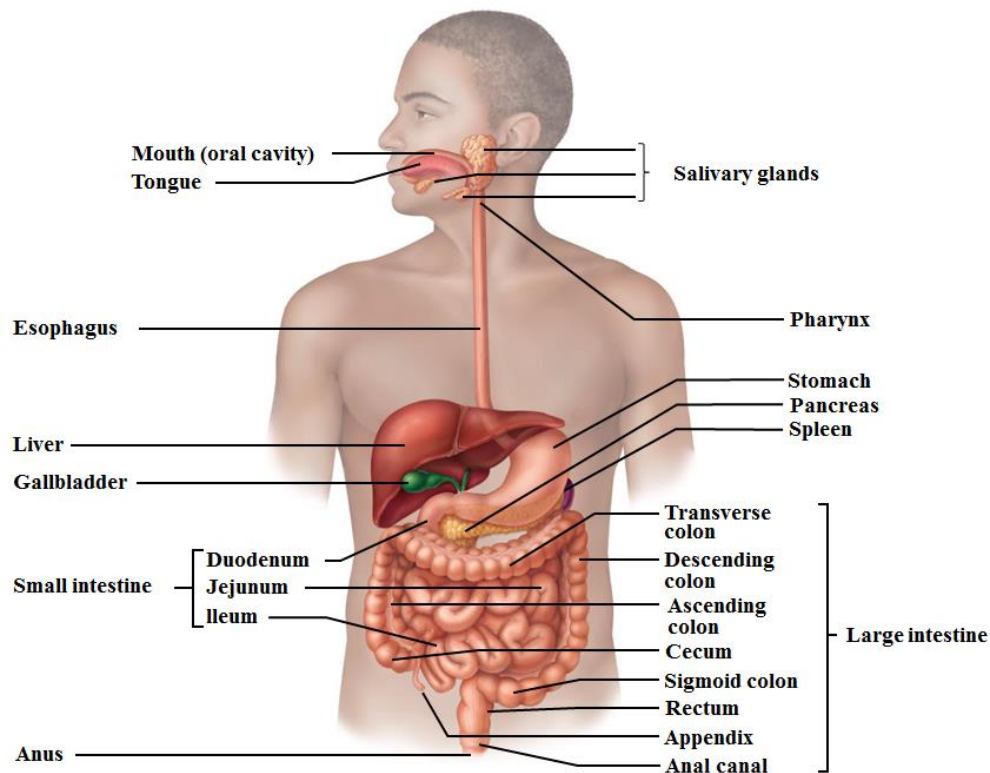


Figure 1: The gastrointestinal tract [7]

Early diagnosis of these diseases is crucial but it is difficult to achieve. Medical technologies such as ultrasonography have been applied but they were reportedly low in producing the desired results. [8, 9, 10] Early diagnosis of GI diseases are crucial. For instance, GI diseases such as cancer are most responsive to treatments when diagnosed in the early stages but become deadly when untreated after a long period. Consequently, there is a need to enhance the technology and methods to cater for the health needs of the world's teeming population and for proper diagnosis and monitoring of diseases of the GI tract medical imaging must be implemented.

Medical imaging is a technique used in visualising the internal part of the human body for medical analysis and treatments. An area of ground-breaking imaging application is capsule endoscopy. A capsule endoscope is an ingestible wireless miniature camera for getting images of the gastrointestinal (GI) mucosa. [11] The endoscope used in capsule endoscopy is a capsule in the size and shape of a vitamin pill and popular designs contain a tiny camera occasionally called a "pillcam". Unlike conventional endoscopy methods capsule endoscopes can easily examine parts of the GI tract that are invisible to other types of endoscopy without pain and discomfort to the patient. They are particularly useful in identifying numerous pathologies within the small intestine such as Crohn's disease, tumours and gastrointestinal bleeding. [12] Capsule endoscopy can be categorised based on the mode of capsule delivery. They are the tethered capsule endoscopy (TCE) [13] and the wireless capsule endoscopy (WCE) [14]. Figures 2 and 3 illustrate the WCE and TCE systems respectively.

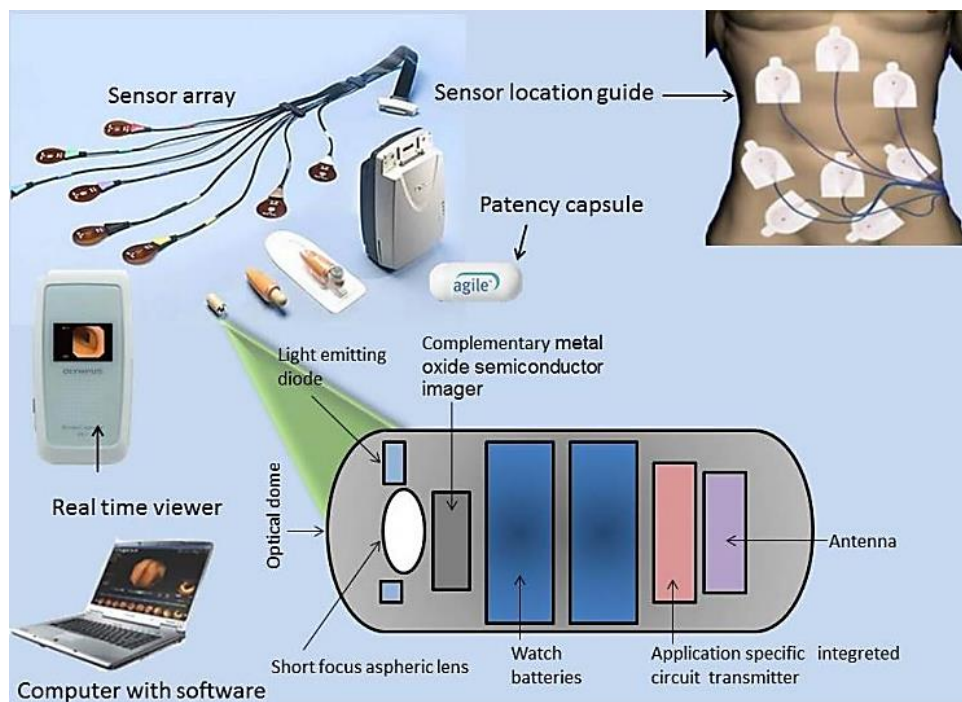


Figure 2: The components of a WCE system [15]

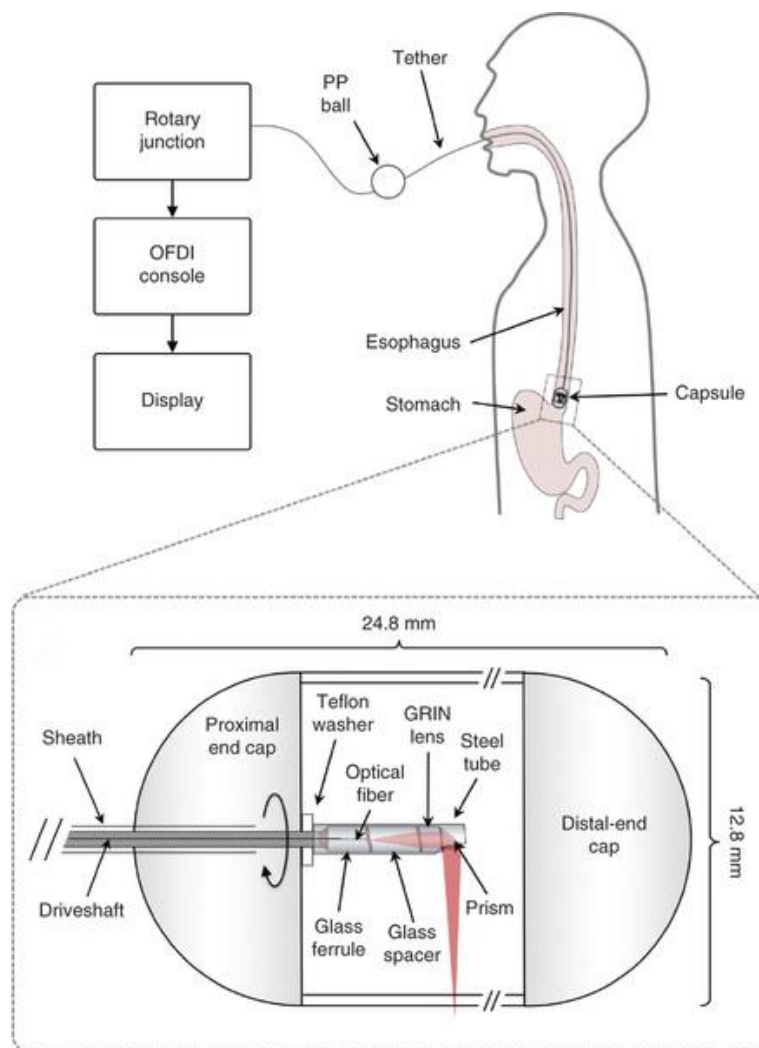


Figure 3: An illustration of a TCE system [13]

In contrast to the WCE, the TCE provides the endoscopist with total command of the imaging process and produces high quality images, while reducing overall cost. [16] A typical tethered capsule endoscope is shown in figure 6. It consists of a tether made from optical fibre which scans a surface using optical illumination as the backscattered light is recorded to form a non-confocal image. [17] Once the tethered capsule is swallowed the walls of the GI tract constrict around the capsule and descend it down the tract by peristalsis. After the point of interest is imaged the capsule is pulled back using the tether while it images the GI tract. [13] Figure 7 illustrates a block diagram of a TCE.

Although WCE and TCE have improved the capacity for the diagnosis of the GI tract, the diagnosis is limited to the mucosa surface. [18] This led to the research on a capsule with ultrasound imaging capabilities. [18]

1.1.2 Ultrasound Capsule Endoscopy

Ultrasound is described as a sound that is above 20 000Hz, which is the range of human hearing. [19] In endoscopy, ultrasound (also termed ultrasonography) is a test in which ultrasound waves are reflected off tissues and the resulting signals are converted into a picture called a sonogram for analysis. [20]

The concept of a WCE with ultrasound capabilities was suggested long-ago. [18, 21, 22] Lee, et al [18] explained that the major difference between ultrasound imaging and optical imaging is the need for an acoustic coupling between an ultrasound transducer and the object of interest. [18] According to S. Lay, et al. [23] signal attenuation in the GI tract is minimised due to the thinness of the gut wall, which is a great advantage for high-fidelity imaging using USCE. It was also observed that the application of ultrasound imaging is popular in conventional endoscopy but currently no form of an ultrasound capsule endoscope is commercially available. [23]

Professor Sandy Cochran [24] and a team of ingenious clinicians at Ninewells Hospital, Dundee, have adopted two ways of achieving progress in the field of microultrasound [25] imaging for clinical applications. One of the pathways adopted was the deployment of microultrasound for non-invasive applications within the body through Ultrasound in a Needle (USIN) Ultrasound Capsule Endoscopy (USCE). The reality of using a USCE is near as significant funding from the Engineering and Physical Sciences Research Council (EPSRC) through the UK government has promoted research work trademarked as the “Sonopill” at Ninewells Hospital, Dundee, Scotland. [25] According to Seetohul, et al. [26] The ultrasound capsule endoscope could be TCE or WCE, with the TCE providing the medium for transmission of power and control signals which favours research. Secondly, the ultrasound device requires acoustic coupling for imaging. Finally, ultrasound capsule endoscope offers the possibility for both imaging and therapeutic applications which places a demand for robotic actuation. [26]

1.1.3 Sonopill

The Sonopill is a £5 million project funded by the European Physical Sciences Research Council (EPSRC) and led by Professor Sandy Cochran [26]. The research base is located at the University of Dundee, Scotland and includes research teams from Heriot Watt University and the University of Glasgow, all in Scotland. The core aim of the Sonopill programme is the exploration of ultrasound imaging and therapeutic capabilities deployed in an ingestible capsule format that is anchored by extensive pre-clinical work to signify the compatibility of ultrasound and visual imaging, along with studies of multimodal diagnosis and therapy, and

the mechanics to control the motion of the Sonopill as it travels through the GI tract. [27] The focus of the ultrasound capsule will be in the small intestine of the GI tract. [23] Figure 4 below shows a conceptual rendering of an ultrasound endoscope named Sonopill, by the research team.



Figure 4: The conception of the Sonopill. The blue ring denotes the position for an ultrasound imaging array and the black ring represents the potential for an autonomous positioning system [25]

In view of the Sonopill project aims it is of paramount importance that prototypes of the intended ultrasound capsule endoscopes are produced and tested to the required standards and functionality before crucial investments are made in the final product. It is also essential that the prototype and final product are produced rapidly in order to meet the demands of patients and also for research purposes. 3D printing is the pathway to achieving these goals.

3D printing refers to the method of building a three-dimensional (3D) prototype with the aid of a 3D printer. A 3D printer is a machine in which consecutive layers of material are formed using computerised control methods to create an object. 3D printing process allows for customization and many products can be built in a 3D printer simultaneously. [28] In this literature, 3D printing will be dealt as an additive manufacturing and rapid prototyping technique.

This Master of Science (MSc) project is part of the £5 million UK EPSRC-sponsored Sonopill project and is aimed at the 3D design and 3D printing of capsule endoscope prototypes for rapid testing and research on the GI tract. The capsule endoscope was also referred to as the “pill” in this project. Two versions of a tethered ultrasound capsule endoscope (abbreviated as TUSCE) namely version 2-2 and version 3-1 will be 3D-printed. The SolidWorks (version 2015) will be used for the 3D modelling of the TUSCE while photopolymer materials are selected with stereolithography (SLA) technique to 3D-print the pills.

The tether design is the actuating system of choice and also used for electric power and control signal transmission. The integration of the tether to the pill will be achieved with an adhesive bonding. As part of quality assurance and control measures in the design of the device

mechanical tests which constitute tensile strength test and bending test and bond strength test will be carried out to ascertain the mechanical characteristics of the tether and its constituent materials. The tensile strength tests will provide the ultimate tensile strength for the tether and tether-to-pill bonding strength while the bending test will be used to evaluate the maximum bending radius needed to access the flexibility of the tether.

A biocompatibility test will only focus on ensuring that the material of the designed tether and the type of adhesive used in the assembly of the ultrasound capsule endoscope are of medical grade. The results of this project will also aid the Sonopill research team in making rapid prototypes of the TUSCEs for rapid testing. This will enable a better understanding of how these devices will perform in vivo and allow the Sonopill team to make evaluations so that corrective actions can be taken where deviations occur.

CHAPTER 2 LITERATURE REVIEW

The main sections in this chapter include:

- ❖ Tethered Capsule Endoscopy (TCE)
- ❖ Design considerations in capsule endoscopy
- ❖ 3D printing
- ❖ Mechanical evaluation of materials for tether design
- ❖ Adhesive bonding and bond strength
- ❖ Biocompatibility
- ❖ Maximum actuation force for endoscopy

2.1 Tethered Capsule Endoscopy (TCE)

Rachlin, et al. [29] described tethered endoscopy as an imaging device fixed to a flexible linkage (for example a cable) that is capable of providing pulling forces alone on a terminating payload that consists of a device for imaging. There are 3 stages involved in tethered endoscopy namely: the introduction (ingesting the imaging capsule), imaging, and retrieval of the imaging device. [29] The tether is also described as a channel for transmitting power and control signals and also generates the most accurate results in research. [26]

2.2 Tethered Capsule Endoscopes and Tether Systems

2.2.1 Tethered Endoscope

Rachlin, et al. [29] invented a tethered endoscope in which a flexible tether was joined to an imaging capsule for diagnostic endoscopy of the oesophagus. The imaging mode designed for the tethered capsule is a video camera. [29] Figure 5 below shows the design of the invented TCE.

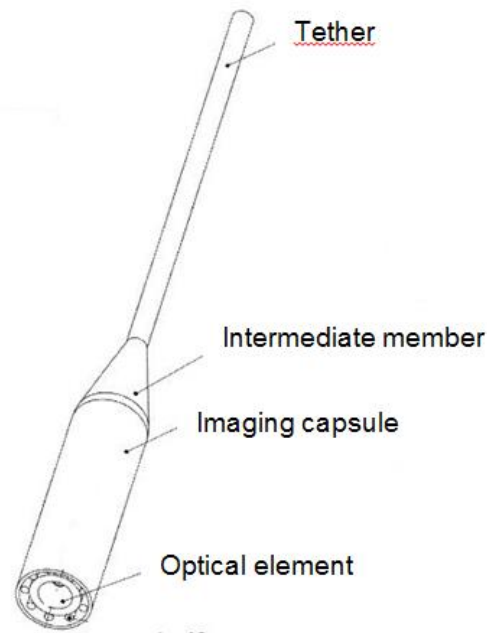


Figure 5: The tethered capsule endoscope invented by Rachlin et al [29]

It was observed in the literature of Rachlin, et al. [29] that the tether prevents the pains generated when using conventional endoscopy methods by allowing some degree of flexibility for position control. The designed tether is made of a long cable with a flexible jacket. The tether length is made long enough to assess the end of the oesophagus. The proximal end of the tether connects to a control station which supplies electricity and the electronics for data acquisition. The tether length should be minimal so as to avoid signal loss. The tether should be flexible enough in order to avoid the use of high force when retrieving the capsule. The diameter of the tether should be limited to 1mm for the purpose of reducing slight pains. [29]

2.2.2 Cytosponge

According to Topfer [30], the Cytosponge is a small reticulated sponge inside a capsule made of soluble gelatine and is discharged orally by a clinician to gather oesophageal cells for examination. Cytosponge is specified for diagnosing Barret's Esophagus (BE). [30] Figure 6 below shows the design of the Cytosponge.



Figure 6: The Cytosponge in mesh form and enclosed in a capsule [30, 31]

The Cytosponge is composed of a small reticulated sponge, measuring roughly 30m in diameter and is held in a string-attached gelatin capsule [32]. The capsule dissolves when it is swallowed with water due to the solubility of the gelatin coating. At the end of 5 minutes, the clinician retracts the extended sponge which gathers cells with its somewhat abrasive structure as it moves through the oesophagus. This retraction is done by pulling back the sponge with the attached string [30, 31].

2.2.3 Tethered Endoscope Endomicroscopy

Michalina, et al. [33] invented a tethered endoscope endomicroscopy which is composed of a cylinder measuring 12.8mm in diameter and 24.8mm in length covered by hemispherical end caps. A flexible sheath of 0.96mm (diameter) fixed to the capsule formed the tether. The sheath (tether) is composed of an optical fibre and a driveshaft. The optical fibre transmits and receives light from small optical components housed in the capsule while the driveshaft transfers rotational torque from the capsule's optics. 3D images are acquired as well as cross-sectional images during the actuation of the tethered capsule in the digestive tract. The tethered capsule can be disinfected for re-use. [33] Figure 7 shows the tethered endoscope endomicroscopy device.

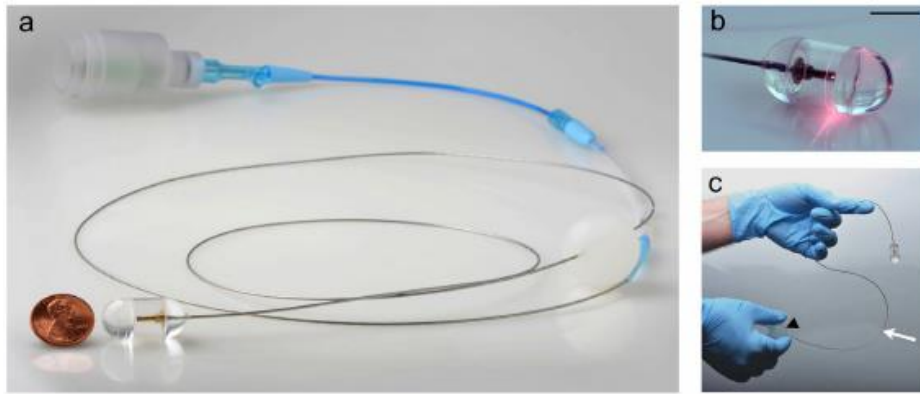


Figure 7: Photograph of the tethered capsule endoscopy device showing: (a) The capsule size compared to a penny coin (b) The activation of the transmission light in the optics system (c) The tether with a plastic ball attached to allow for easy handling of the device. [33]

2.3 Design Considerations in Capsule Endoscopy

2.2.1 Form factor

Lee, et al [18] proposed that the size of wireless capsule endoscopic ultrasound (WCEU) is limited to about 1cm diameter by 3cm length, beyond which the risk of GI obstruction increases. [18] Professor Sandy Cochran [34] in his interview with the piezo Institute news team [35] stated that the aim of the Sonopill is to design capsules for oral ingestion within the size of about 10mm in diameter and no more than 30mm in length. But according to Rachlin et al. [29] an imaging device with a larger diameter allows for firmer peristaltic “grip”. [29]

2.2.2 Power

The system complexity (especially of the electronics) and power design of the capsule must be minimised to lessen the power usage and capsule form factor. [18]

2.2.3 Capsule Weight

The capsule weight through gravity exerts a downward pull of the capsule while aiding the peristalsis action. The capsule weight must overcome the primary frictional forces that hinder the downward movement of the device through the open lumen. [29]

2.2.4 Aiding the ingestion of the Capsule

Use of palatants

A palatant or swallowing aid is applied on the imaging device to give it an appealing taste to the mouth. The swallowing aid also adds weight to the imaging device to enhance its descent through the lumen. [29]

Peristalsis

Lee, et al. [18] described peristalsis is the contraction and relaxation of the muscles to move food down the tract. [18] Hardcastle and Mann [36] defined peristalsis as a continuous wave of contraction moving through the bowel at a constant rate, which leads to the onward motion of the contents. [36] Peristalsis can exert a downward force on the capsule [29] and is a natural mode of squeezing the pill and enabling the requisite contact for coupling [18].

Low friction

Low friction surfaces around the capsule and tether allow for an easy retrieval and also facilitates the gravitational pull on the device into the oesophagus during the introduction process. This can be achieved by using lubricous or hydrophilic coatings. [29]

2.4 3D Printing

2.4.1 Definition of 3D Printing

Miscalleff [37] described 3D printing as an additive fabrication process that converts geometry designed with a digital computer into physical models built via a layer-by-layer procedure using different materials. Miscallef [37] added that the unique feature of 3D printing in comparison to other forms of manufacturing technologies is its accessibility to anyone with a drive for converting their ideas into finished products. [37]

Gibson, et al. [38] used the term “additive manufacturing” or AM as an endorsed term for rapid prototyping and 3D printing. A three-dimensional Computer Aided Design (3D CAD) generated model can be fabricated at first hand without process planning. [38] The term “rapid prototyping” [39] was defined by Pham and Dimov [39] as a technology for fast fabrication of parts (models or functional prototypes) straight from Computer Aided Design data in small sets. [39]

According to the American Society for Testing and Materials (ASTM) International, Designation: F2792-12a (Standard Terminologies for Additive Manufacturing Technologies) made with reference to the International Organisation of Standards (ISO) ISO10303-1: 1994 [40], 3D printing is defined as “*the fabrication of objects through the deposition of material using a print head, nozzle, or another printer technology.*” [40]

Chia and Wu [41], in their literature, referred to 3D printing as all Solid Freeform (SFF) technologies [42, 43] and as a liquid binder-based inkjet technology. [41]

2.4.2 Additive Manufacturing

3D printing is called an additive manufacturing (AM) process because the synthesis of a 3D object involves an additive process. The object is created via building successive layers of material and these layers can be viewed as thinly sliced horizontal cross-sections of the final product. [44]

2.4.3 The 3D Printing Process

According to Gibson, et al. [38] the 3D printing or AM process has in eight stages. The stages are namely:

- I. Conceptualization and CAD [38]
- II. Conversion to CAD file to STL format [38]
- III. Transfer and manipulation of STL file on AM machine [38]
- IV. Setting up the machine [38]
- V. Building the part [38]
- VI. Part removal and cleaning [38]
- VII. Post-processing techniques [38]
- VIII. Evaluation of the part [38]

I. 3D Modelling

All 3D parts start with a virtual design or 3D software model of the object to be created. The 3D software model completely describes the external geometry of the printed object. This can be achieved by using Computer Aided Design (CAD) application software. [37, 44, 45]. The object can also be copied to a 3D digital format by using a 3D scanner [44].

II. 3D Modelling Software

The 3D modelling software produces a CAD drawing of the object in the 3D form. Examples of licensed 3D CAD application software include SolidWorks, Autodesk Inventor, and 3DS MAX while examples of opensource versions are FreeCad, 123apps, Blender, Sculptris, OpenScad, and Tinkercad. [37]

III. SolidWorks

SolidWorks [46] is solid modelling CAD and Computer-aided Engineering (CAE) software founded by Jon Hirschtick, with a company named Solidworks Corporation that is headquartered in Waltham, Massachusetts, United States of America (USA) in December 1993. In 1997, a France-based company called Dassault Systemes [47] acquired SolidWorks Corporation which now runs the publishing of the SolidWorks software. [47]. The latest version

of the SolidWorks software is version 2016. [46] Figure 8 below shows the graphical user interface of the SolidWorks 2016 software.

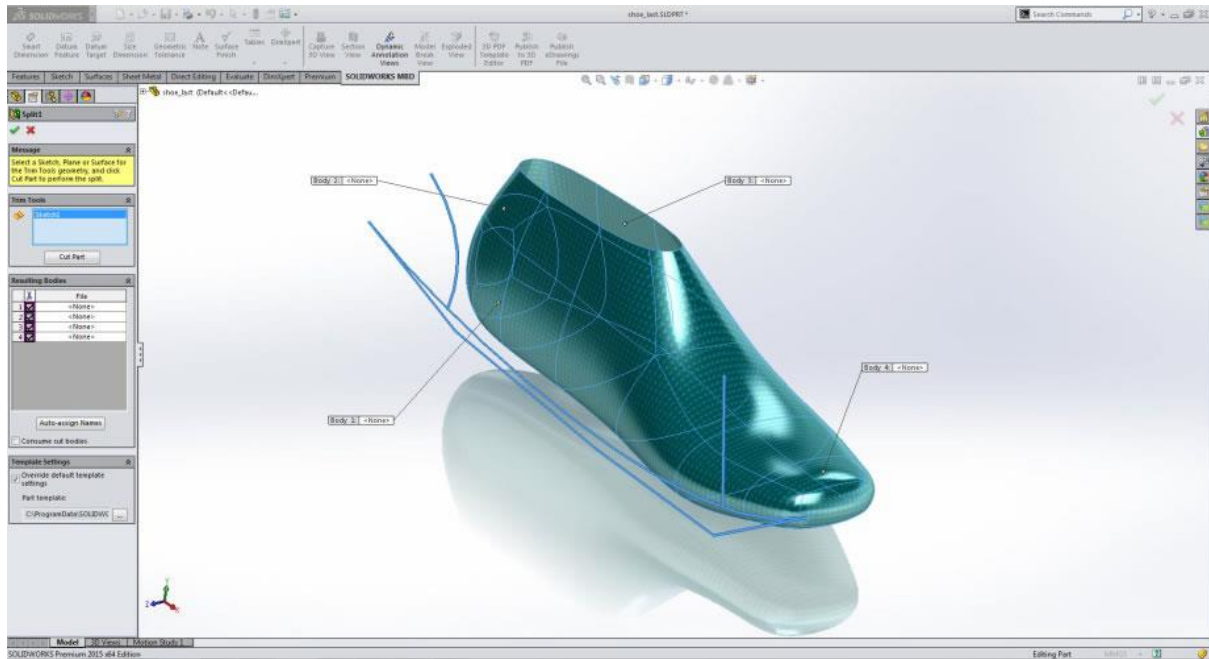


Figure 8: SolidWorks 3D modelling graphical user interface (GUI) [48]

IV. Conversion to STL File Format

The STL File Format

The STL (Stereolithography Tesselation Language or Standard Tesselation Language) [49] is a file format peculiar to the stereolithography [50] CAD developed by an American firm, 3D Systems in 1987 for transferring 3D CAD models to the first stereolithography (SLA) machines. [49, 50, 51] The STL file is the most implemented common interface for transferring a CAD model to an RP system. [45, 52] The principle of the STL format is such that the geometry defined within the 3D CAD model is represented using a mesh of triangles over the surface of the designed part as illustrated in figure 9. The triangulated 3D CAD model is sliced in layers of uniform thickness. Slicing refers to the breaking of a 3D model into many horizontal layers and is implemented with CAD software. [53] The sliced 3D model is the file sent to the 3D printer. [37]

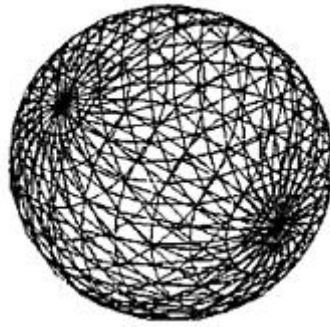


Figure 9: A STL file from a tessellated sphere [53]

V. Transfer to 3D Printer (Additive Manufacturing Machine) and STL File Manipulation

The STL is transferred to the 3D printer. The STL file is checked for correct dimensioning, orientation and manipulated if any errors are found before building the final product. [37]

VI. 3D Printer Configuration

The 3D printer is configured to the desired settings prior to the build-up process. [38]

VII. Building the Part

The building process (that is printing) is monitored for quality assurance and control. Important aspects of the monitoring include the rate of material consumption, power supply and freezing of software [38] and orientation of the parts on the print bed. [37]

VIII. Removal

The built parts are removed with safety measures by ensuring that operating temperature of the 3D printer and product is sufficiently low that the movable parts of the printer are at rest. [38]

IX. Post-Processing

The part is checked for defects and treated carefully. Priming and painting are applied to give the part a good appearance. [38]

X. Evaluation

The part is tested to see if it meets desired standards. [38]

2.4.4 3D Printing Materials

A study was made to understand the types of 3D printing materials that could be used for fabricating the capsules. The features of the final products used in 3D printing are characterised by the materials used in the fabrication. The 3D printing processing methods also influence the quality of the final product. [43] Factors to consider when selecting 3D printing materials include the design, application, function, and the product life span [54]. It was observed that the major materials used in 3D printing include photopolymers, thermoplastics, metals and powder. [54] The photopolymer material was the focus for the application.

Photopolymers

A photopolymer is a polymer that alters its features when exposed to ultraviolet (UV) light or visible light. [55] Photopolymers are composed of monomers, oligomers, and photoinitiators that combine to form a toughened polymeric material through a process called curing as shown in figure 10 below. [56, 57]

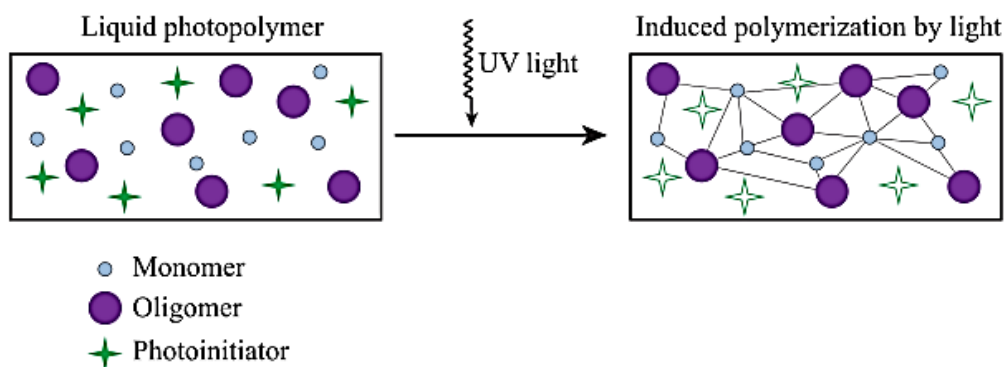


Figure 10: The photopolymerization process [58]

In 3D printing, photopolymer materials are liquid resins that undergo a photocuring process where an oligomer is photo cross-linked on when exposed to UV light and finally develops into a hardened plastic prototype and part. [54, 59] Photopolymers are applied in the SLA and Stratasys Polyjet 3D printing technology. In SLA photopolymers are usually based on epoxies and acrylics chemistry.

2.4.5 Rapid Prototyping Technologies in 3D Printing

Prototyping [60] is a vital component of the production required for testing the form, fit and functionality of a new design before crucial investments are made in tooling. [60] Rapid prototyping (RP) refers to a range of established technologies for fabricating accurate parts directly from CAD models in a few hours with the need of little or no human intervention [45, 60]. This implies that physical models of CAD drawings can be produced more often for easy assessments and further development [60]. Established rapid prototyping technologies used in the medical field [45] include stereolithography, fused deposition modelling, selective laser sintering, inkjet printing and laminated object manufacturing [45]. The stereolithography process was the rapid prototyping technology of interest.

Stereolithography

Stereolithography (SLA) [41] was invented in 1986 by Charles Hull [61, 62], the founder of the American company, 3D Systems [47] which is headquartered at Rock Hill, South Carolina in the United States of America (USA). SLA uses a vat [44] of a liquid photopolymer that is photocurable by ultraviolet (UV) laser to synthesise the object's layers one by one. [41, 47] The UV laser beam traces in each layer a sample of the part pattern on the surface of the liquid resin. [44] The traced pattern on the liquid resin is cured and solidified on exposure to the UV light. A bottom-up and top-down system is used to position the platform for introducing a new layer of uncured liquid resin. In the bottom-up system, a movable platform with the cured composition is lowered by a distance equal to the thickness of one layer (typically 0.05mm to 0.15mm) [44] and a new layer of uncured liquid resin is spread over the top by a resin-filled blade as illustrated in figure 11 below.

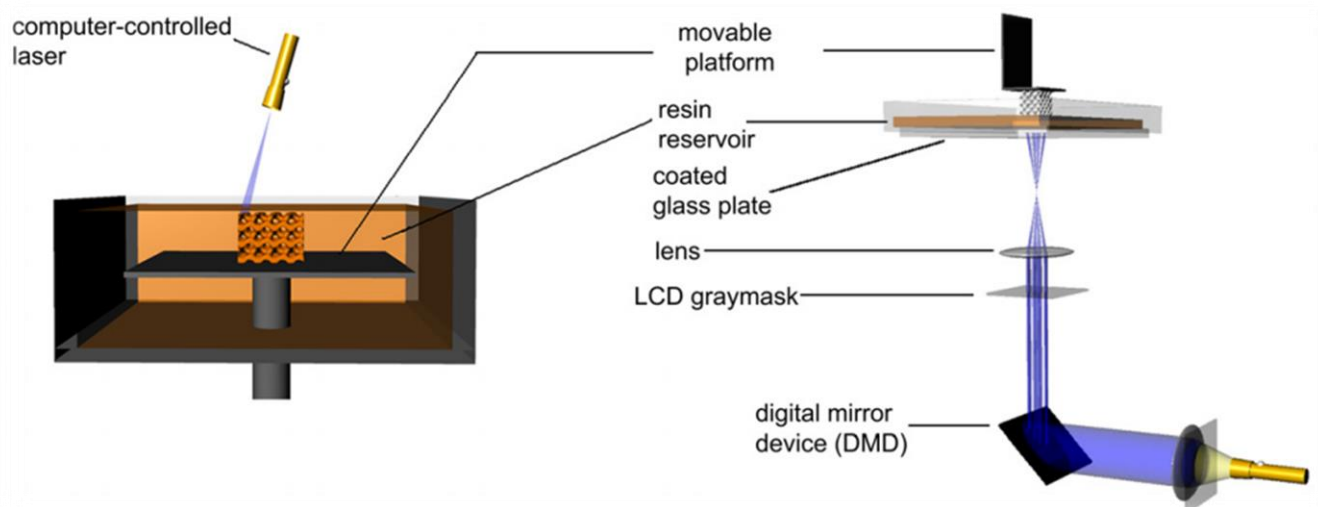


Figure 11: The stereolithography (SLA) process [41, 63]

At this stage, the topmost layer is prepared to get patterned. The topdown system is illustrated in figure 22 where a light source is projected onto a clear plate initially kept close to the base of the vessel holding the liquid resin. [41, 63] After a layer is patterned through the clear plate, the cured structure is disengaged from the clear plate and raised to permit uncured liquid resin to occupy the space between the structure and the clear plate. Thus, the next layer is prepared to be patterned. For processing of large parts, the masked lamp technique [41] was designed to cure a full layer of photopolymers at once. [41] Post-processing methods used in SLA include draining out unpolymerized liquid resin, strengthening and curing unreacted parts in an oven. [41, 64]

Materials used in STL technology must have photocurable moieties for crosslinking. These include acrylic and epoxy materials [41] and photocrosslinkable poly(propylene fumarate) (PPF) [41, 65].

Advantages of SLA include the capability of making complex designs with internal architecture and making allowance for easy clearance of unpolymerised resin. SLA also has an exceedingly high resolution of approximately 1.2 μ m [41, 66]. The main disadvantage of SLA is the insufficiency of biocompatible resins with genuine SLA processing qualities [41]. Parts produced by SLA have remarked shrinkage and distortion which affects the accuracy of its dimensions. [64] Also, SLA requires the addition of temporary support structures into the CAD model to construct unsupported features like overhanging levers [41].

The Stratasys Objet30 PolyJet 3D Printing Technology

Stratasys Limited (Ltd), based in Eden Prairie, Minnesota, USA [67] is a manufacturer of 3D printing systems for both office and industrial applications. [67, 68, 69] “Objet” is one of the brands of Stratasys Ltd and the latest 3D printing technology applied in the Objet line of Stratasys 3D printers is the polyjet 3D printing technology. Polyjet 3D printers have the ability to give the best resolution with a layer thickness of 16 μ , resulting in parts with a smoother texture that voids the need for post-processing [70]. PolyJet is also the sole 3D printing process to utilise multiple materials with varied durometers [65]. Models of polyjet 3D printers include the bio-compatible Objet30 Prime and Objet30 Pro [71]. Detailed specifications of the Objet 30 and Objet Prime models of Stratasys polyjet 3D printers are given in FILE 1 of the Appendix-CD. Figure 12 shows the Stratasys Objet30 Prime 3D printing machine [72].



Figure 12: The stratasys objet30 prime polyjet 3D printer [73]

2.4.6 Examples of 3D-Printed Capsule Endoscopes

Case Study 1: Endoscopic Submarine Capsules

Hoang et al, [74] developed endoscopic submarine capsules [74] with an aim of assessing the benefits of using a capsule swarming system in the GI tract while carrying out the endoscopy of a liquid-bloated stomach. The capsule shell measuring 46.25mm long and 14.90mm in diameter was designed on Creo Parametric 2.0 software [75] and fabricated with a VeroWhite material [54] on a Stratasys Objet Alaris30 3D printer [76]. Figure 13 below shows the endoscopic submarine capsule design. The shell dimensioning is described on 2A and the 3D-printed shell with the electronics framed on 2B.

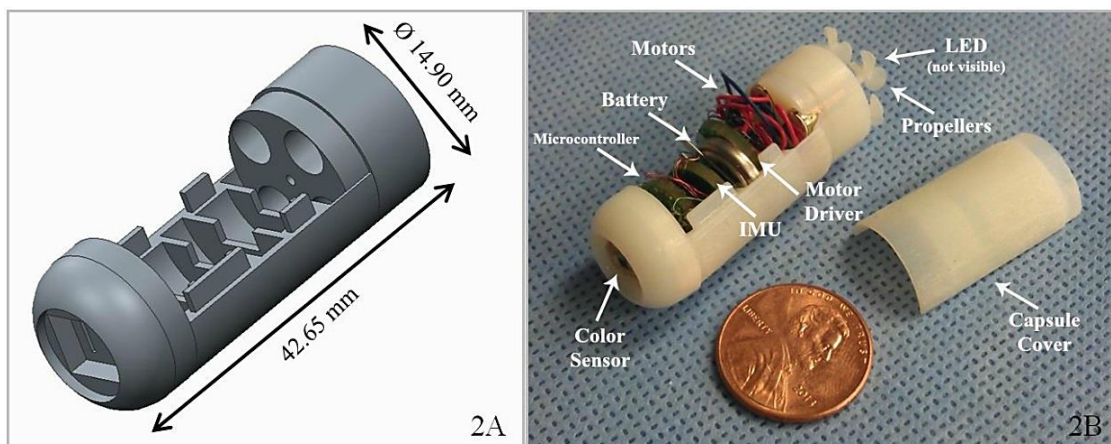


Figure 13: Endoscopic submarine capsule [74]

Case Study 2: Magnetically Actuated Capsule Endoscopy for Obesity Treatment

Thanh et al [77] developed an ingestible magnetically actuated capsule endoscope controlled by a magnetically remote-controlled balloon for obesity treatment. Figure 14 below shows an image of the magnetically actuated capsule prototype fabricated with a powder 3D printer SLM500HL, designed by the German company, SLM Solutions Group AM. [77]

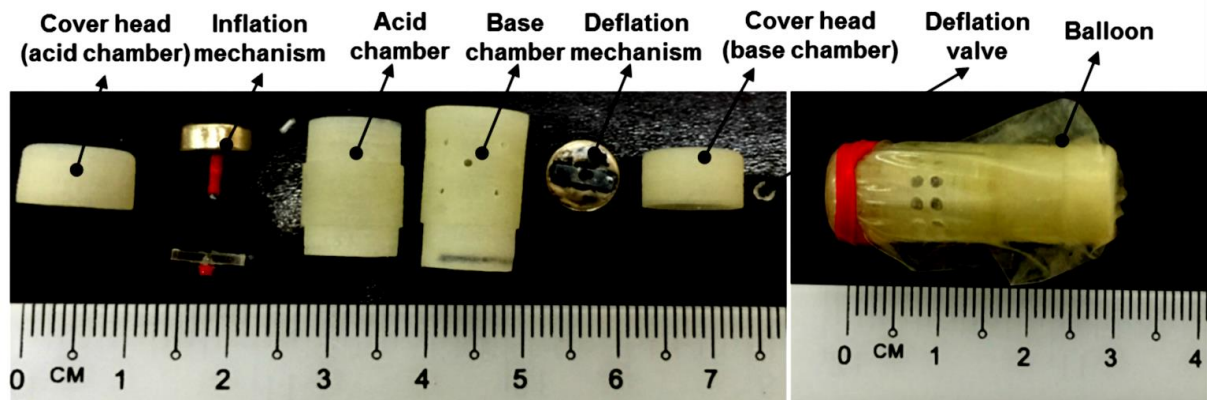


Figure 14: A magnetically actuated capsule endoscope for obesity treatment [78]

2.5 Mechanical Evaluation of Materials for Tether Design

In order to select cables for the tether design, a study of the specifications of small diameter micro coaxial (micro-coaxial) and power cables was carried out.

2.5.1 Micro coaxial Cables

Micro coaxial cable [79], also called micro-coaxial cable [80] is an easy-routing cable solution that saves space and it is mostly used in medical applications such as probes and endoscopy apparatus. Figure 15 shows the parts of a micro-coaxial cable.



Figure 15: The layout of a micro-coaxial cable [80]

The micro-coaxial consists of a layer of dielectric, outer jacket, and a centre conductor. The layer of dielectric provides the micro-coaxial with low capacitance [79] while outer jacket maintains the quality of the signal and a stable impedance. [79] Coaxial cables are deployed in the transmission of radio frequency signals. Coaxial cables have the inherent quality of shielding signals from the influence of external electromagnetism. [81]

2.5.2 Hook-up Cables

Hook-up wire is small-to-medium gauge [81] single insulated conductor wire, [82] used for low voltage, low current applications [82]. They are either solid or stranded and used mostly within the casings of electrical or electronic devices. [81, 82] Figure 16 below shows the strand and solid core types of hook-up wires. The insulation types used in hook up wires include polyvinylchloride (PVC), ethylene-propylene diene elastomer (EDPM), hypalon, perfluorotetraethylene (PTFE), and neoprene. [81]

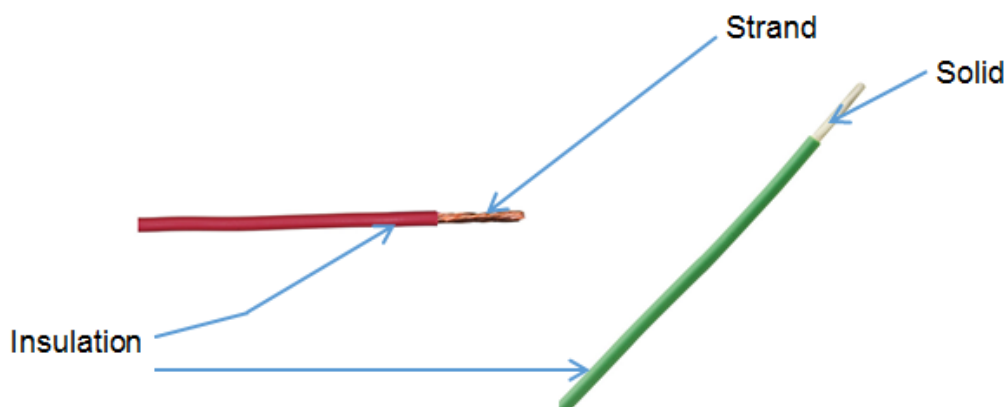


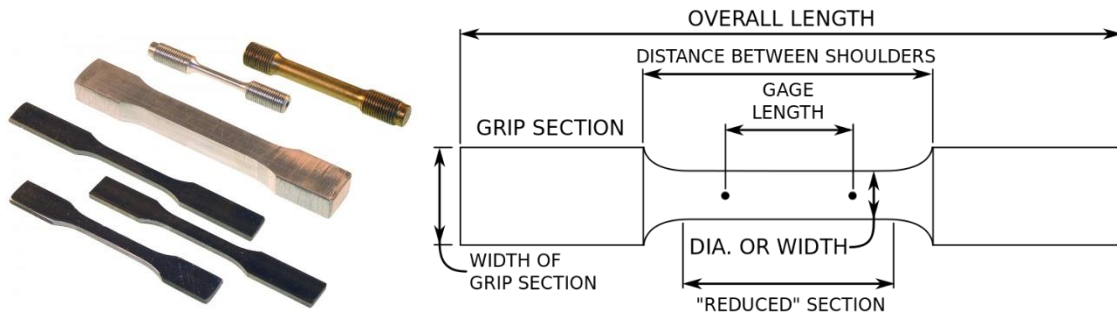
Figure 16: Hook-up wire (strand conductor type) with insulation [83]

2.5.3 Mechanical Evaluation of Cables

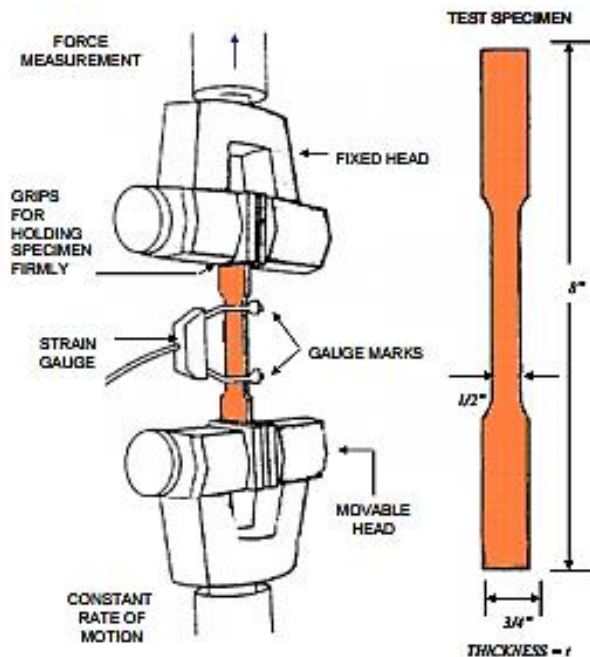
The mechanical characteristics of materials can be assessed by conducting lab-based experiments that recreate to a great extent the service trends. The type of load applied, the application time and environmental effects are factors to be considered. Another important mechanical characteristic is ductility. Lab-based experiments carried out to cables include the ultimate tensile strength test (UTS) and bending test. [84]

Ultimate Tensile Strength Test

The ultimate tensile strength (UTS) is described as the maximum stress above the yield strength [84] on the engineering stress-versus-strain curve with units in megapascals (MPa). [84, 85] The simplest method of evaluating a material is by a tensile test. [85] This can be obtained by using the pull test as shown in figure 17 below.



(a)



(b)

Figure 17: The Tensile test method (a) The “dogbone” specimen [86, 87] (b) The test machine setup [88]

The specimen is usually in the form of a “dogbone” shape and it is fixed to the holding grips of the testing machine which elongates the specimen steadily and continuously measures the elongations obtained using an extensometer and the resulting instantaneous applied load with a load cell. The output graph from the testing machine is plotted on a computer as a load or force versus elongation curve [84, 85]. To minimise geometric problems [85] the load and elongation parameters are normalized [85] to engineering stress and engineering strain parameters respectively. [85] The graphical descriptions of the load versus elongation curve and the stress versus strain curve are shown in figures 18 below and a more detailed description of the stress-strain curve is given in figure 19.

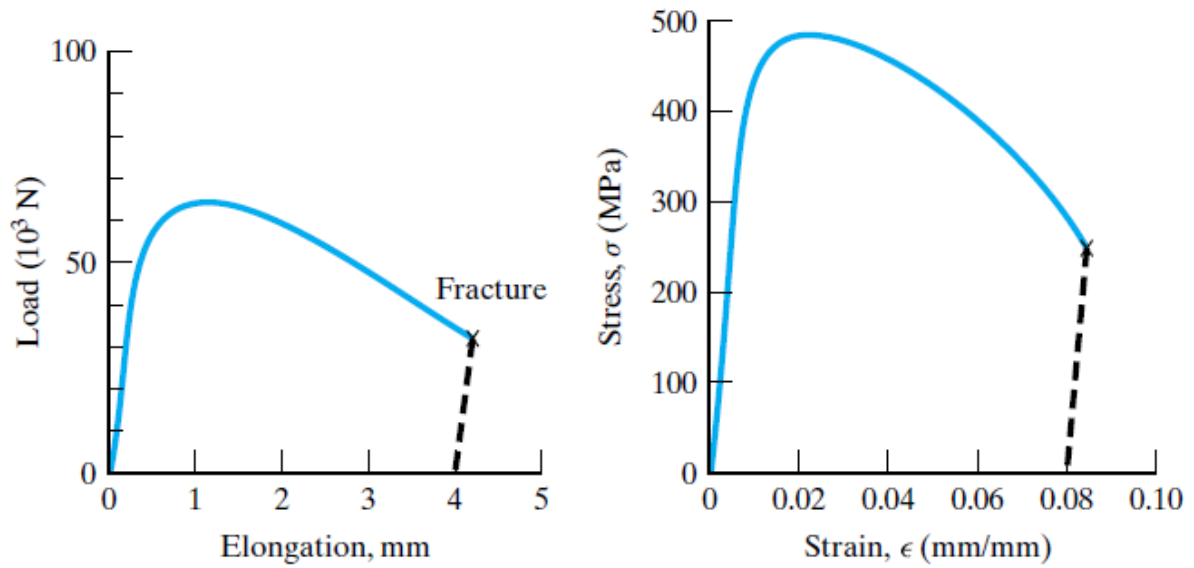


Figure 18: Load versus elongation curve for an aluminium specimen (left) and stress versus strain curve acquired from normalization of the load versus elongation data. [85]

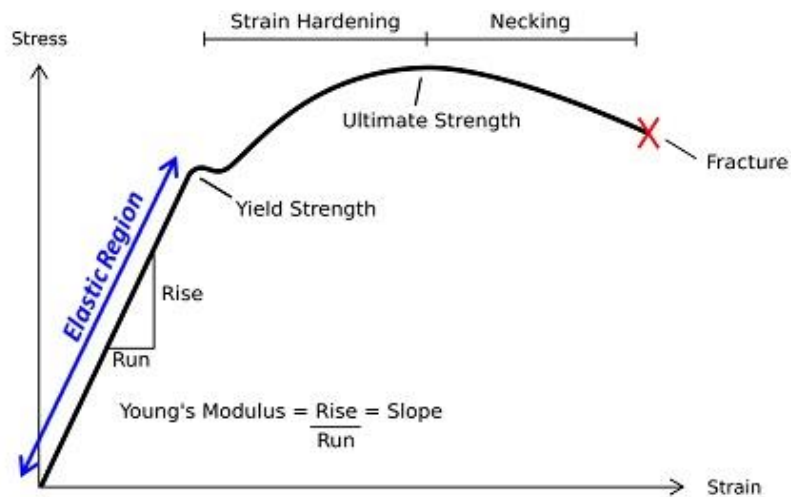


Figure 19: A detailed description of the behaviour of a stress-strain curve [89]

From figure 18 the engineering stress, σ , is defined as

$$\sigma = \frac{P}{A_0} \quad (1)$$

where P is the load on the specimen with an original cross section area or zero-stress cross section area. [85] The engineering strain is also defined as

$$\epsilon = \frac{l - l_0}{l_0} = \frac{\Delta l}{l_0} \quad (2)$$

where l represents the gauge length at a given load, and l_0 represents the original or zero-stress length. [85]

According to John [90], the tensile strength (TS) can be calculated as nominal stress given by

$$\text{TS} = \frac{\text{maximum load applied}}{\text{original cross sectional area}} \quad (3)$$

Raymond Higgins [91] calculated the tensile strength (T) [91] by dividing the maximum load sustained by the specimen during the test by the actual area of cross-section given by

$$T = \frac{P_{max}}{A_0} \quad (4)$$

where P_{max} is the maximum load sustained and A_0 is the actual cross-sectional area of the specimen. [91]

The “dogbone” shape of the specimen

The specimen shape is in a “dogbone” shape in order to restrict the deformation of the material within the narrow centre region and also to minimize the possibility of fracture happening at the ends of the specimen. [92, 93]

The tensile strength results will be different for two samples of the same piece of material if they are tested at different strain rates. For consistent results, it is advised to run the tests on all materials at the same strain rate. Samples with a small diameter will exhibit a negligible change in force for a given extension. This reduces the accuracy of the force and stress measurements. Strengthening the grips can reduce slippage but this increases the stress on that area. [88]

Ductility

Ductility is defined as an assessment of the degree of plastic deformation [85] that a material sustained at the time of breakage [84]. Higgins [91] described ductility as the level of extension

in a tensioned material before failure. [91] The description of ductility is illustrated in figure 20 below.

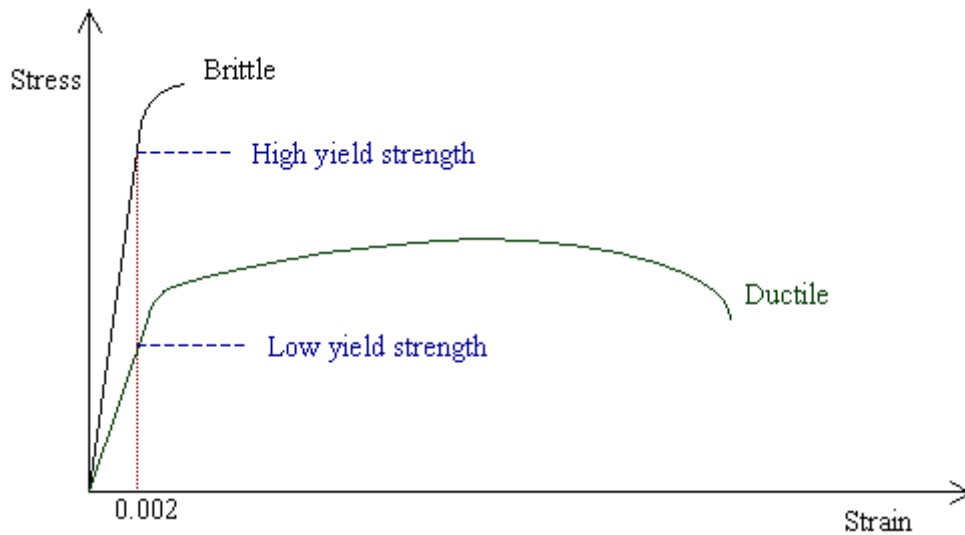


Figure 20: Schematic graph of tensile stress versus strain characteristics for ductile materials [94]

From the figure 37 it can be observed that a very small plastic deformation is termed brittle [91, 94] while a ductile material has the ability to sustain considerable geometric change when it is tested.

2.5.4 Bending Tests

Bending test [84, 95] or flexure test [95] is a mechanical evaluation test for brittle materials with the application of a load on a rectangular specimen at either one or two spots. A bending test method where the vertical application of the load is in one spot is termed a three-point bending test [95]. Similarly, a four-point bending [95] test has a vertical application of the load on two points. [95] The bending test method is shown in figure 21 below.



Figure 21: Three-point and four-point bending test methods [95]

The specimens experience longitudinal stresses which are tensile on the top surface and compressive at their bottom surface. [95]

Bend Radius

The bend radius is the smallest permissible radius a cable, wire, tube or pipe can be bent without causing any damage. [91] The flexibility of a material increases with a decrease in bending radius. [96]

Figure 22 shows a cable with an outer diameter (OD) of 2 inches bent about a radius of 12 inches. [97] The minimum bend radius of the cable is calculated [97] as

$$\text{Minimum bend radius} = \text{cable outer diameter} \times \text{cable multiplier}$$

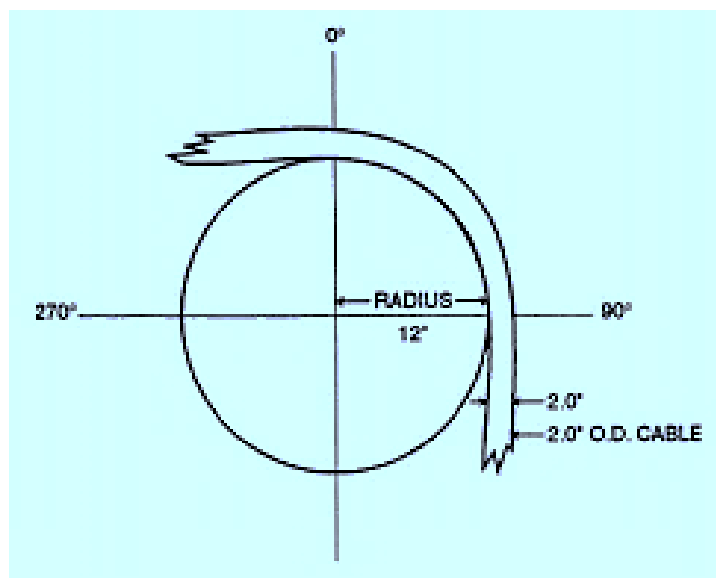


Figure 22: Illustration of the minimum bend radius of a cable [97]

Bending Test Procedure

In order to carry out a tether bending test, an investigation into the standard procedures for the test was studied based on a test carried out by the National Aeronautics and Space Administration (NASA), [98] an agency of the government of United States of America (USA). A wire and cold bending test was used to evaluate the effect of a low temperature (75 Kelvin) on the physical and mechanical characteristics of different wire samples. [99]

Case Study: National Aeronautics and Space Administration (NASA) Wire and Cable Cold Bending Test

Colozza [99] aimed at providing information on the mechanical behaviour of wires under cold, cryogenic temperature, [99] conditions by cold soaking 35 various samples of wires and cables in a cold liquid nitrogen bath. Thereafter, a bending test was conducted to evaluate the

flexibility of the wire samples and the bending force required to bend it in relation to the temperature of the liquid nitrogen. The test equipment used is shown in figure 23. The equipment consists of an automated bending press utilising a force sensor, an actuated bending fixture, and a wire support bracket for the wire samples and cables. [99]

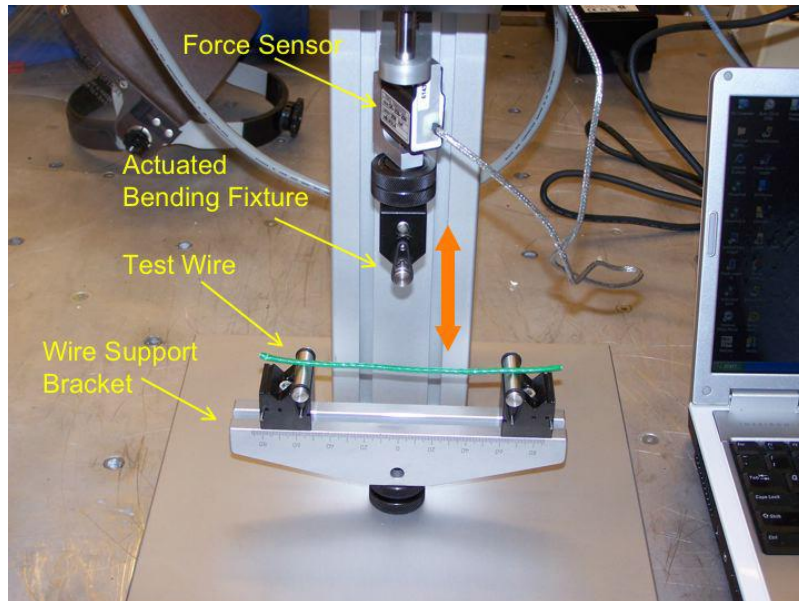


Figure 23: Jig for the cable and wire bending test [99]

Mathematical evaluation of the bending force

Figure 24 shows a 2D design of the bend test jig. The torque [100] needed to unreel the cable was calculated by multiplying the radius (r) of the wire reel by the bending force (F), as expressed in Equation (5). [99]

$$T = Fr \tag{5}$$

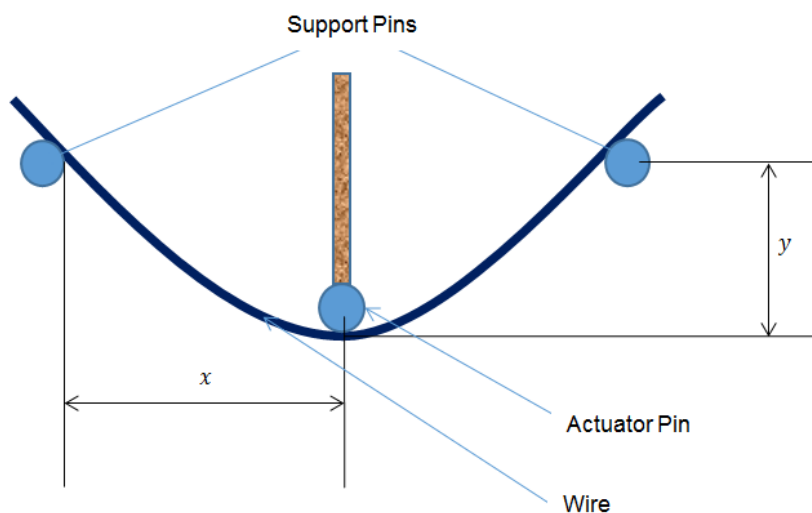


Figure 24: Diagram of the three-point bending test used on the test jig [99]

General Trend of Bending Force Curves

By plotting a graph of the bending force against time, together with the bending radius [101] for the different wire types or gauge, Colloza [99] derived the following results. Generally, a decrease in the bending radius caused an increase in the required bending force. The change in the bending radius and, also the bending force was significant at the start of the bending test and diminished with time. The bending force increased considerably between the room temperature and the liquid nitrogen temperature tests. Figure 25 shows the failure in the cable.

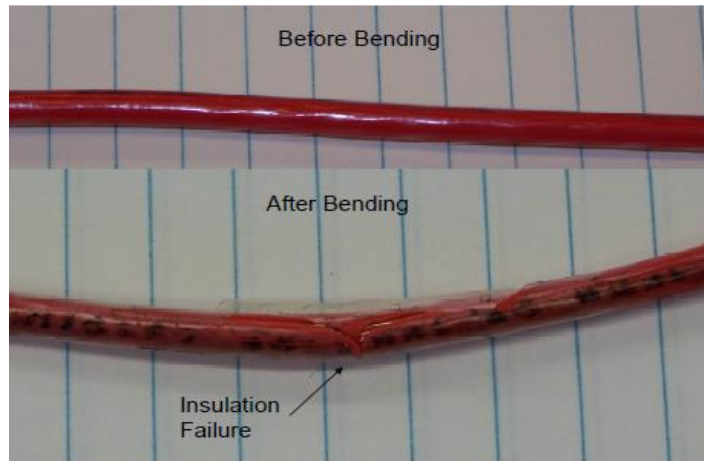


Figure 25: Insulation failure of the 6-gauge wire before and after bending test [99]

Bending curve for a Teflon and Peek Insulated Wire

As illustrated in figure 26 the bending force required for 18 and 20 gauge wires with Teflon and Peek insulation was lower than the values obtained in the other tests.

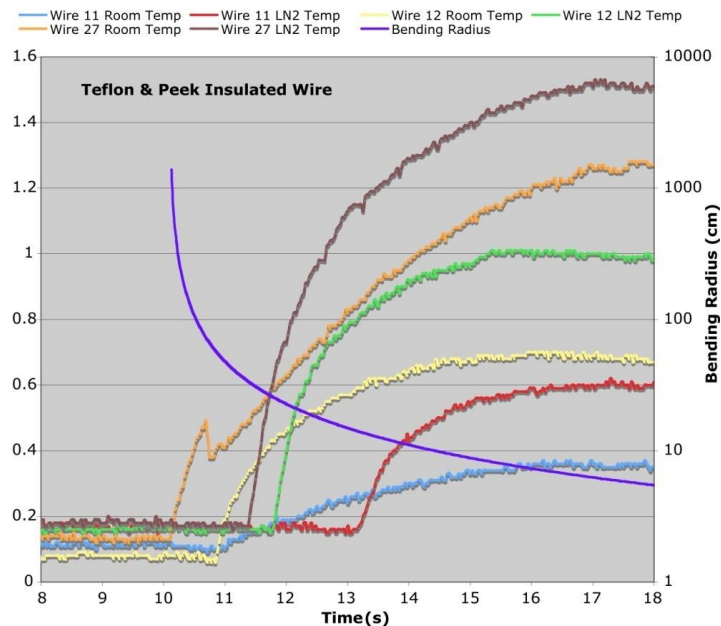


Figure 26: The bending force curves for 18 and 20 gauge Teflon and peek insulated wires [99]

Colloza [99] summarised that failures in insulation are a function of wire size; lower gauge wires and those with thick insulation failed the most. The insulation thickness was a critical factor in determining the required bending force because a thicker insulation generates a higher bending force at cold temperatures. The results of multiple wire cables and dual coaxial cables showed that the deployment force of a cable is minimised by reducing the number of wires in a given cable or using multiple cables with low wire counts. [99]

2.6 Biocompatibility

A medical device needs to be biocompatible for a safe and healthy application in humans. [102, 103, 104] For the capsule endoscope biocompatibility will focus on the materials and the adhesives used for binding the 3D-printed parts together.

2.6.1 Standards used in the Evaluation of Medical Devices

The International Organization for Standardization (ISO) [105] provides the standards: ISO 13485 for quality management in medical device design [106], and ISO 10993-1:2009 for biological evaluation of medical devices (evaluation and testing within a risk management process) [107].

2.6.2 Biocompatible Fluoropolymers used in Endoscopy

In the medical device market, the use of fluoropolymers centres on two key properties: lubricity and biocompatibility. Fluoropolymers exhibit very good lubricity and biocompatibility compared with other plastics. [108] The high-grade properties of fluoropolymers are linked to their chemistry; fluorine is the most electronegative element and is very reactive. The commonly used fluoropolymers in the medical arena [108] are Perfluorotetraethylene (PTFE), and Perfluoroalkoxy (PFA) and Fluorinated Ethylene Propylene (FEP). [108]

PTFE

Perfluorotetraethylene (PTFE) also called Teflon [109] is by far the most chemically resistant fluoropolymer. [110] PTFE is the most lubricious polymer, with a very low coefficient of friction (COF) of 0.1 and is considered hydraulically smooth. [111] PTFE is widely applied in making artificial tendons, ligaments, blood vessel guide catheters, prosthetics and vascular grafts. [112] However, PTFE is prone to radiation attacks. [111] Figure 27 below shows samples of PTFE tubes.



Figure 27: PTFE [113]

PFA

Perfluoroalkoxy (PFA) is a fluoropolymer with similar physical and chemical properties and to PTFE such as use temperature and also combines the melt processability of FEP. [114] PFA has the highest permeation performance and the best finish of all of the fluoropolymers. [114] Another advantage of PFA over PTFE is its high transparency with a good transmittance of both ultraviolet (UV) and visible light wavelengths and extremely low refractive index of 1.34. [112] PFA is prone to radiation effects, and degradation in the air starts at a roughly higher dose than that of PTFE. It is popularly used for critical fluid handling. [112] Figure 28 below shows a PFA tube.



Figure 28: Transparent tube and bottles made with PFA [115]

FEP

FEP is transparent and has a good transmittance of both UV and visible light wavelengths with a similar refractive index to PFA. It lacks the near universal chemical resistance exhibited by PTFE and PFA. [111] FEP is also attacked by radiation, and its degradation in air is ten times higher than that of PTFE. [110] FEP is utilised in electrocautery devices and fusing sleeves. [112] Figure 29 below shows an FEP tube.



Figure 29: FEP [116]

The relative tensile strength values of the fluoropolymers reviewed are given in table 1 below.

Fluoropolymer	Tensile Strength(ψi)	Tensile Strength(MPa)
PTFE	2500	17.24
PFA	4000	27.58
FEP	3000	20.68

Table 1: Tensile strength values for fluoropolymers [112]

2.7 Adhesive Bonding

According to Cummins and Desmulliez [117], biocompatible adhesives are obtainable for the assembly of medical devices some of which are epoxies, silicones, and acrylics. [117] The silicone adhesive was selected for this project.

2.7.1 Silicone

Silicones are used for sealing seams. [117] Silicone adhesives are flexible, durable [117, 118] and have high wettability. [117, 119] They are also good insulators which make them good for applications in electronics. [117, 120] According to Yoda [121] silicones are obtainable in different grades of hardness. The superficial properties and biocompatibility of silicone suggest a minimum possibility of damage to tissues and blood cells. [121] Silicones are utilised in high sensitive diagnostic procedures such as peristaltic pump tubing for heart-lung machines [122] and some blood circuitry equipment. [121] A setback for using silicone adhesives is that they have an extended cure time for bonding in comparison to other adhesives but the bond strength increases with time. [117]

2.7.2 Bond strength of adhesives

The tensile strength of a medical adhesive is the maximum force required to break the bond divided by the area of the specimen. Table 2 shows the different tensile strengths of medical

adhesives. The higher the tensile strength the higher the force required to break the bond. [123]

Adhesive	Tensile Strength (psi)	Tensile Strength (MPa)
Epoxy	8000	55.16
Acrylic (light cure)	2500	17.24
Silicone	150	1.03

Table 2: Tensile strengths of popular medical adhesives [123]

2.7.3 Elongation property of silicone adhesive

Elongation indicates the flexibility of the adhesive. The higher the elongation the greater is the flexibility of the adhesive. The flexibility of an adhesive is crucial for devices that bend or actuate during use. Medical devices such as catheters and tubing connections embody flexible adhesive joints. Silicones are the most flexible because they have higher percent elongation values. Cyanoacrylates and epoxies have low percent values for elongation. [123]

2.8 Maximum Pulling force for endoscopy

Shergill et al. [124] summarised that a threshold of 10N should not be repeatedly exceeded in an endoscopy process so as to avoid injuries to patients. [124] The greatest pinch forces during a colonoscopy endoscopic process was exerted by the right thumb. [124]

CHAPTER 3 MATERIALS, METHODS, AND RESULTS

3.1 Project Flowchart

The project flowchart is illustrated in figure 30. The lengthy test data generated from the mechanical tests are stored on the CD accompanying this project report. The main sections include:

- ❖ 3D design of pills
- ❖ 3D printing
- ❖ Mechanical evaluation of 3D-printed pills
- ❖ Tensile tests for cables and tether
- ❖ Three-point bend tests
- ❖ Adhesive Bonding
- ❖ Tether-to-pill bond strength test
- ❖ Biocompatibility statement

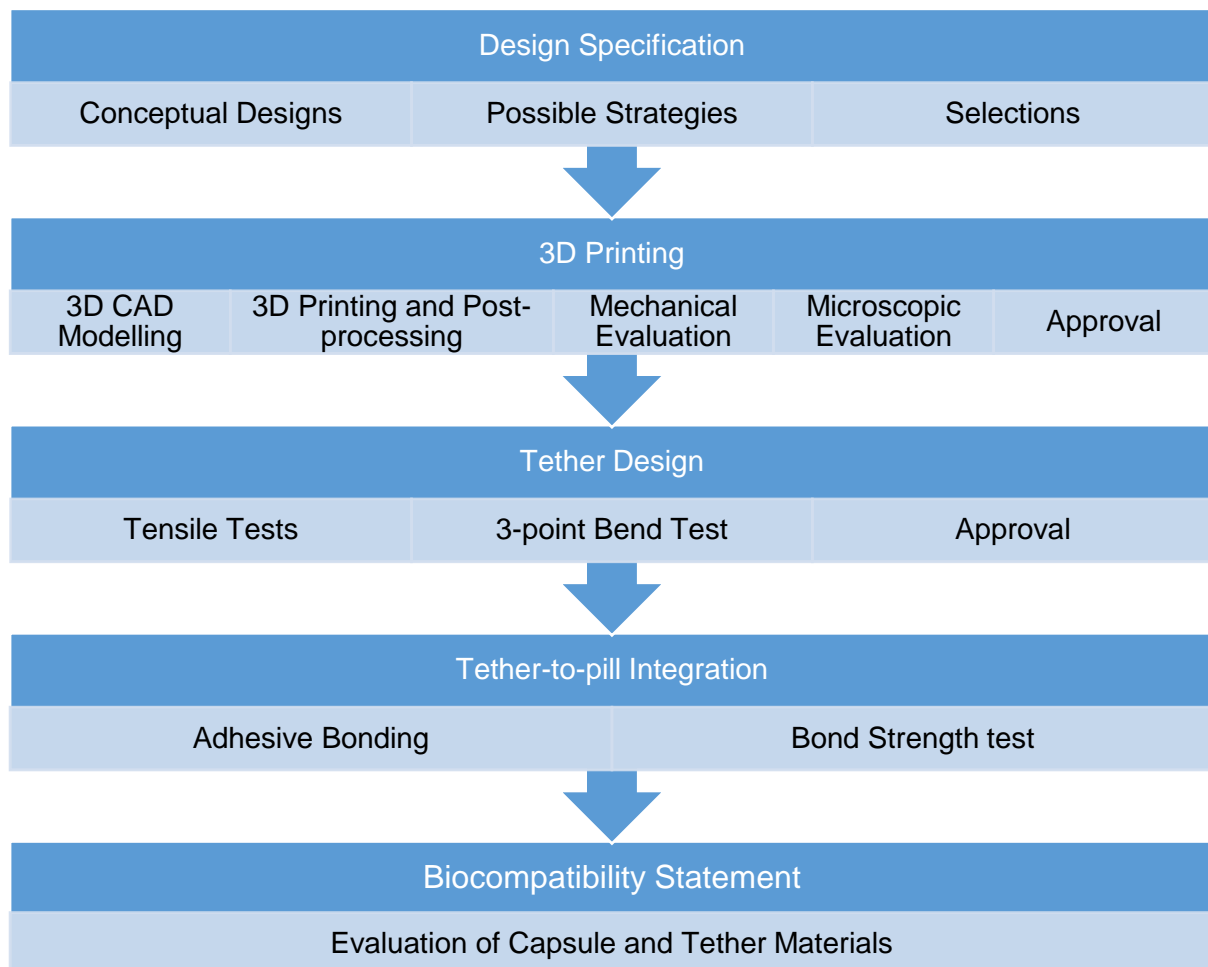


Figure 30: Flow chart of project methods

3.2 Specification

The capsule shell is to create room for the following components:

- 4 ultrasound (UT) transducers measuring 5mm diameter with a variable thickness of 3mm to 5mm.



Figure 31: The Ultrasound Transducer (Courtesy: Dr. Yongqiang, Sonopill)

- Either a thermocap printed circuit board (PCB) measuring 17mm x 6mm or a sonocap PCB with dimensions, 18.25mm x 6.25mm.

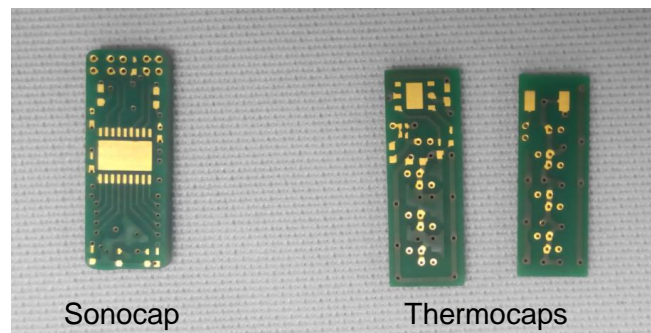


Figure 32: The Sonocap and thermocap PCBs (Courtesy: Dr. Holly Lay, Sonopill)

- Provision for tether integration.

Table 3 gives an outline of the specification for the ultrasound capsule endoscopes. The dimensions given were approximate values

Feature	Specification
Capsule type	Tethered Ultrasound Capsule Endoscope (USCE)
Form factor	Pill diameter: 10mm Pill length: 30mm
Technical dimension	10mm x 30mm
Imaging mode	Ultrasound imaging
Communication mode	Tether system
Power mode	Batteryless, grid-tied system
Actuation mode	Manual actuation

Table 3: Ultrasound capsule endoscope design specification

3.3 Design Concept

It was aimed that the final capsule endoscope should be easily opened into two halves with structures to contain the specified components. The final product will have the shape of a vitamin pill.

3.4 Possible Strategies

Two-dimensional (2D) sketches of various design ideas were made preceding the actual 3D CAD modelling. The various designs are shown in figure 33 below.

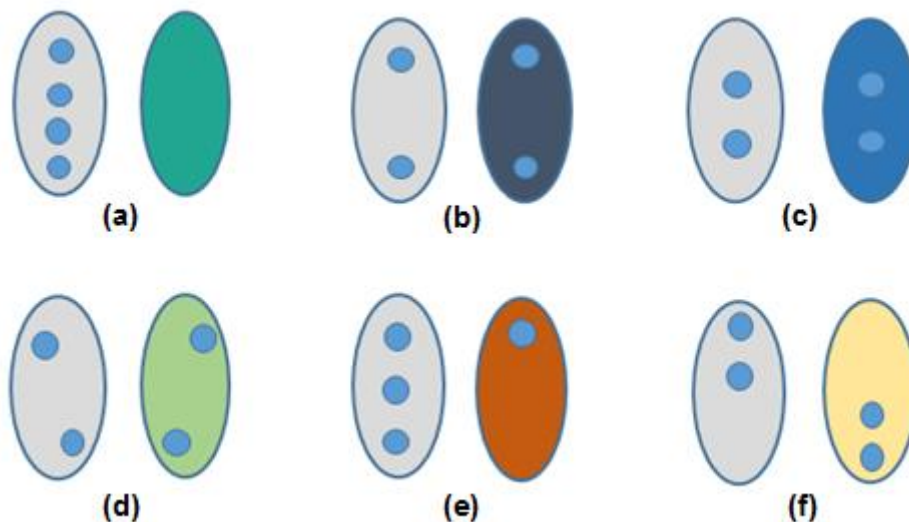


Figure 33: Ideas for pill design showing the different configurations for placing the ultrasound transducers on the pill caps.

Only two ideas were used; ideas “c” and “e”. The reasons were that idea “c” will give a good weight balance since it has 2 equally spaced transducers on both pill caps and allowance for electronic tools when fixing the PCB and UT transducers. The spacing for the PCBs will be designed with a rectangular “cut extrude” method. Although idea “e” has 3 UT transducers on one cap and 1 UT transducer on the other cap, its weight problems will be solved by fixing the PCBs on the second cap by using a “shell” method for its design. Ideas “c” and “e” were renamed Version 2-2 (V 2-2) and Version 3-1(V 3-1) respectively. V 2-2 denotes a pill design with two UT transducers on both caps of the pill while V 3-1 denotes a design with 3 UT transducers on one cap and one UT transducer only on the other cap.

3.5 Method: 3D Modelling of Pills

The pills were designed on SolidWorks 3D CAD modelling software, version 2015 using a rectangular “box” method for V 2-2 and a “shell” method for V 3-1. The aim for using the rectangular “box” and “shell” was to provide space to house the thermocap and sonocap boards in each pill. Dimensions are in millimetres (mm).

3.5.1. Design of V 2-2

Drawing the hemispherical end cap

The V 2-2 and V 3-1 designs began on the top plane with the design of a hemispherical end cap by revolving a three-point arc (radius of 5mm) about a 5mm axis through an angle of 360° as shown in figure 34.

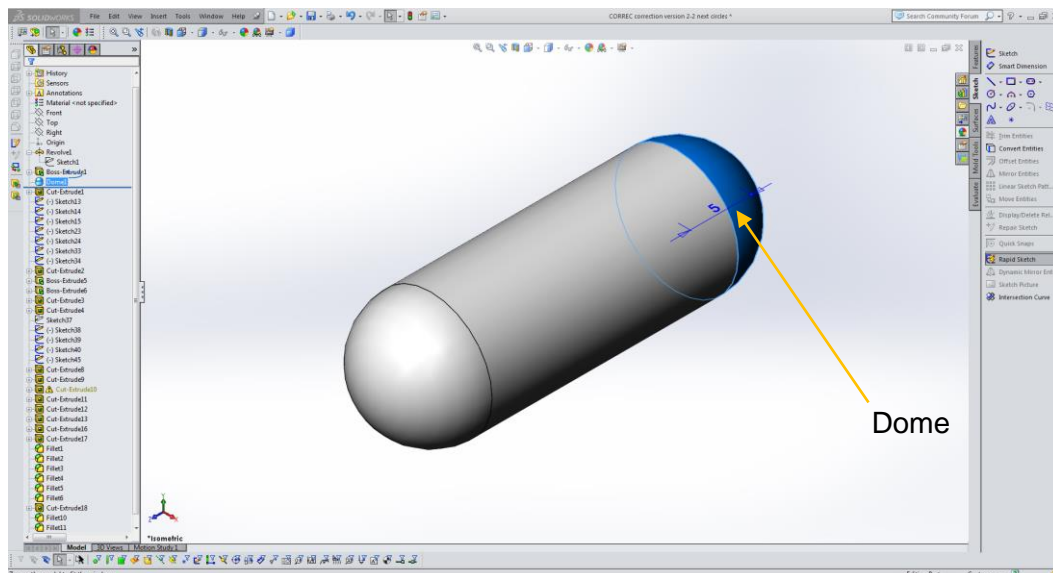


Figure 34: A full pill design with the inserted domes on the cylinder

Base cap design and tether inlet (integration) design

The design for the tether inlet was achieved by using a circular “cut extrude” command from the end of the base cap where space had been provided at the early stages of the design. The tether inlet design is spotted by the red ribbon in figure 35 below.

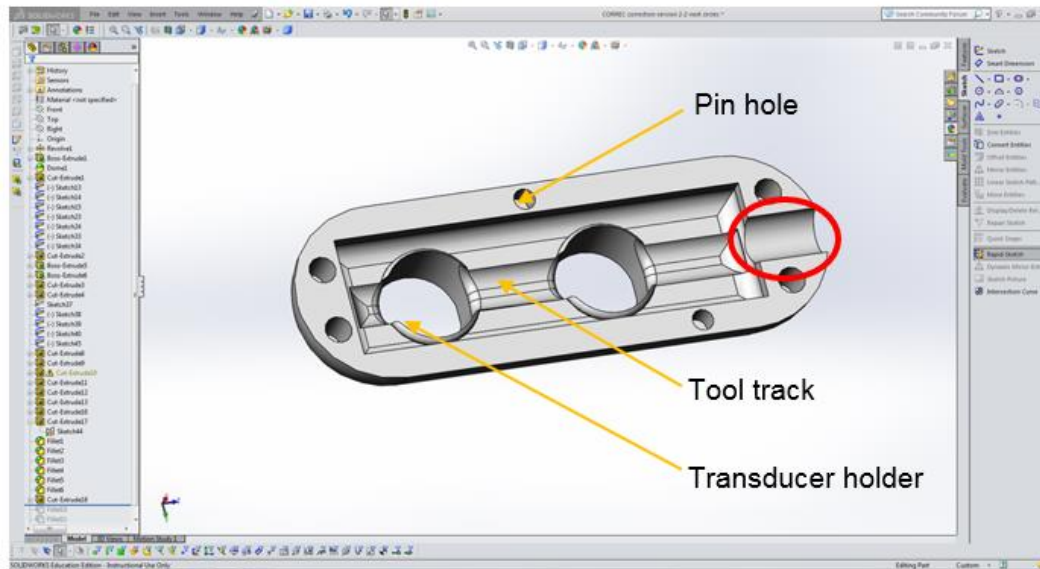


Figure 35: Base cap design with tether inlet

Smoothering edges with the “fillet” tool

The edges were smoothed to enhance the appearance of the design with the aid of the “fillet” tool as shown in figure 36.

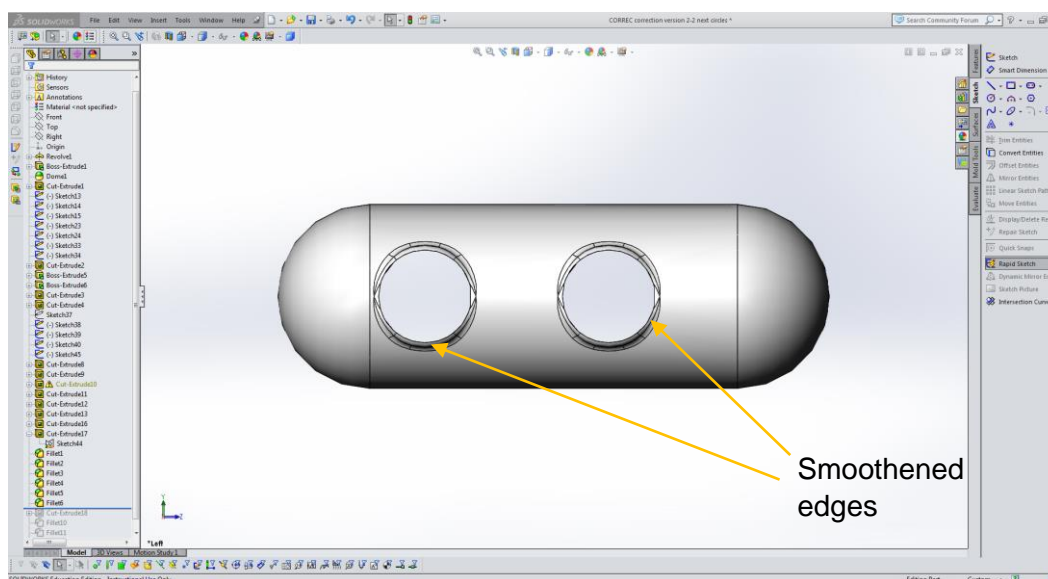


Figure: 36 Application of the “fillet” tool on the edges

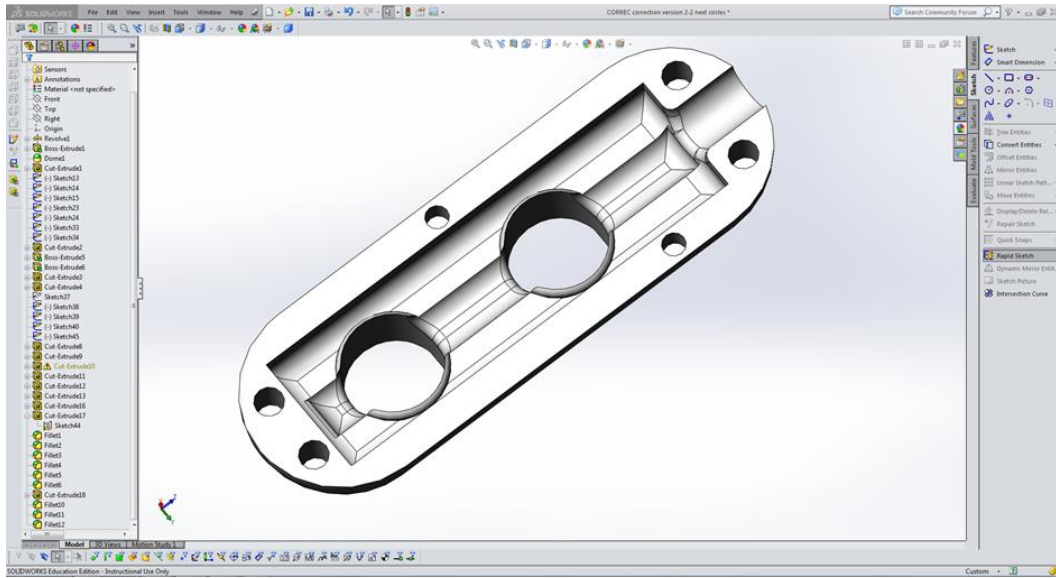


Figure 37: 3D design view of final base cap design showing the “box” layout

Pill cover design (cover cap)

The second pill cap which was later called the “cover cap” is a mirror design of the base cap at the design for tether inlet stage. The part file at that stage was simply copied to design the cover cap but the pin holes were deleted. Figure 38 below shows the copied part file for the design of the cover cap with the retained tether inlet design. The colour of the cover cap was made blue in order to differentiate it from the base cap during the design and after the assembly process. Assembling pins are designed on the thickness of the cover cap to latch the pill caps efficiently during the assembly process. Tether reinforcement pins are used to hold the tether for a firm bonding with the pill.

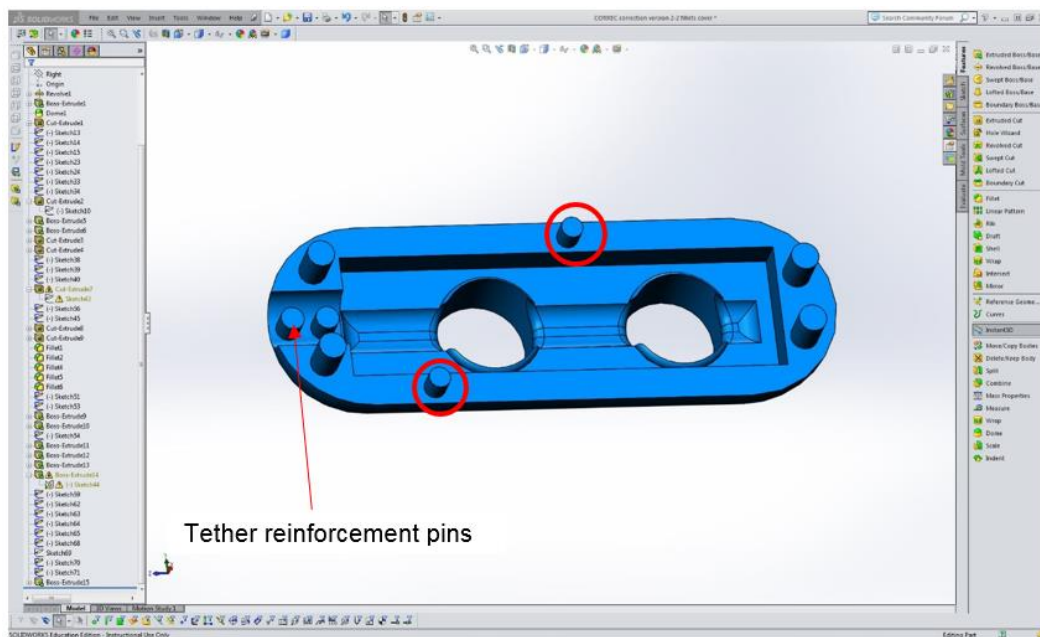


Figure 38: Design of assembling and tether reinforcement pins

3.5.2 Design of V 3-1

Application of shelling

The “shell” tool was used to design a shell for housing the components in the V 3-1 pill. The transducer holders were also designed in an octagonal structure as illustrated in figure 39 below.

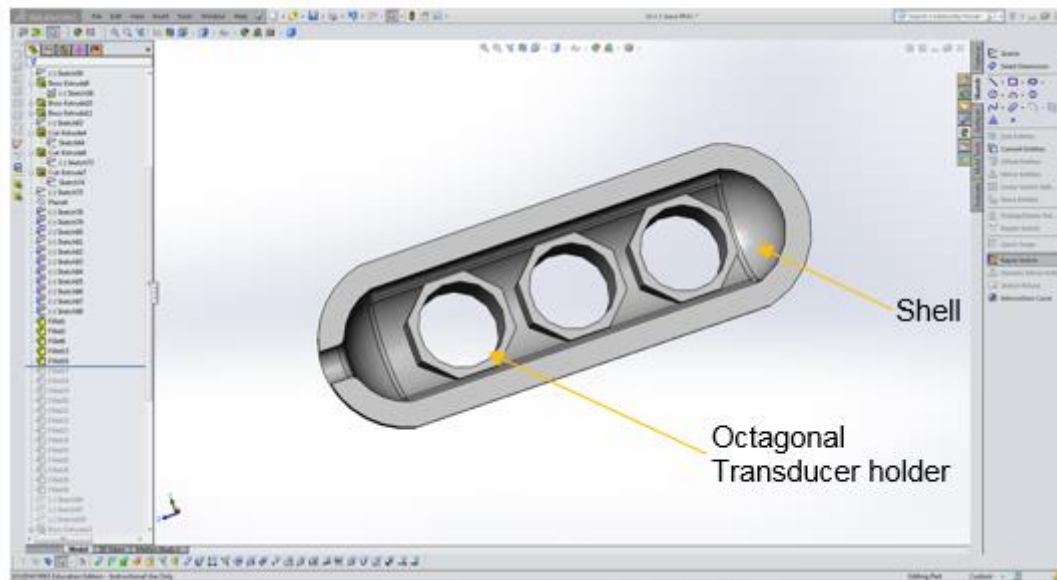


Figure 39: “Shell” tool design method and the octagonal structure of the transducer holders

Smoothing the edges with the “fillet” tool

The edges of the transducer holders in the shell and on the body of the pill cap as shown in figure 40 were smoothed with the “fillet” tool neat and less-protruding forms as illustrated in figure 41.

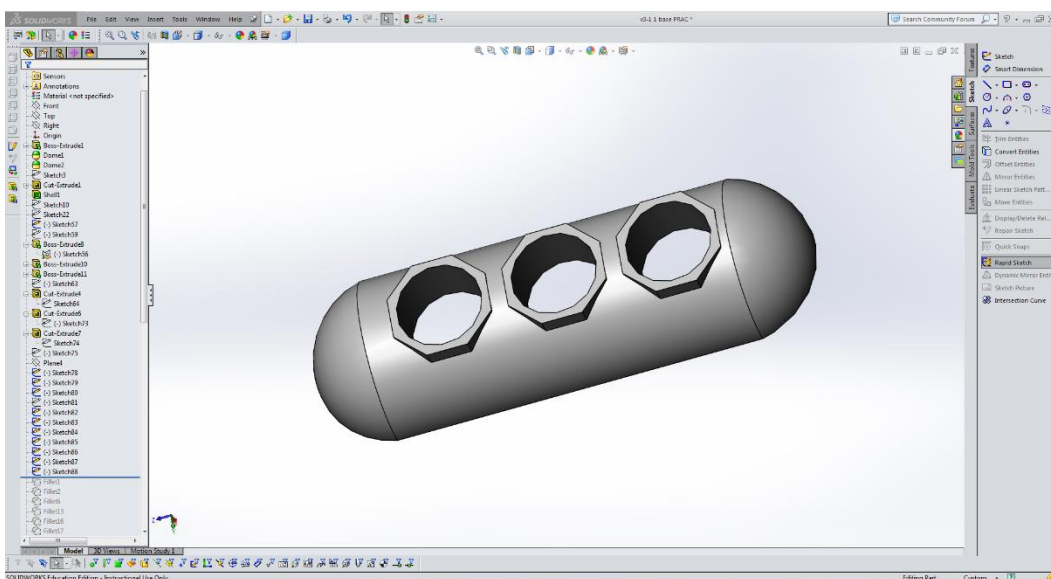


Figure 40: The protruding transducer holders before the application of the “fillet” tool

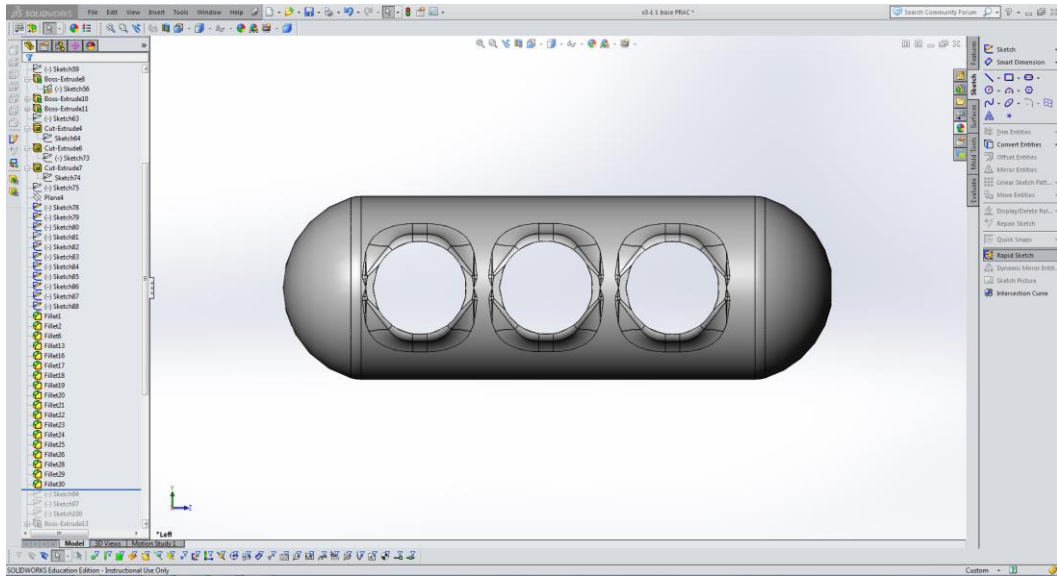


Figure 41: The smoothed protruding transducer holders after the application of the “fillet” tool

Tether inlet (integration) design and pin hole design

The thickness of the V 3-1 pill had to be increased around the edges to make provision for the tether inlet design as shown in figure 42. Pin holes were also designed for assembly purpose.

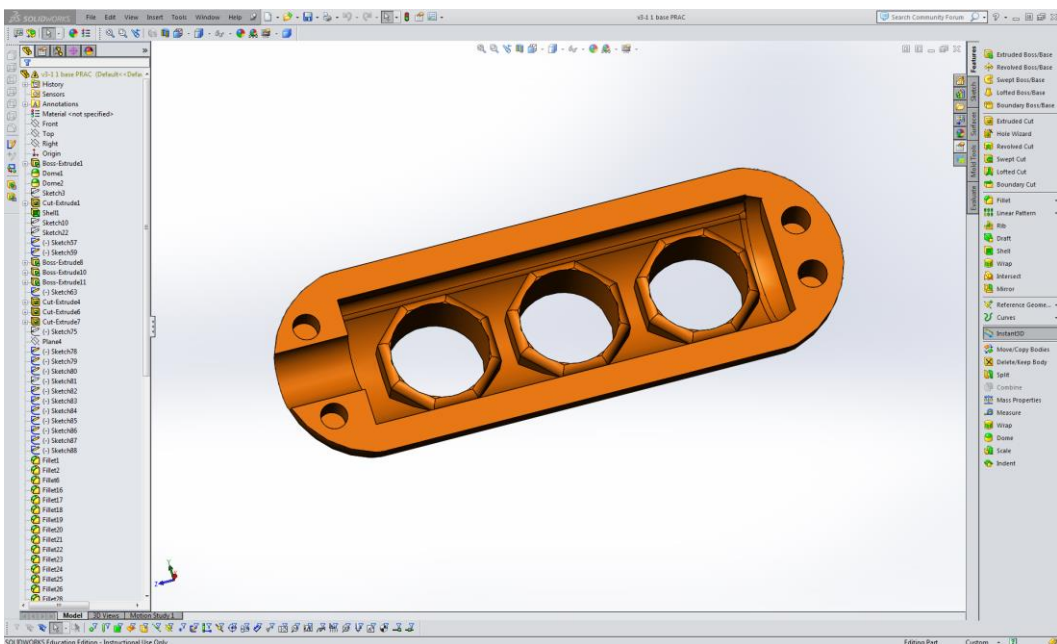


Figure 42: The tether inlet design with extended thickness of the ends to accommodate pin holes

Cover cap design

To design the cover cap 2 transducer holders were deleted from the base cap drawing and the pin holes were simply converted to assembly pins as shown in figures 43 below.

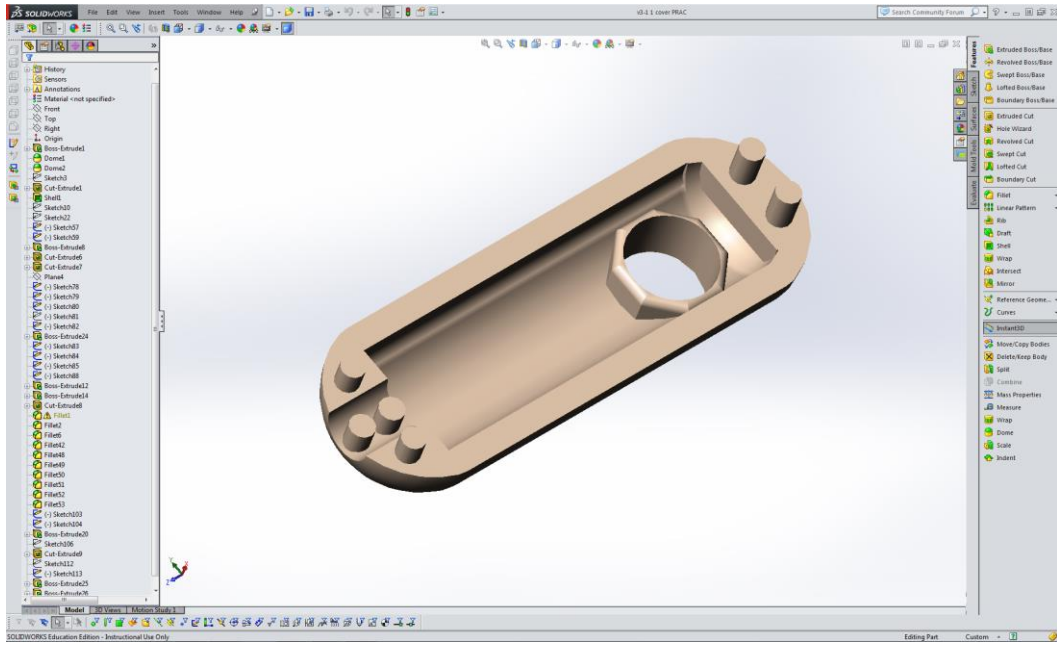


Figure 43: Final cover cap design with assembly pins

The transducer holder and edges of the cover cap were also smoothed with the “fillet” tool as shown in figure 44 below.

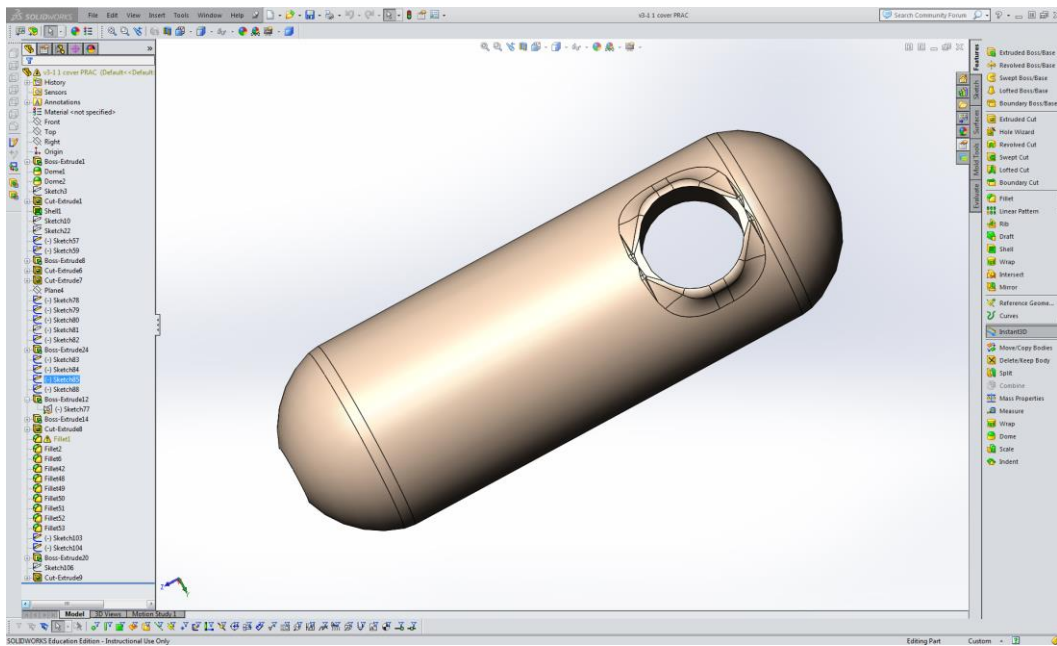
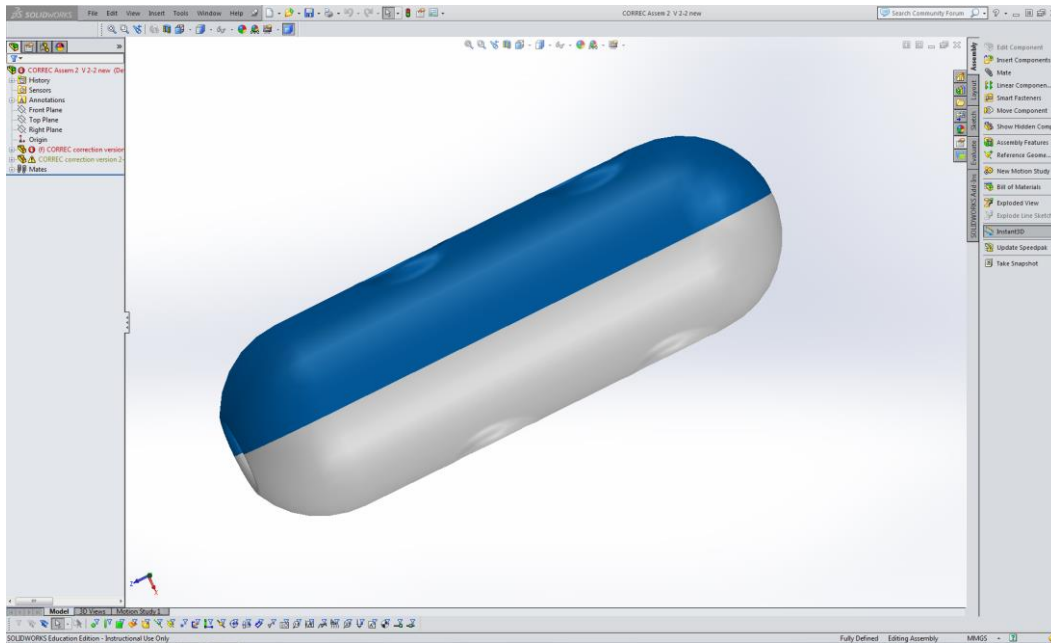


Figure 44: Smoothed transducer holder with “fillet” tool

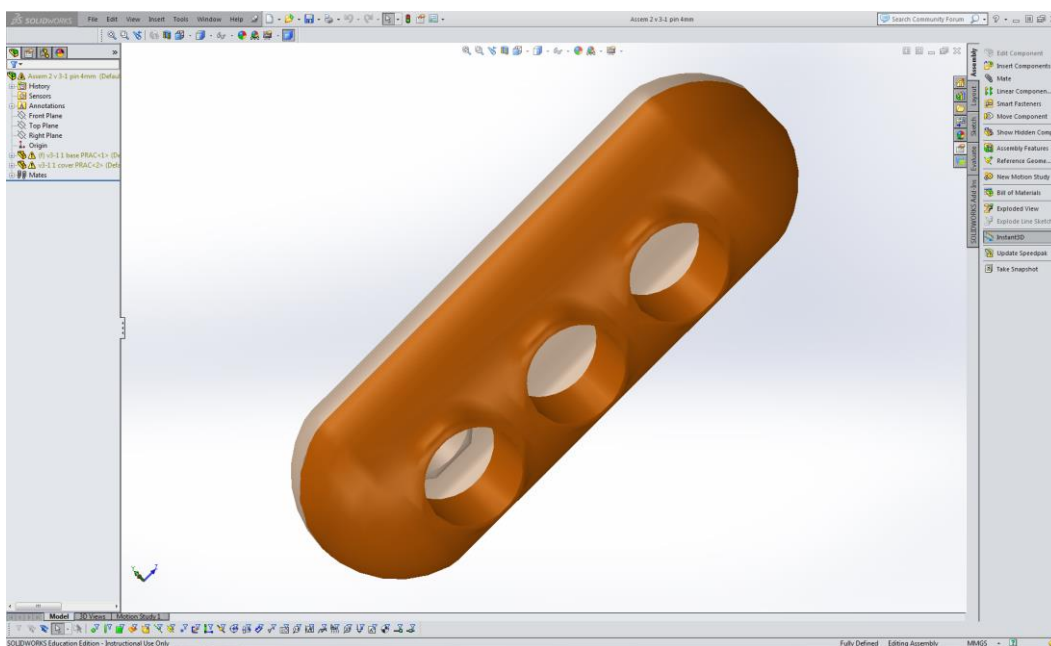
3.5.3 Results for 3D modelling of pills

Pill Assembly 3D Design

The assembly designs of the pills are shown in figure 45. The shape of the pills is similar to the shape of a vitamin pill. A blue colour was used on the cover cap in V 2-2 in contrast to the brown colour that was used for V 3-1. The pill caps are in white colour.



V 2-2 after assembly



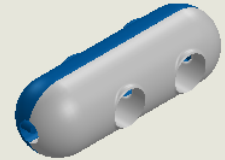
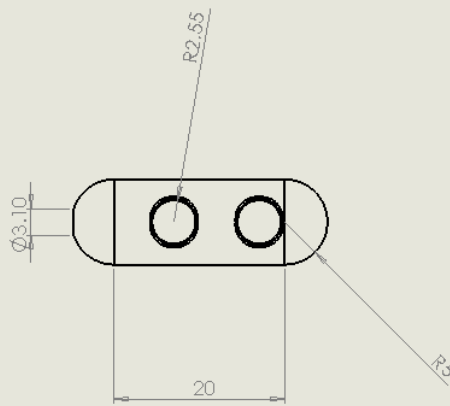
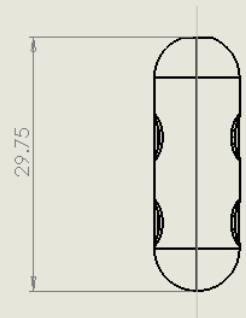
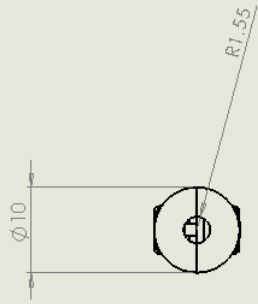
V 3-1 after assembly

Figure 45: V 2-2 and V 3-1 after assembly

The orthographic and sectional views are shown in figures 46 to 49. They allowed for a better assessment of the internal geometry of the pills. The dimensions of the pills from the assembly design are given in table 4 below.

Pill	Diameter (mm)	Length (mm)
V 2-2	10	29.83
V 3-1	9.84	29.90

Table 4: Pill size after 3D modelling



Document Title	Orthographic View
Pill Name	V 2-2
Type	Tethered Ultrasound Capsule Endoscope (TUSCE)
Designer (Mat. No.)	2245703A
Date	August 2016

Figure 46: Orthographic drawing of V 2-2

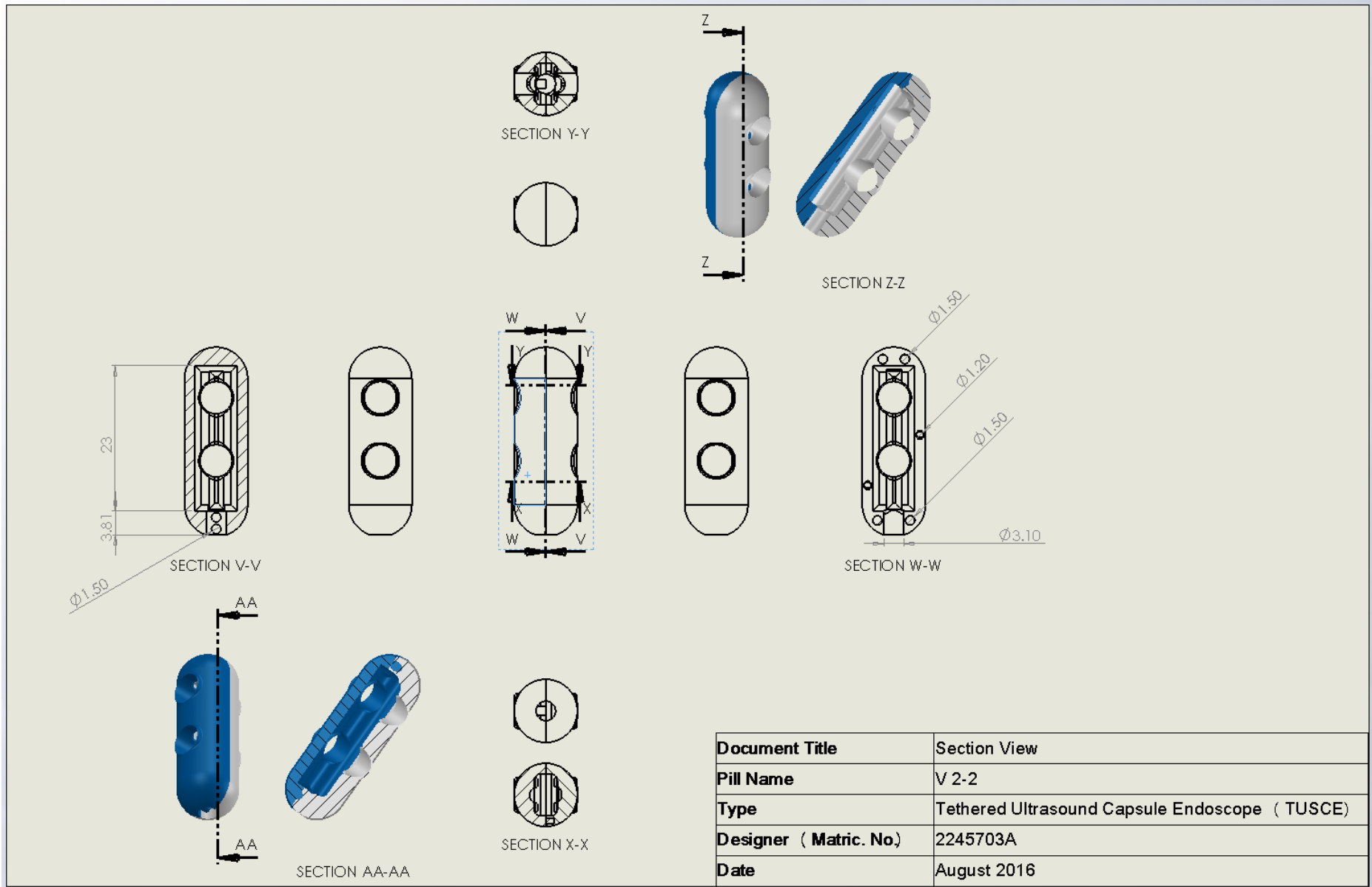


Figure 47: Section view of V 2-2

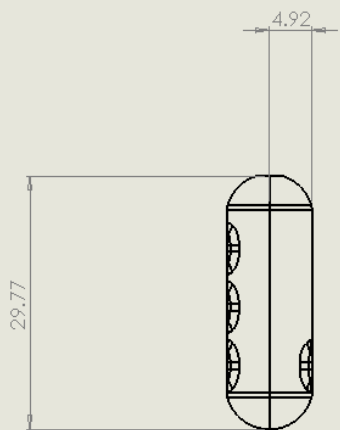
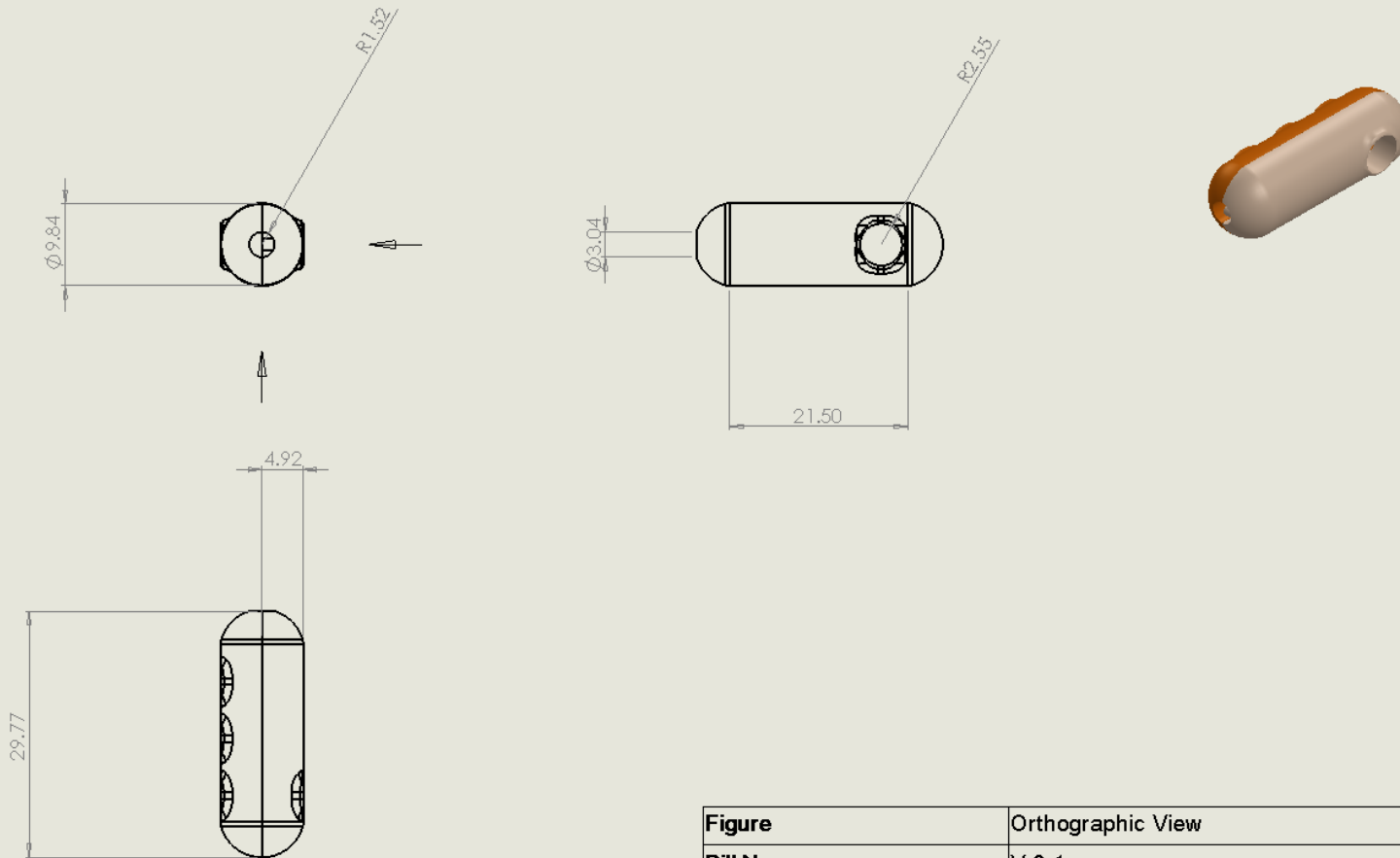


Figure	Orthographic View
Pill Name	V 3-1
Type	Tethered Ultrasound Capsule Endoscope (TUSCE)
Designer (Matric. No.)	2245703A
Date	August 2016

Figure 48: Orthographic Drawing of V3-31

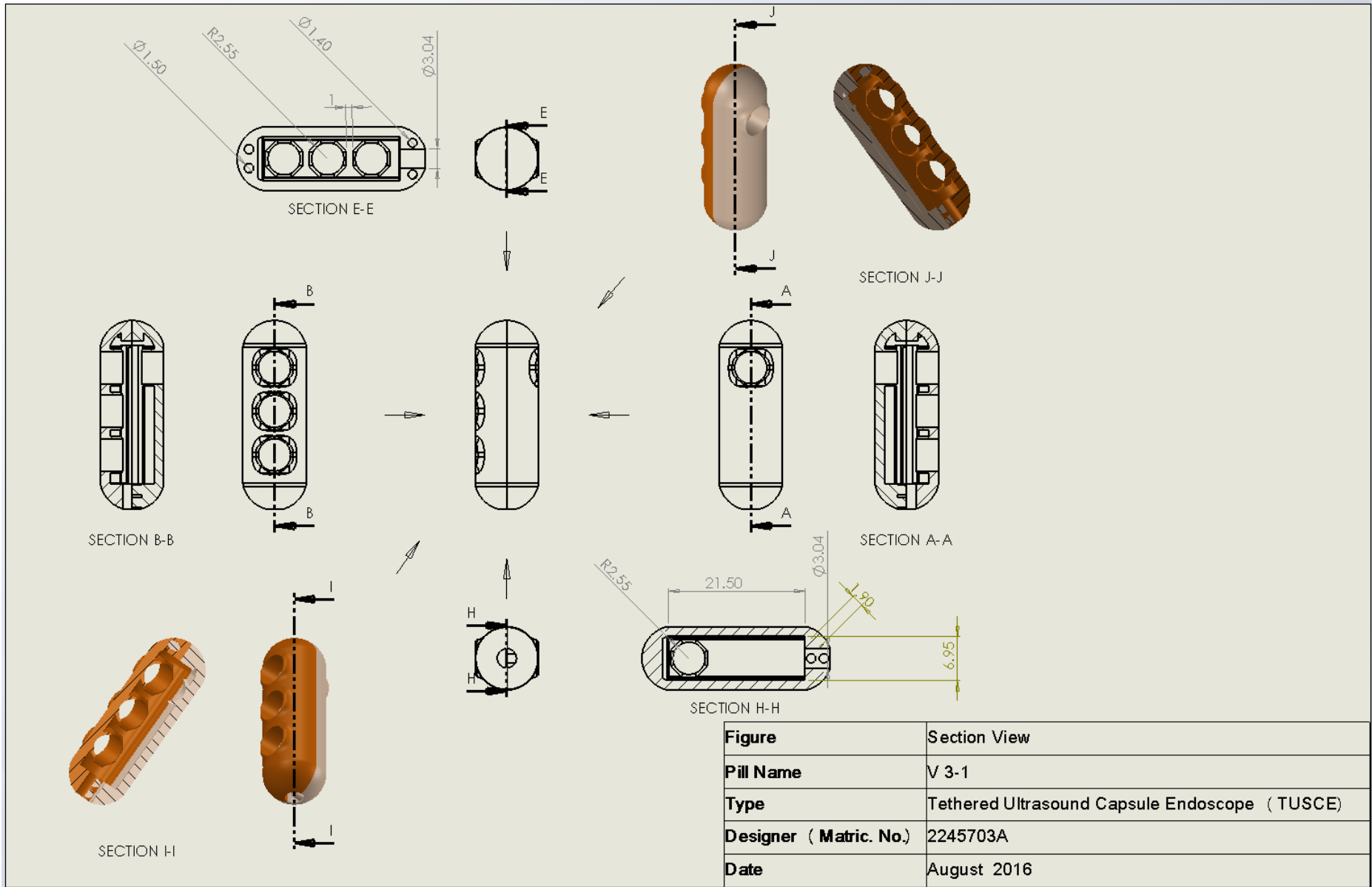


Figure 49: Section view of V 3-1

3.6 3D printing of the designed pills

3.6.1 Conversion to STL file format

The 3D designed pills which were originally saved in SolidWorks 2015 part format (.SLDPRT) were converted to STL file format (.STL) for 3D printing.

3.6.2 3D printing machine

The 3D printing of the designed pills was done with the materials outlined in table 5 below.

3D Printer	Printing Material	Colour of material	Print time (minute)
Stratasys Objet30 Pro	VeroWhite Photopolymer	White	75

Table 5: Material used for the 3D printing

Figure 50 shows the photopolymer material contained in liquid form and the loading bed for the material in the 3D printer.



Figure 50: The loading bed for the photopolymer in the Stratasys Objet30 Pro 3D printer

3.6.3 Post-processing

The 3D-printed pills were flushed with a waterjet machine to remove the uncured materials attached to the pills. The post-processing technique is shown in figure 102 below.



Figure 51: Post-processing technique with a waterjet machine

3.6.4 Results of 3D printing

STL File Format

After the conversion of the drawing part files to STL format as shown in figure 52 it was observed that the STL forms of the pill caps have a triangular geometrical form and a uniform layered profile.

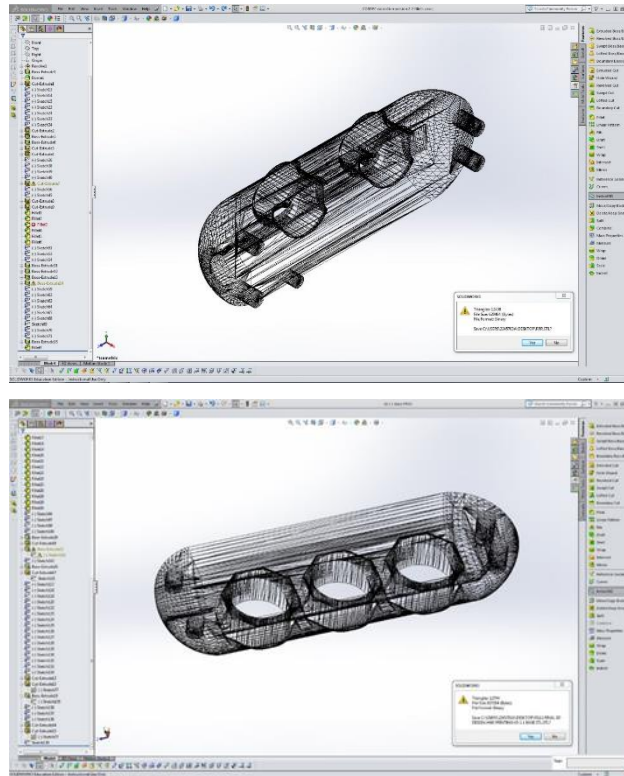


Figure 52: STL form for the V 2-2 cover cap (above) and V 3-1 cover cap (below)

3D-printed parts after post-processing

Flushing the parts with a high-pressure waterjet machine revealed the true design of the fabricated parts. The 3D designed structures were visible but the appearance of some parts looked rough and also lacked gloss. The appearance of the pills after flushing with the waterjet is shown in figure 82 below.

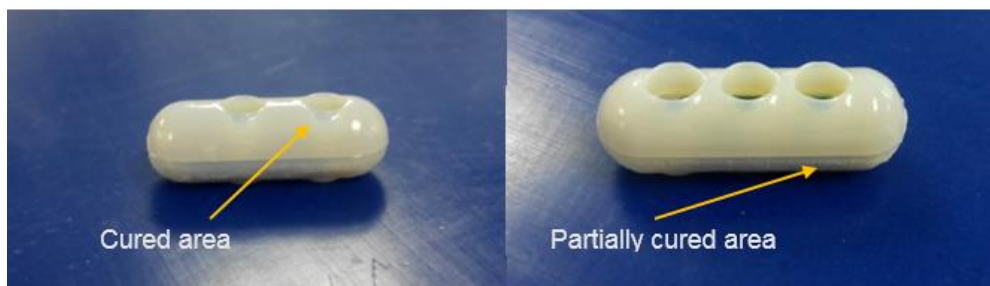


Figure 53: Result of 3D printing using VeroWhite Material

3.7 Mechanical Evaluation 3D-printed Pills

3.7.2 Measurement of the pill mass

The mass of the pills in grammes was determined using a weighting scale as shown in figure 83 below.



Figure 54: The weighing scale

The tray of the weighing scale was cleaned to avoid the influence of dust particles on the results. Tweezers were used for picking and placing the pills on the weighing scale. The measurements for each pill version was done in 4 measurements and the average for the two sets of measurements were compared to give a final value. The measurement method used is summarised in table 6 below.

Pill	Results (g)		
	Empty	With Sonocap	With Thermocaps
V 2-2			
V 3-1			

Table 6: Adopted weighing method

3.7.4 Pill size

The dimensions of the pills were measured with a digital vernier calliper as shown in figure 55 below.



Figure 55: Measuring the pill size with a Vernier calliper

3.7.5 Microscopic evaluation of pills

A USB (Universal Serial Bus) microscope was used to evaluate the structure of the pills. The microscope was connected to a laptop where the images of the pills were taken through a software interface as shown in figure 56 below.

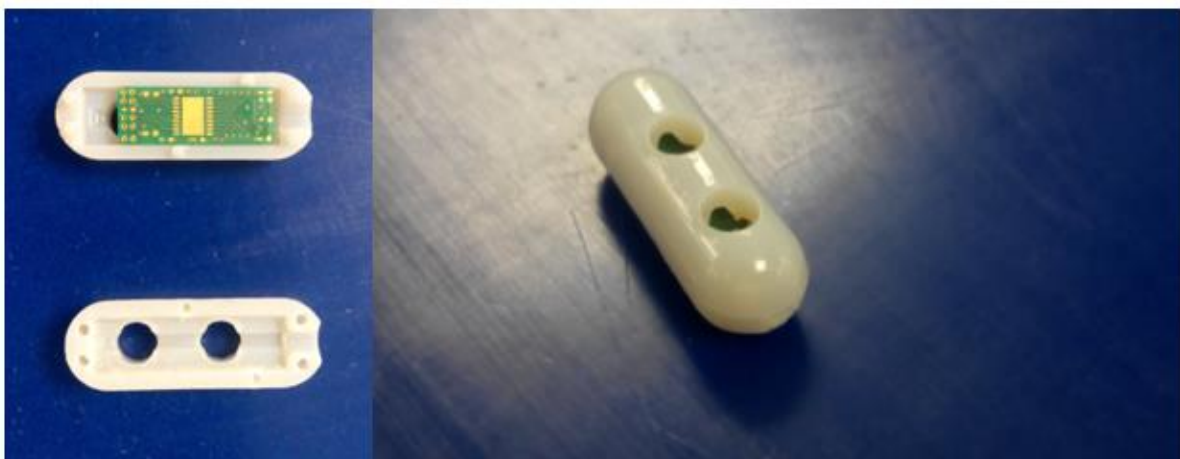


Figure 56: The setup for the microscopic evaluation

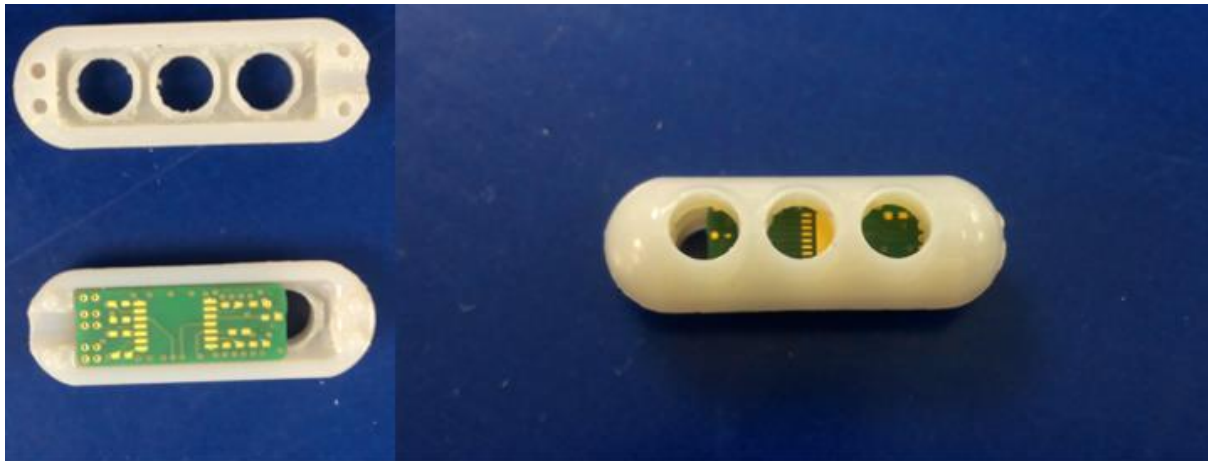
3.7.6 Results of mechanical evaluation of pills

Evaluation of PCB slots and transducer holders

The sonocap and thermocap boards were adequately housed in the pill. The assembly is shown in figure 57 below.



(a) V2-2 assembly



(b) V 3-1 assembly

Figure 57: The assembly of the capsule with the PCBs

Measurement of the pill mass

The result for the measurements of the mass of the pills is given in table 7 below.

Results (g)			
Pill	Empty (Average)	With Sonocap (Average)	With Thermocap (Average)
V 2-2	1.523	1.934	2.000
V 3-1	1.496	1.793	1.865

Table 7: Results for measurements of pill mass

From the results table shown above, it can be observed that V 2-2 is heavier than V 3-1 by 1.81% when they are both empty, 9.43% when they have sonocap PCBs, and by 7.2% when they both have thermocap boards.

Results for measurement of pill size

The dimensions of the pills as measured using a Vernier calliper and compared to the actual dimensions in the 3D CAD design are given in table 8 below.

Pill	Vernier Calliper Readings		3D CAD Design Values		Deviation in diameter %	Deviation in length %
	Diameter (mm)	Length (mm)	Actual Diameter (mm)	Actual Length (mm)		
V 2-2	10.13	29.43	10	29.83	1.3	-1.34
V 3-1	9.89	29.90	9.84	29.90	0.5	None

Table 8: Results and comparison of the Vernier calliper readings of the pill size to the 3D CAD design values.

Results from the microscopic evaluation of the pills

The results of the microscopic evaluation of the pills are shown in figure 58 below.

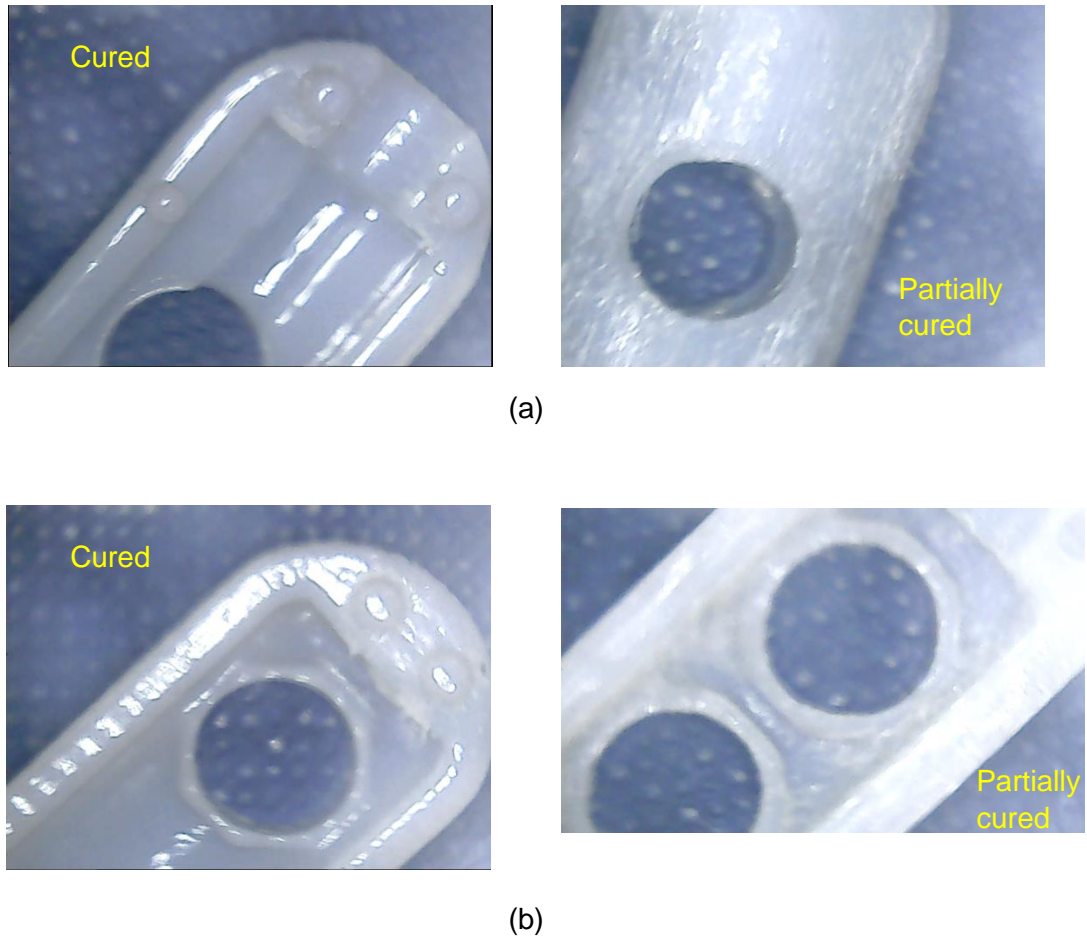


Figure 58: Microscopic evaluation of the pills showing the cured and partially cured areas after 3D printing (a) V 2-2 (b) V 3-1

3.8 Design of the tether

Destructive (mechanical) tests were carried out in order to properly select the cables and Teflon tube for the tether design. The tests were ultimate tensile strength (UTS) test and three-point bend test. The UTS test was performed on different cable samples and on the tether to find their maximum tensile strength while the three-point bend test was used to find the maximum bend radius of the tether.

3.8.1 Measurement principle

The test specimen was subjected to a pull and allowed to stretch under a constant pulling force. The force value to be determined is the maximum force at which the specimen is stretched to weakness, failure or deformation.

3.8.2 Selection of cable samples

The cables used in this test were selected based on the meetings with the Microengineering & Microelectronics team of Sonopill and factors like cost, size, current/voltage rating and signal attenuation were considered. Micro-coaxial cables [79] and power cables [82] were selected.

Sample	Type	Core diameter (in)	Core diameter (mm)	Insulation Type	Jacket diameter (in)	Jacket diameter (mm)	
1	Coax1	Micro-coaxial	0.0029	0.07366	PFA	0.0059	0.14986
2	Coax2	Micro-coaxial	0.0037	0.09398	PFA	0.0068	0.17272
3	Coax3	Micro-coaxial	0.0045	0.11430	PFA	0.0078	0.19812
4	Coax4	Micro-coaxial	0.0062	0.15748	PFA	0.0105	0.26670
5	Coax5	Micro-coaxial	0.0077	0.19558	PFA	0.0120	0.30480

Table 9: Technical specification for micro-coaxial cables

Sample	Type	Core diameter (in)	Core diameter (mm)	Insulation Type	Jacket diameter (in)	Jacket diameter (mm)	
1	P1	Hook-up wire	0.0090	0.22860	PTFE	0.0220	0.55880
2	P2	Hook-up wire	0.0120	0.30480	PTFE	0.0240	0.60960

Table 10: Technical specification for power cables

3.8.3 Material Test Machines

Zwick/Roell Z2.0 and Zwick/Roell Z250

The UTS test was conducted with the Zwick/Roell Z2.0 and Zwick/Roell Z250 materials testing machines which had a wired communication link to a desktop computer. The Zwick/Roell TestExpertIII application software was used as the communication interface. Load cells of 500N and 2.5KN were used on the Z2.0 and Z250 machines respectively for tensioning the specimens.

Method

Figure 60 shows the test setup for the UTS test.

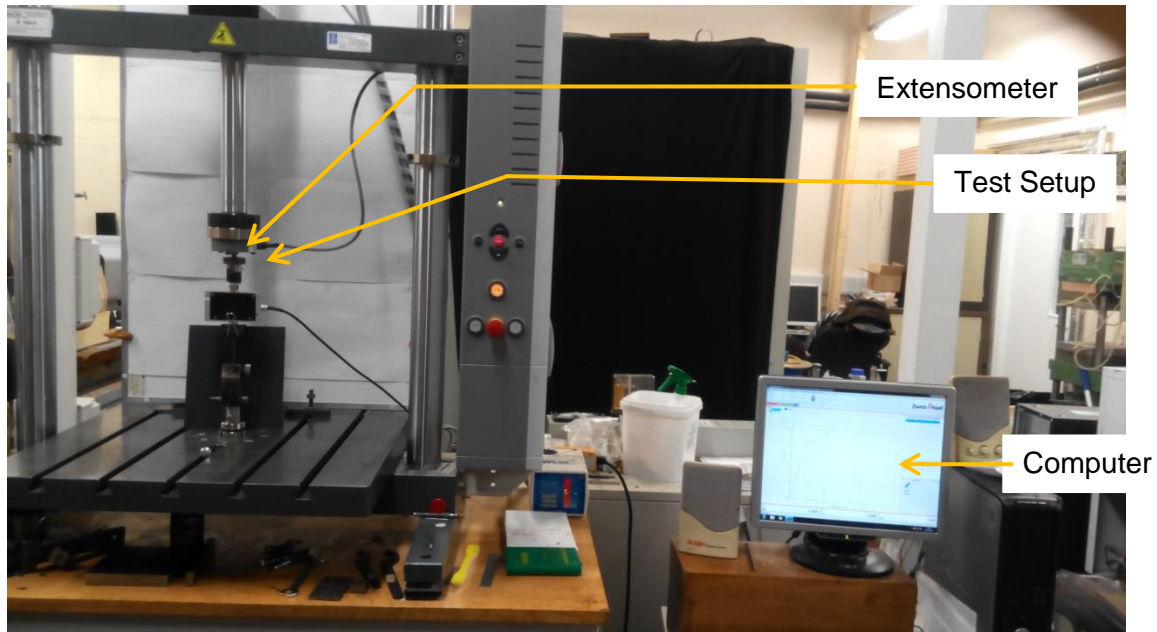


Figure 59: Test setup on the Zick/Roell Z2.0 material test machine

Cable samples were cut into three specimens of equal lengths of 130mm. In order to ensure a quality test procedure, a pre-test was done and the right operating parameters and correct support structure were set. Figure 61 below shows the test setup on the test machine. The specimens were tested one at a time. The tested specimen was clamped at the base by the holding grip and pulled upwards by the crosshead. A 500N load cell was applied to the specimen while the extensometer recorded the standard travel of the wire (elongation). The resulting instantaneous force and elongation were recorded on the desktop computer. Figure 62 shows a similar setup in the Zwick/Roell Z250 with a load cell of 2.5KN.

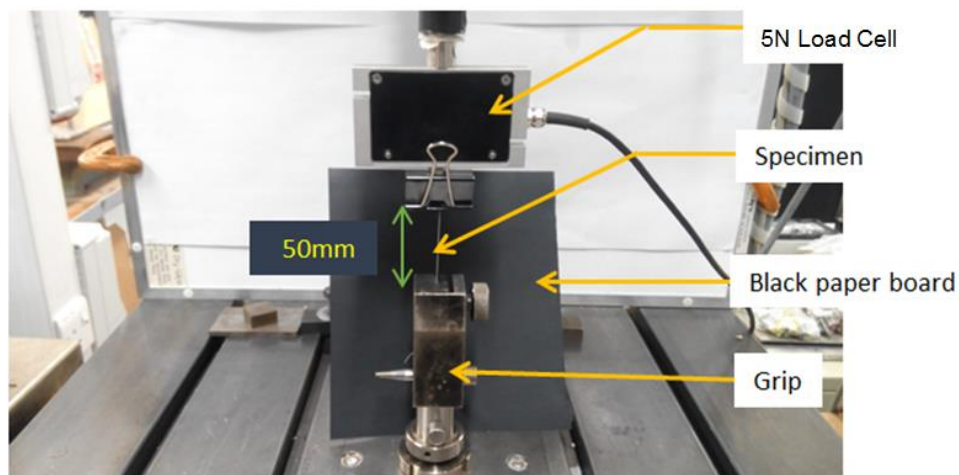


Figure 60: The maintained cable length before test process and the blackboard on the Zick/Roell Z2.0

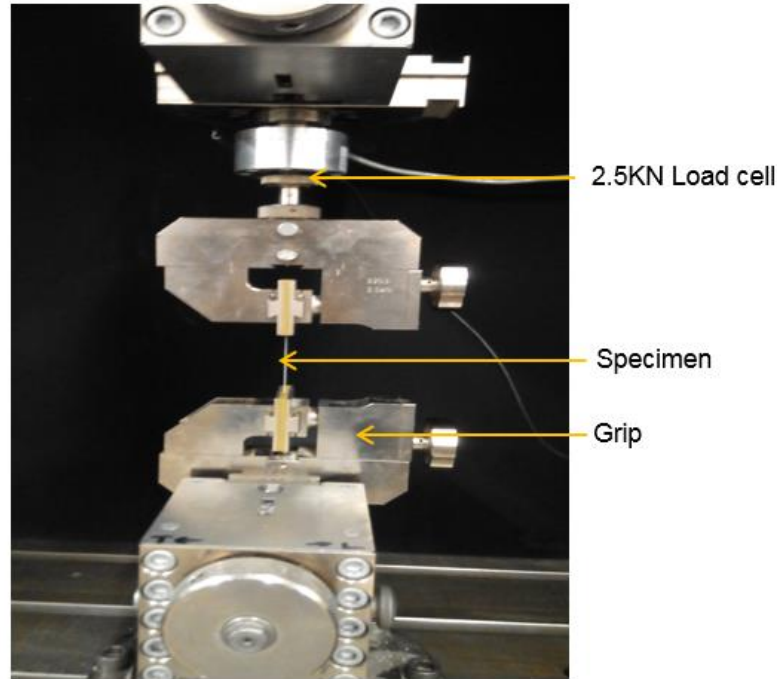


Figure 61: Test setup using the Zwick/Roell Z250 material test machine

A gage length of 50mm between the load cell and clamp support was maintained. At the end of each test, the specimens were placed on a black sheet for post-test evaluation. Each test lasted for an average of 40 minutes in order to obtain accurate results.

While the tensile stress test lasted, a graph of force (N) versus standard travel (mm) was plotted on the computer screen to determine the force in Newton (N) at which the maximum stress on each sample occurs before failure. The maximum force (F_{max}) obtained at the maximum stress, the change in length (dL) at the maximum force, the force at breakpoint (F_{Break}) of the specimen and the dL at the breakpoint was generated with the graphs.

The failure parameters used in assessing each specimen were insulation failure and breaking of the conductor. In total 3 tests were carried out for each cable sample at room temperature. To calculate the UTS of the samples, equation (4) was used with F_{max} substituted for the maximum load on the specimen, P_{max} .

Precautions

- ❖ The test machine was always reset to zero after each test by clicking on the reset tab on the application software interface.
- ❖ The clamping of the specimen was always checked before testing to avoid the graph plotting at an offset from the origin.

The test data for the graphs are given in FILE 3 in Appendix-CD.

3.8.2 Results of UTS test for micro-coaxial cable samples

Coax 1

Figure 63 below shows the graphical plot of the UTS test for coax1.

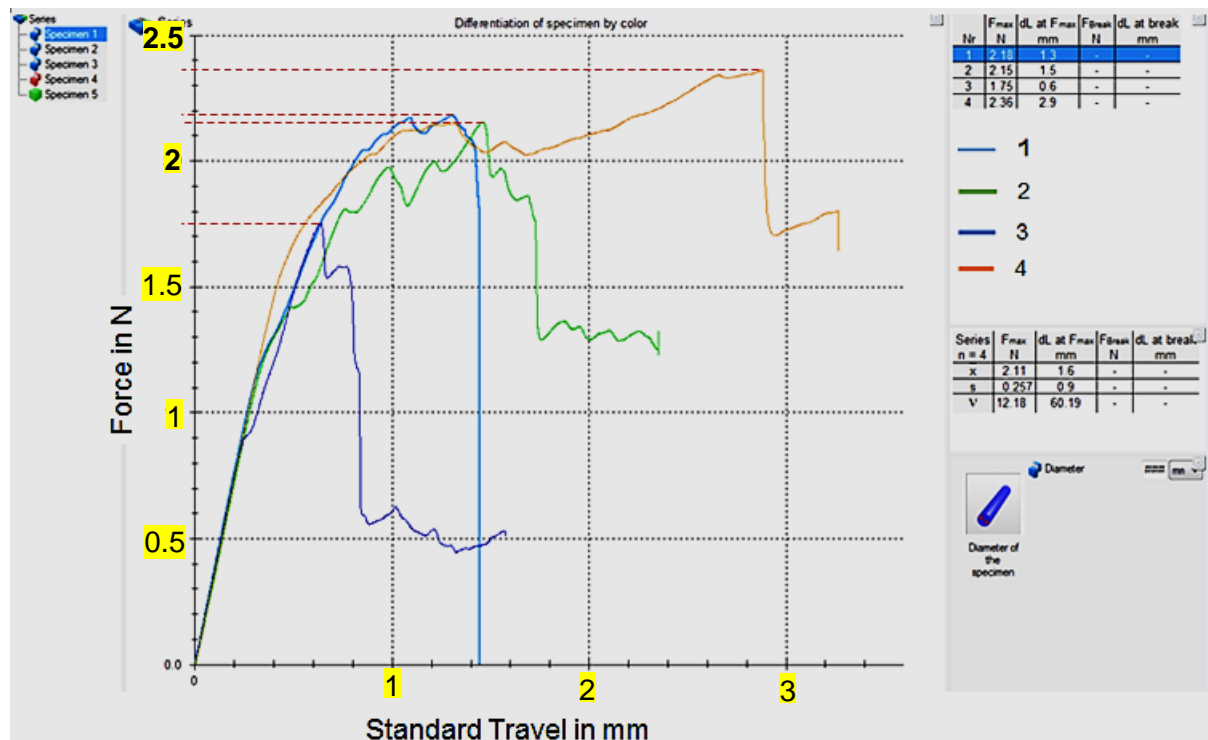


Figure 62: UTS curve for sample coax1 showing the force at maximum stress for each specimen

The values for specimen 3 were not considered as true values of the force at maximum stress because the UTS test on specimen 3 was repeated after it had pulled out of the holding grip. The fourth test was done on a new specimen obtained from Coax1. Specimen 1 failed the test after a 1.3mm change in length. Figure 64 shows the deformation of the specimens after the test. Investigations revealed breakage in the specimen.

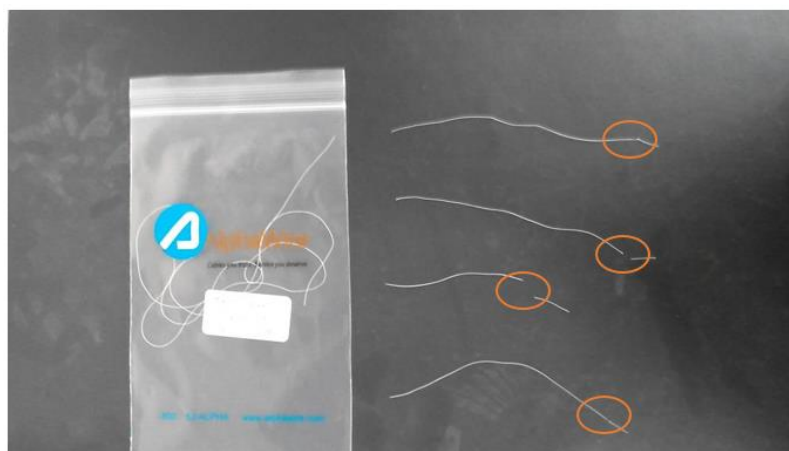


Figure 63: Deformation of coax1 specimens 1 to 4 (from the top) after the UTS test. Points of failure are spotted in the orange ovoids

The results from the graph are summarised in table 11 below. The values for specimen 3 were excluded from the “average” calculations for F_{max} , dL and UTS.

Specimen	Area (m ² x 10 ⁻⁸)	F _{max} (N)	dL at F _{max} (mm)	UTS (MPa)	F _{max} Average (N)	dL Average (mm)	UTS Average (MPa)
1	1.764	2.18	1.3	123.58	2.23	1.9	126.42
2	1.764	2.15	1.5	121.88			
3	1.764	1.75	0.6	99.21			
4	1.764	2.36	2.9	133.79			

Table 11: UTS test results for coax1 specimens

Coax2

Figure 65 below shows the graphical plot of the UTS test for coax2.

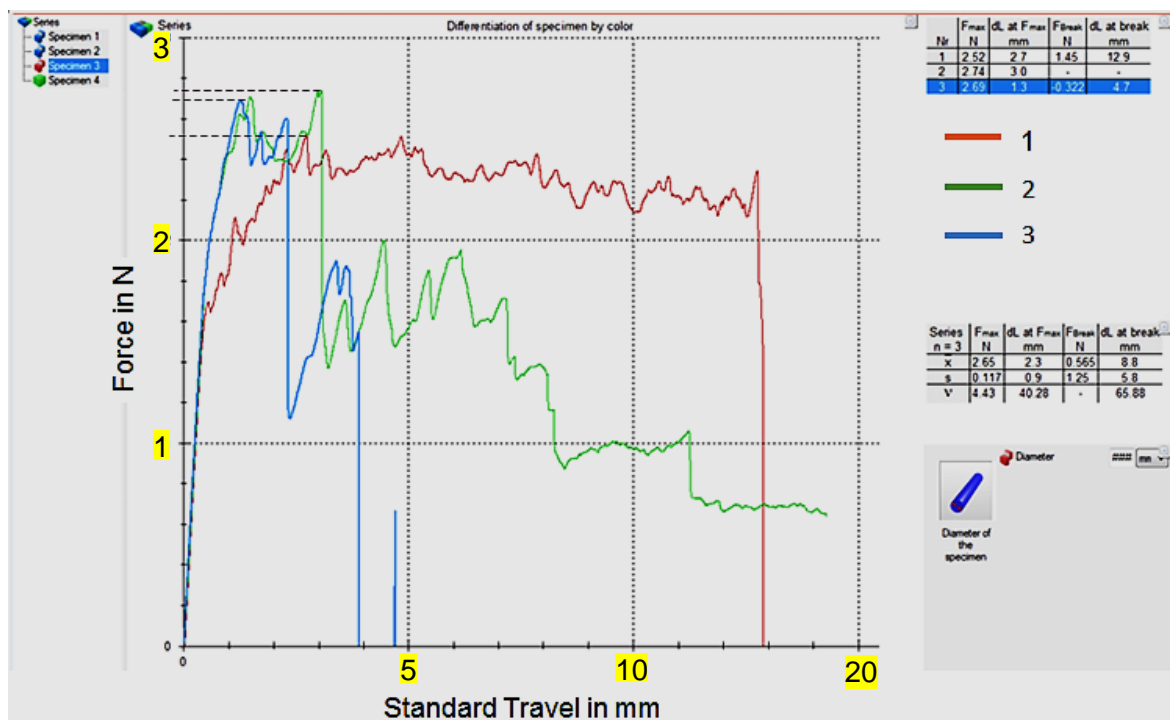


Figure 64: UTS curve for sample coax2 showing the force at maximum stress for each specimen

The highest value of F_{max} was 2.74N on specimen 2 with a dL of 3.0mm. Both specimens 1 and 3 failed the test after being stretched to 2.7mm and 1.3mm respectively. Figure 66 shows the deformation of the specimens after the test. Investigations revealed breakage and failure in insulation.

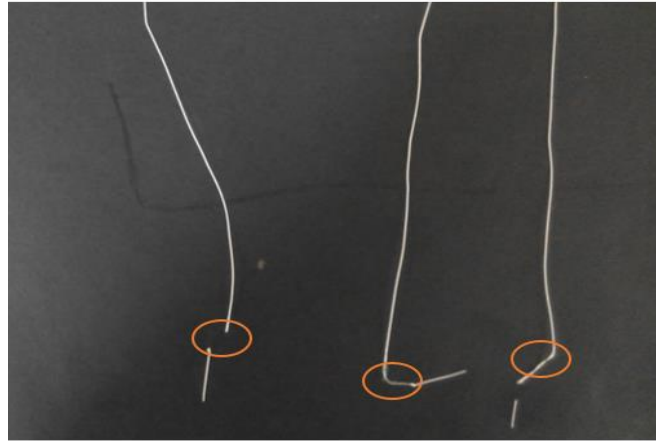


Figure 65: Deformation of coax2 specimens 1 to 3 (from the right to left) after the UTS test Points of failure are spotted in the orange ovoids.

Table 12 below gives the calculated values for the UTS.

Specimen	Area (m ² x 10 ⁻⁸)	F _{max} (N)	dL at F _{max} (mm)	UTS (MPa)	F _{max} Average (N)	dL Average (mm)	UTS Average (MPa)
1	2.343	2.52	2.7	107.55	2.65	2.3	113.10
2	2.343	2.74	3.0	116.94			
3	2.343	2.69	1.3	114.81			

Table 12: UTS test results for coax2 specimens

Coax3

Figure 67 below shows the graphical plot of the UTS for coax3.

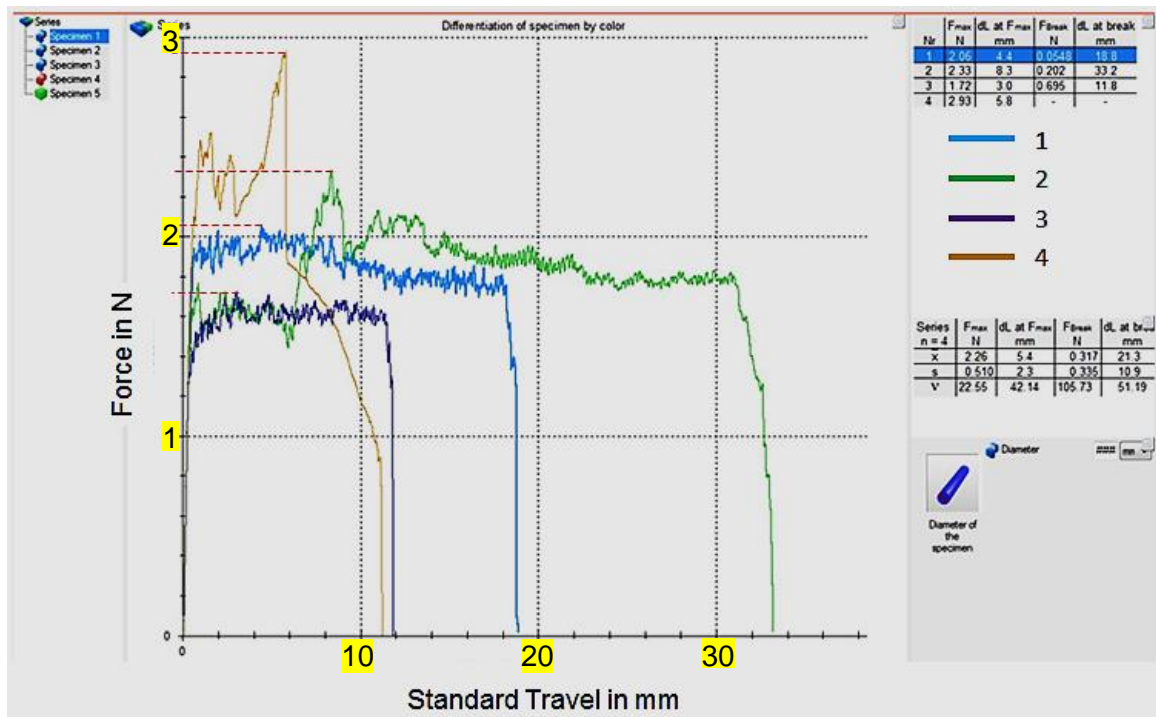


Figure 66: UTS curve for sample coax3 showing the force at maximum stress for each specimen

The highest value of F_{max} occurred at 2.93N on specimen 4 with a corresponding dL of 5.8mm which is almost two times the value of the elongation in coax2. All the specimens failed during this test at 18.8mm, 33.2mm and approximately 11.2mm for specimens 1, 2, and 4 respectively. Specimen 3 slipped out of the holding grip.

Figure 68 shows the deformation of the specimens after the test. Investigations revealed breaking of the specimen.



Figure 67: Deformation of coax3 specimens after the UTS test, 1 to 3 (from right to left) above and 4 below the other. Points of failure are spotted in the orange ovoids three.

Table 13 below gives the UTS values for coax3 specimens. The values for specimen 3 were excluded from the “average” calculations for F_{max} , dL and UTS.

Specimen	Area ($m^2 \times 10^{-8}$)	F_{max} (N)	dL at F_{max} (mm)	UTS (MPa)	F_{max} Average (N)	dL Average (mm)	UTS Average (MPa)
1	3.083	2.06	4.4	66.82	2.44	6.17	79.15
2	3.083	2.33	8.3	75.58			
3	3.083	1.72	3.0	55.79			
4	3.083	2.93	5.8	95.04			

Table 13: UTS test results for coax3 specimens

Coax4

Figure 69 below shows the graphical plot of the UTS for coax4. From the graph, the highest value of F_{max} recorded was 3.43N on specimen 3 with a corresponding dL of 28.44mm. This is untrue there was a jerk of the holding grip due to the sudden failure and pulling out of the specimen’s insulation. The jerking of the holding grip at insulation failure produced a vertical straight line result on the graph spotted in a red broken circle but the true value of the maximum force produced (as seen in figure 69) was approximately 3.16N.

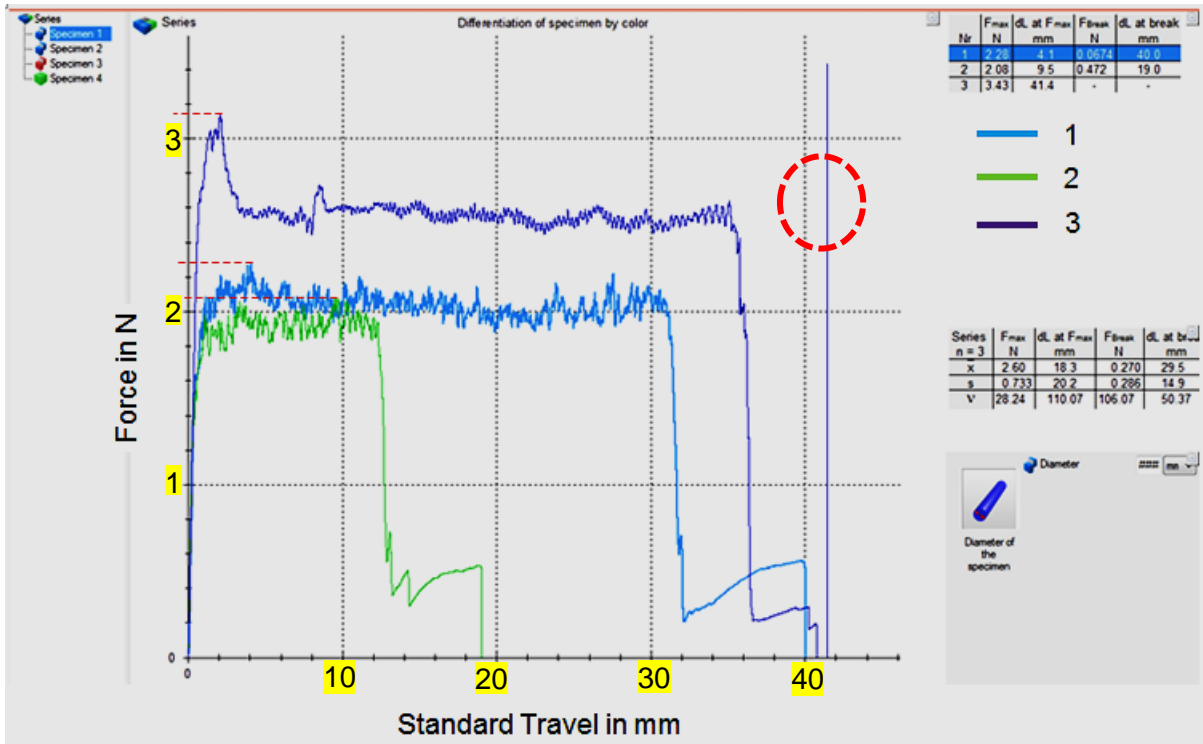


Figure 68: UTS curve for sample coax4 showing the force at maximum stress for each specimen

Figure 70 below shows the deformation of the coax4 specimens after the test. Investigations revealed an insulation failure.

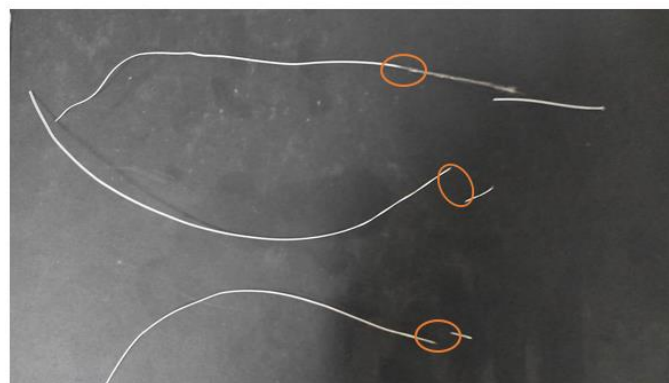


Figure 69: Deformation of coax4 specimens after the UTS test. Points of failure are spotted in the orange ovoids

Table 14 gives a summary of the test results.

Specimen	Area (m ² x 10 ⁻⁹)	F _{max} (N)	dL at F _{max} (mm)	UTS (MPa)	F _{max} Average (N)	dL Average (mm)	UTS Average (MPa)
1	5.587	2.28	4.1	40.81	2.60	18.3	44.87
2	5.587	2.08	9.5	37.23			
3	5.587	3.16	41.4	56.56			

Table 14: UTS test results for coax4 specimens

Coax5

A 2.5KN was used which ensured a better control and firmer gripping of the specimens as shown in figure 71. The 50mm gage length used in the previous tests was maintained as well as room temperature condition.

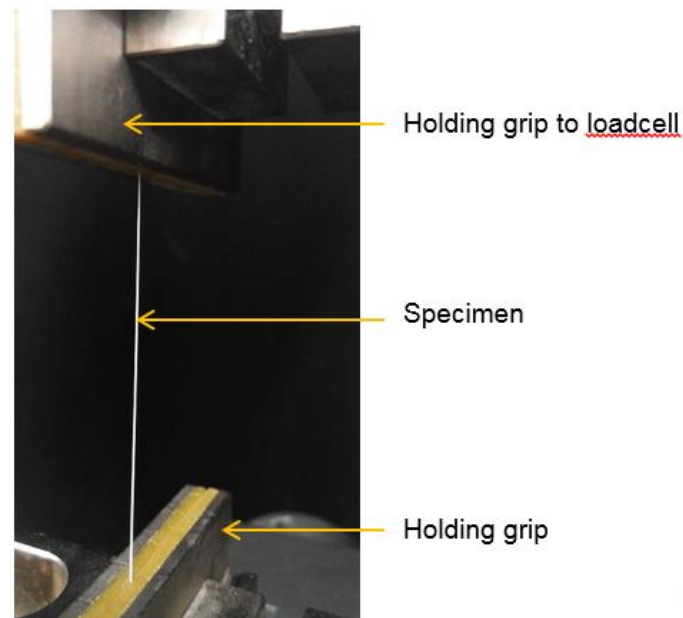


Figure 70: The test setup on the Zick/Roell Z250 showing a firm gripping of the coax5 specimen

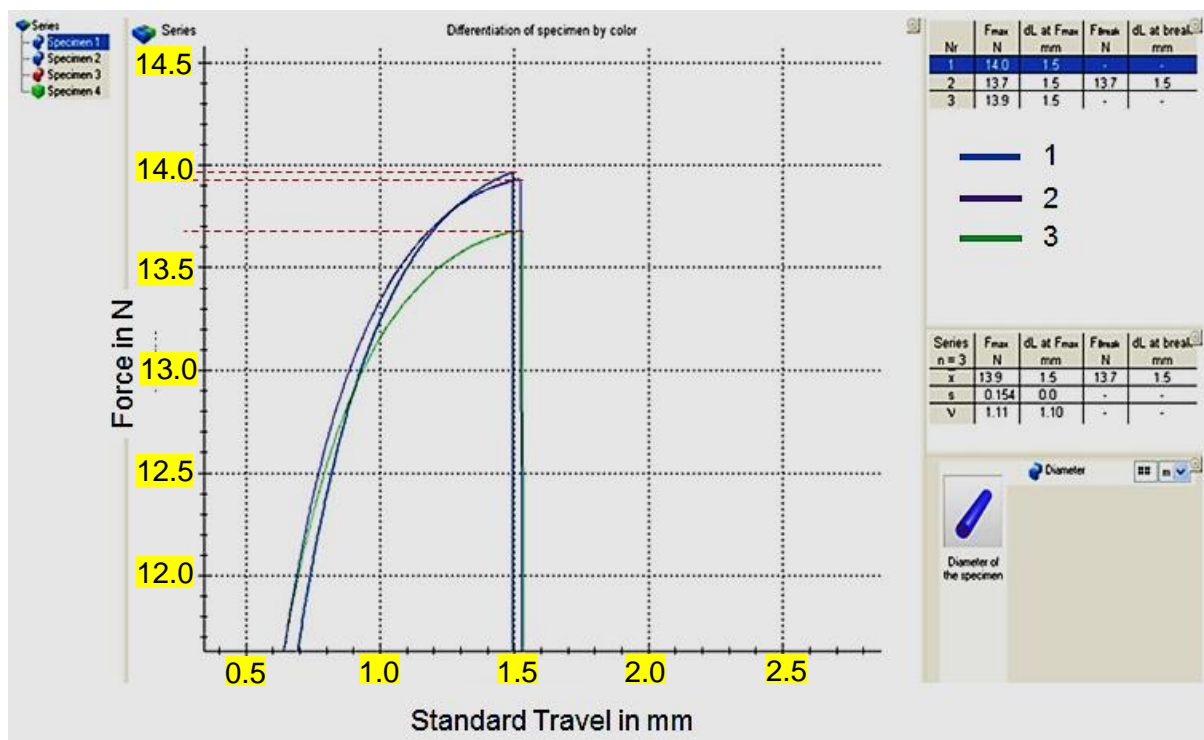


Figure 71: UTS curve for sample coax5 showing the force at maximum stress for each specimen

Figure 72 shows the graphical plot of the UTS curve for coax5 while figure 73 shows the deformation of the coax5 specimens after test examination revealed the insulation failures. The maximum force obtained is 14N and the results of the specimens were very close as can be seen in table 15.

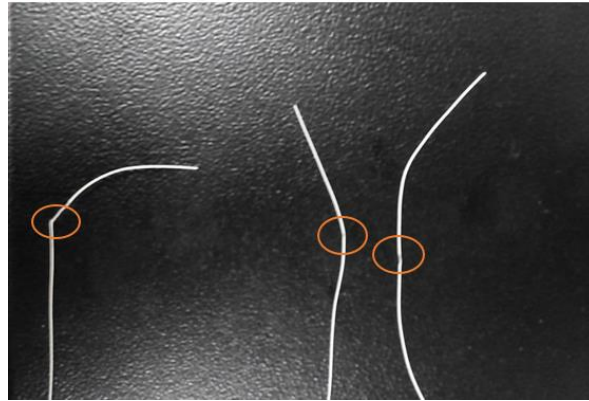


Figure 72: Deformation of coax5 specimens after the UTS test. Points of failure are spotted in the orange ovoids

Table 15 below gives the UTS values for coax5 specimens.

Specimen	Area ($m^2 \times 10^{-8}$)	F_{max} (N)	dL at F_{max} (mm)	UTS (MPa)	F_{max} Average (N)	dL Average (mm)	UTS Average (MPa)
1	7.297	14.0	1.5	191.86	13.9	1.5	190.03
2	7.297	13.7	1.5	187.75			
3	7.297	13.9	1.5	190.49			

Table 15: UTS test results for coax5 specimens

PW1

The UTS curve for PW1 can be seen in figure 74 below. The curve for PW1 is consistent with the smoothness of the coax5 micro-coaxial cable sample graph result. The maximum force obtained from the graph is 10.9N.

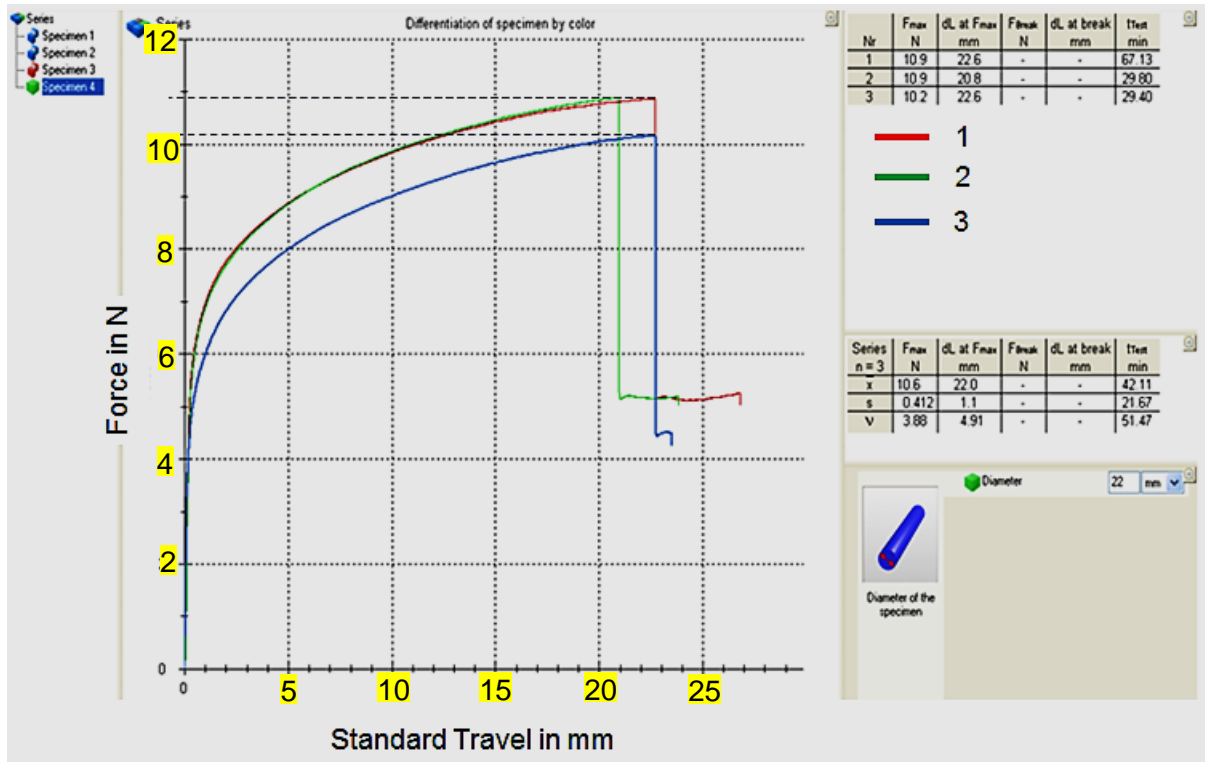


Figure 73: UTS curve for sample PW1 showing the force at maximum stress for each specimen

Figure 75 below shows the deformation of the specimens.

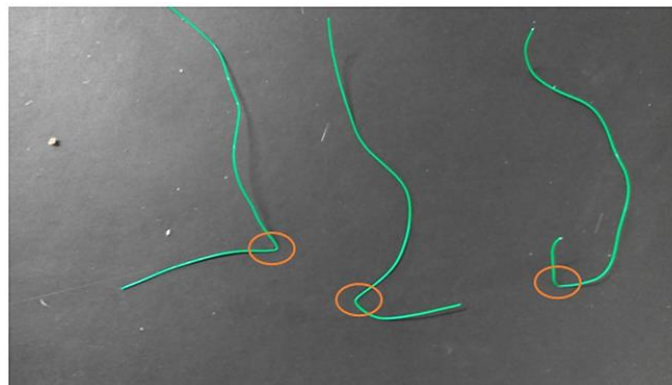


Figure 74: Deformation of PW1 specimens after the UTS test. Points of failure are spotted in the orange ovoids

Table 16 below gives the UTS values for PW1 specimens.

Specimen	Area (m ² x 10 ⁻⁸)	F _{max} (N)	dL at F _{max} (mm)	UTS (MPa)	F _{max} Average (N)	dL Average (mm)	UTS Average (MPa)
1	24.528	10.9	22.6	44.44	10.6	22.0	43.49
2	24.528	10.9	20.8	44.44			
3	24.528	10.2	22.6	41.59			

Table 16: UTS test results for PW1 specimens

PW2

The graph illustrated in figure 76 below is the UTS curve for PW2.

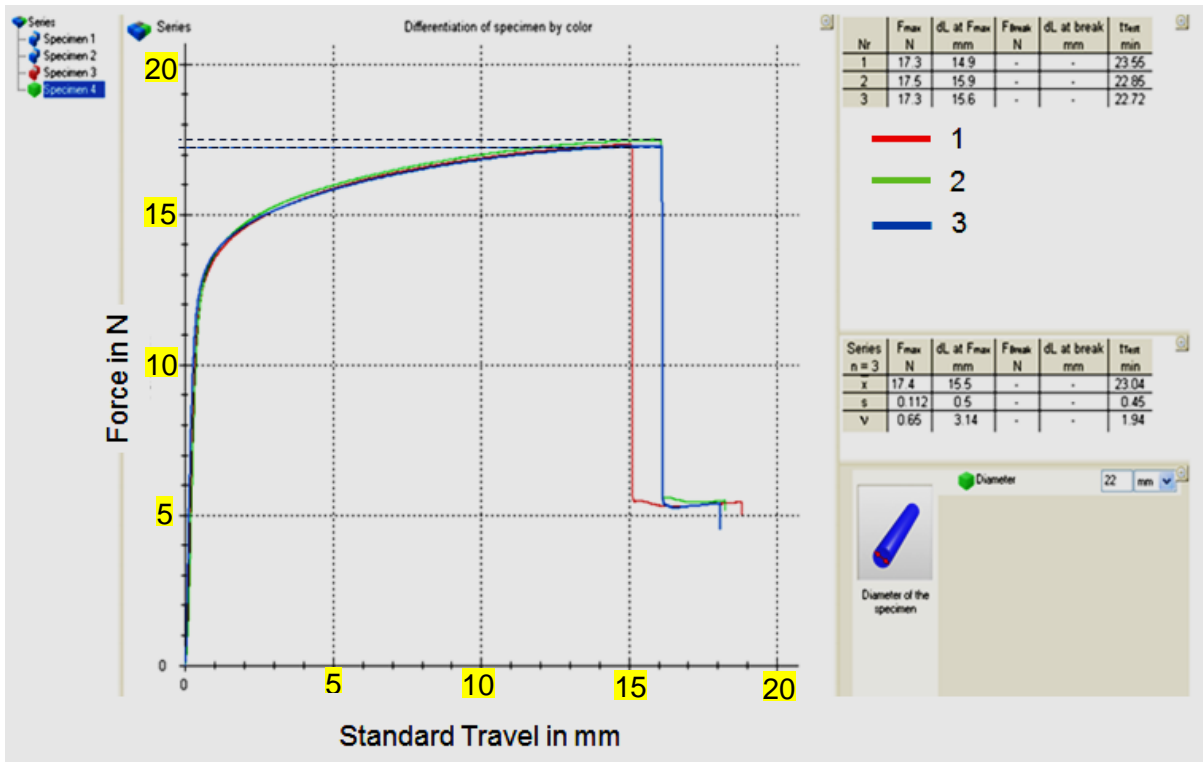


Figure 75: UTS curve for sample PW2 showing the force at maximum stress for each specimen

From the graph above, the maximum force obtained is 17.5N. The load-elongation curve is also smooth-patterned.

The points of failure on the PW2 specimens are shown in figure 77 below.

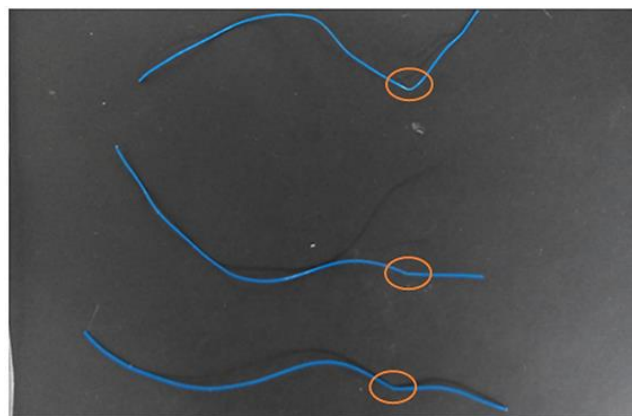


Figure 76: Deformation of PW2 specimens after the UTS test. Points of failure are spotted in the orange ovoids

Table 17 below gives the UTS values for PW2 specimens.

Specimen	Area (m ² x 10 ⁻⁸)	F _{max} (N)	dL at F _{max} (mm)	UTS (MPa)	F _{max} Average (N)	dL Average (mm)	UTS Average (MPa)
1	29.186	17.3	14.9	59.28	17.4	15.5	59.51
2	29.186	17.5	15.9	59.96			
3	29.186	17.3	15.6	59.28			

Table 17: UTS test results for PW2 specimens

3.8.3 Tether tests

Selection of micro-coaxial and power cables

Based on the previous UTS test results for the cables, coax5 and PW1 were selected for the tether design.

Selection of Teflon Tube

PFA Teflon tube was selected for the design. In order to determine the Teflon tube size for the tether the selected cables; coax5 and PW1 were simulated in a cable core design. The core arrangement designs for a 10-gauge wire are shown in figure 78 below.

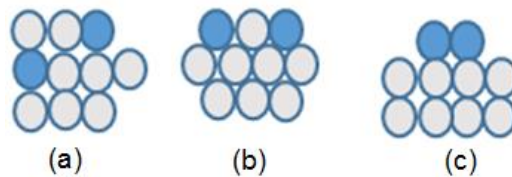


Figure 77: Cable arrangement pattern for the tether. The blue colour depicts the power cable and the white colour is the micro-coaxial cable

From the cable arrangement designs shown above, design (b) was preferred because it has balance and a uniform pattern for flexibility and its structure simplified the calculation for the inner diameter of the Teflon tube that was needed for the tether. The diameters for coax1 and PW1 were denoted by a , and b respectively. Using the values of the diameters from tables 9 and 10 the Teflon diameter d required for the tether was calculated as

$$d = 2(a + b)$$

This generated a result of $d \cong 1.73\text{mm}$. The assumptions made was that the minimum number of power cables (2) will be in a combination of a maximum of 2 micro-coaxial cables along the longest row in the cable arrangement as shown in figure 78(b). Therefore, a Teflon size of with

an inner diameter (ID) of 2mm and an outer diameter (OD) of 3mm was selected. This size was selected to allow for easy passing of the cables through the ID of the Teflon tube.

Materials

The tether consists of ten cables; four pairs of micro-coaxial cables where each pair represents a connection to each of the four UT transducers and two power cables for powering either the used thermocap or sonocap PCBs. The cables were fixed in a biocompatible Teflon tube made from PFA fluoroplastic. A more detailed specification of the Teflon material and other products are given in the datasheet in FILE 5 in Appendix-CD.

Table 18 below gives the composition of the tether.

Specimen	Length (mm)	Number of power cables	Number of micro-coaxial cables
T1	75mm	2	8
T2	75mm	2	8

Table 18: Components of the tether samples

Test Machine

The Zick/Roell Z2.0 was utilised for the tether tests.

Digital Multimeter

The continuity test range of a digital multimeter was utilised in the test.

3.8.5 Test 1: Three-point Bend Test

A three-point bend test was conducted to evaluate the flexibility and bending radius of the tether at room temperature.

Measurement Principle

The test specimens were exposed to a three-point bending test at a constant load of 2KN to create a bending stress. This test was repeated once due to the exhaustion of the cables.

Method

Continuity tests for cables

The micro-coaxial and power cables were tested for continuity using a multimeter before and after the bending test in order to assess any conductor failures in the tether. The power cables were stripped at the edges to expose the conductor to a continuity test. However, the micro-coaxial cables were not stripped because this only shortened their length.

Test Setup

The test setup for the three-point bend test on the Zwick/Roell Z2.0 is shown in figure 79 below.

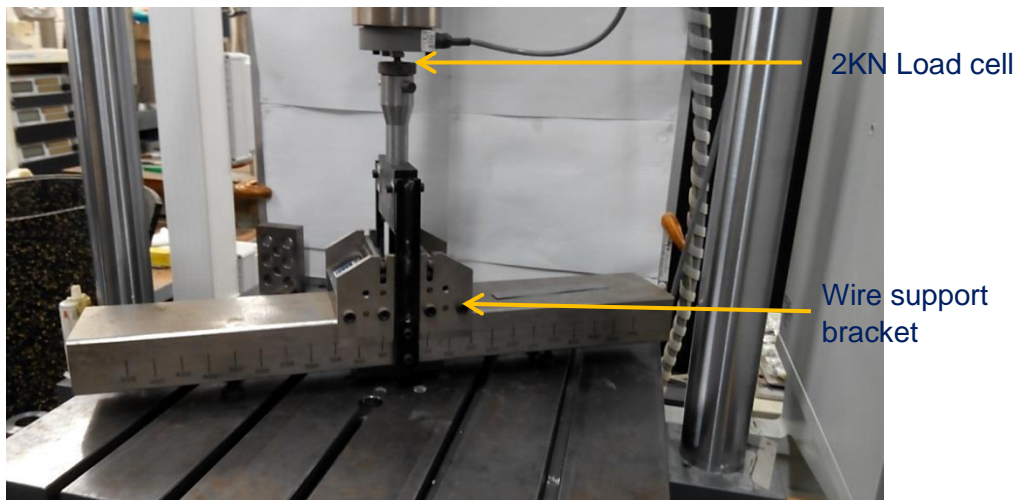


Figure 78: The bending press showing the wire support bracket used for the three-point bend test and load cell

The test setup consists of a wire support bracket with two support cylinders of 10mm diameter which were set to a separation distance of 50mm as seen in figure 80 below. Above the wire support bracket is a 2KN load cell used to exert the bending force in the test. The load cell has an actuator pin of 10mm.

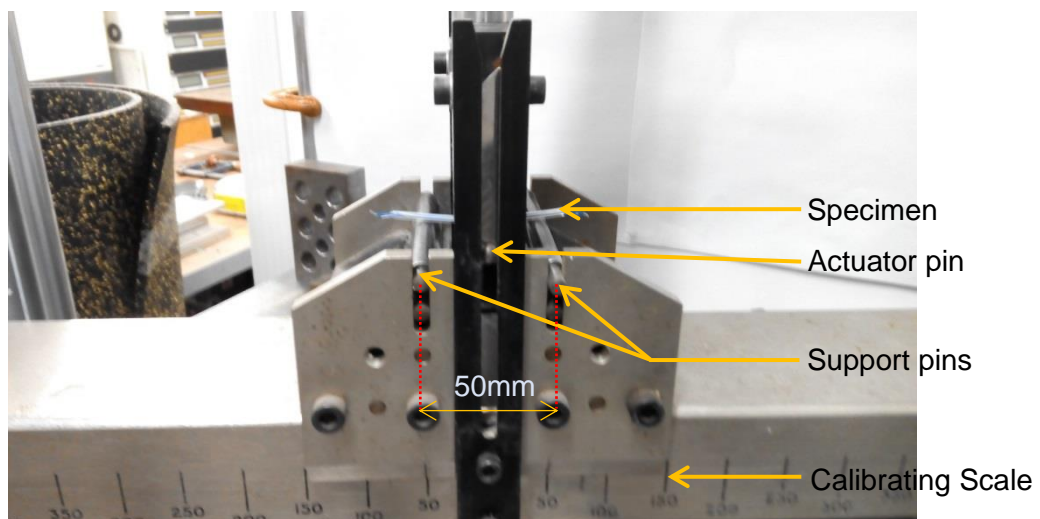


Figure 79: The specimen placed across the wall support bracket and the settings used

The tether specimens were placed across the two cylindrical support pins with a separation distance of 50mm between the centres of the pins as shown in figure 80 above. The test machine was set to a speed of 0.5mm/min and activated. The actuator pin pressed against the tether specimen pushing it downwards through the centre. The descent of the actuator pin on the specimen created a bending radius which continued to increase as the force on the

specimen increased. At the end of the test the specimen was inspected for any failures and the results were recorded. The bending test results were recorded on a computer which also displayed a bending force-versus-radius curve; a graph of the bending force (N) required bending the tether against the standard travel (mm) which is the bending radius. Figure 81 below shows the bent cable during the bending test.

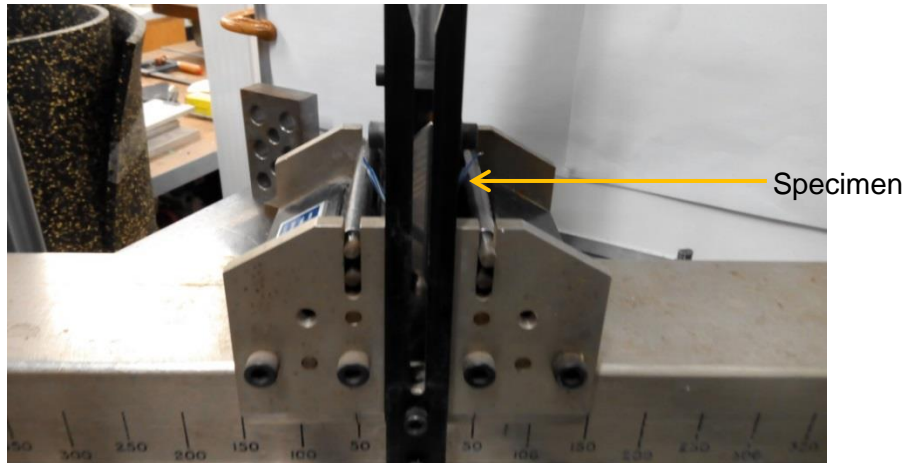


Figure 80: The pushed down specimen during the bending test

3.8.6 Results for 3-point Bend Test

The bending force-versus-radius curves for the tensile strength test is given in figure 82 and an image of the specimens after the 3-point bend test is shown below.

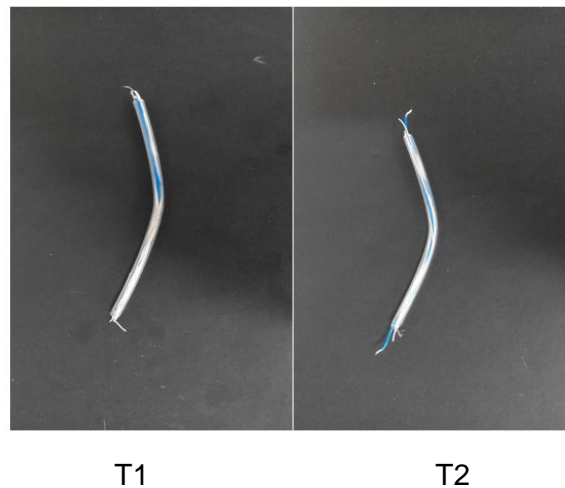


Figure 81: Specimens T1 and T2 viewed immediately after the bending test

The bending force-versus-radius curves for T1 and T2 have a similar pattern. The bending force increased rapidly at the beginning of the test to a maximum value before falling as the bending radius increased. From the graph, it can be seen that T1 had a higher value of maximum bending force of 3.12N at a corresponding bending radius of 9.3mm while T2 had

a lower value of the maximum bending force of 2.74N at a higher bending radius value of 10.7mm.

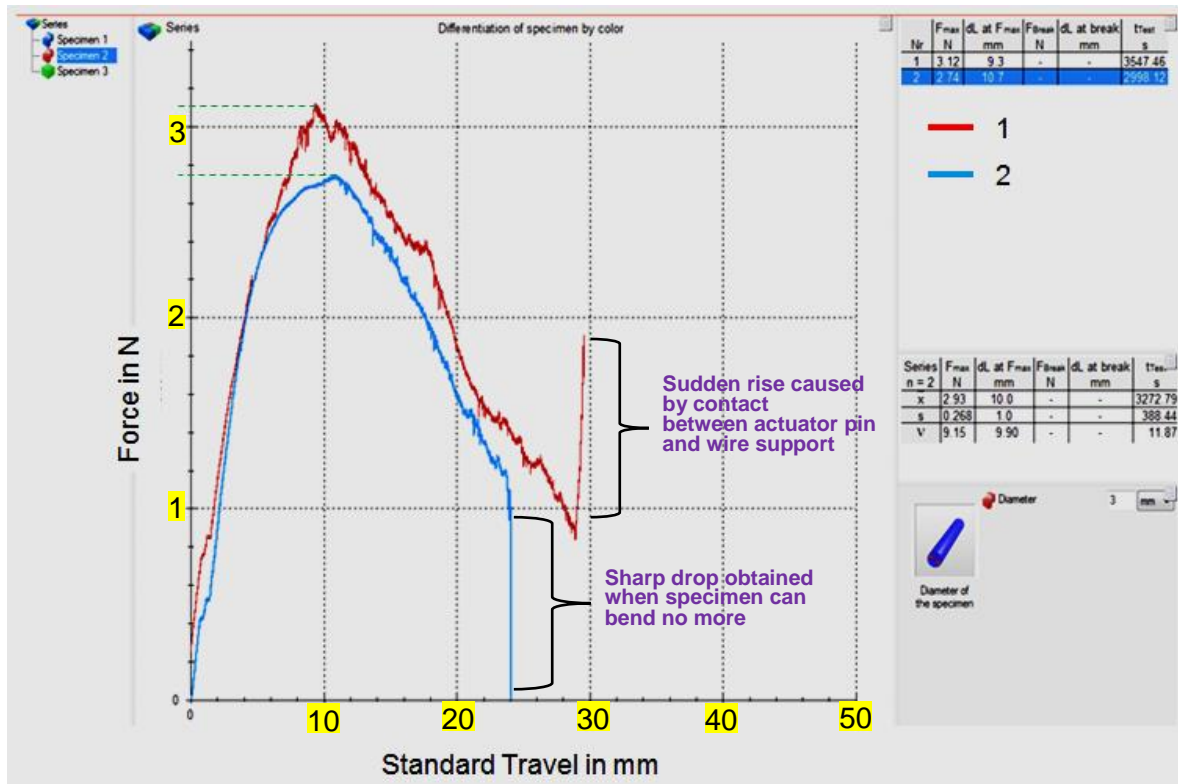


Figure 82: Bending force-versus-radius curves for specimens T1 and T2 after the bending test

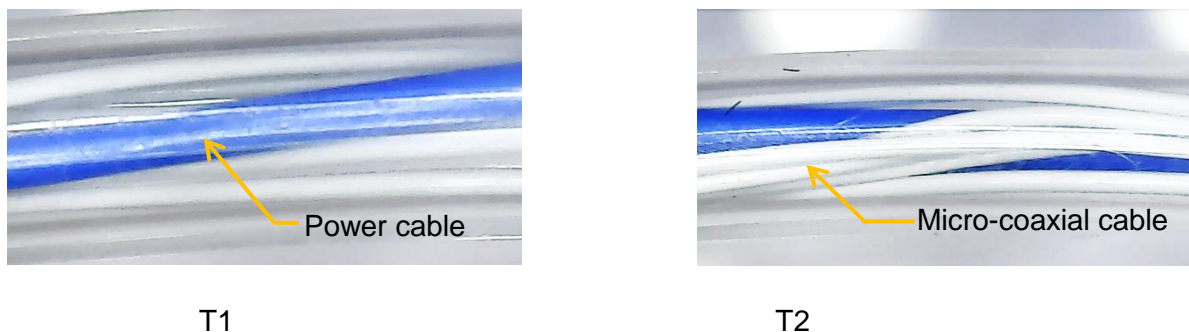


Figure 83: Cables in specimens T1 and T2 showing no signs of failure when viewed with a USB microscope after the three-point bending test

The result of the 3-point bend test is summarised in table 19 below.

Specimen	Radius (mm)	F_{max} (N)	Bending Radius (mm)	F_{max} Average (N)	Bending radius Average (mm)
T1	1.5mm	3.12	9.30	2.93	10.0
T2	1.5mm	2.74	10.70		

Table 19: Three-point bend test results for specimens T1 and T2

Continuity test of cables

The power cables and some selected micro-coaxial cables all passed the continuity test.

3.8.7 Test 2: Ultimate tensile strength test

An ultimate tensile strength (UTS) test was conducted to find the maximum stress the tether can withstand before it deforms.

Materials

The same length and composition of the tether used in the three-point bending test were utilised in the UTS test.

Method

The UTS test was repeated once and carried out at room temperature with the following procedures. Two tests were performed; one UTS test on specimens T1 and T2. The test setup is shown in figure 85 below.

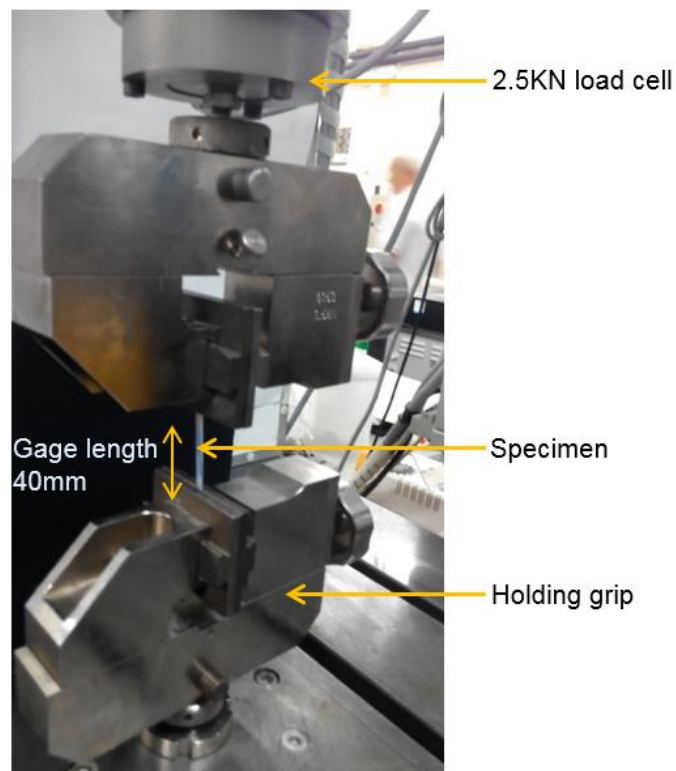
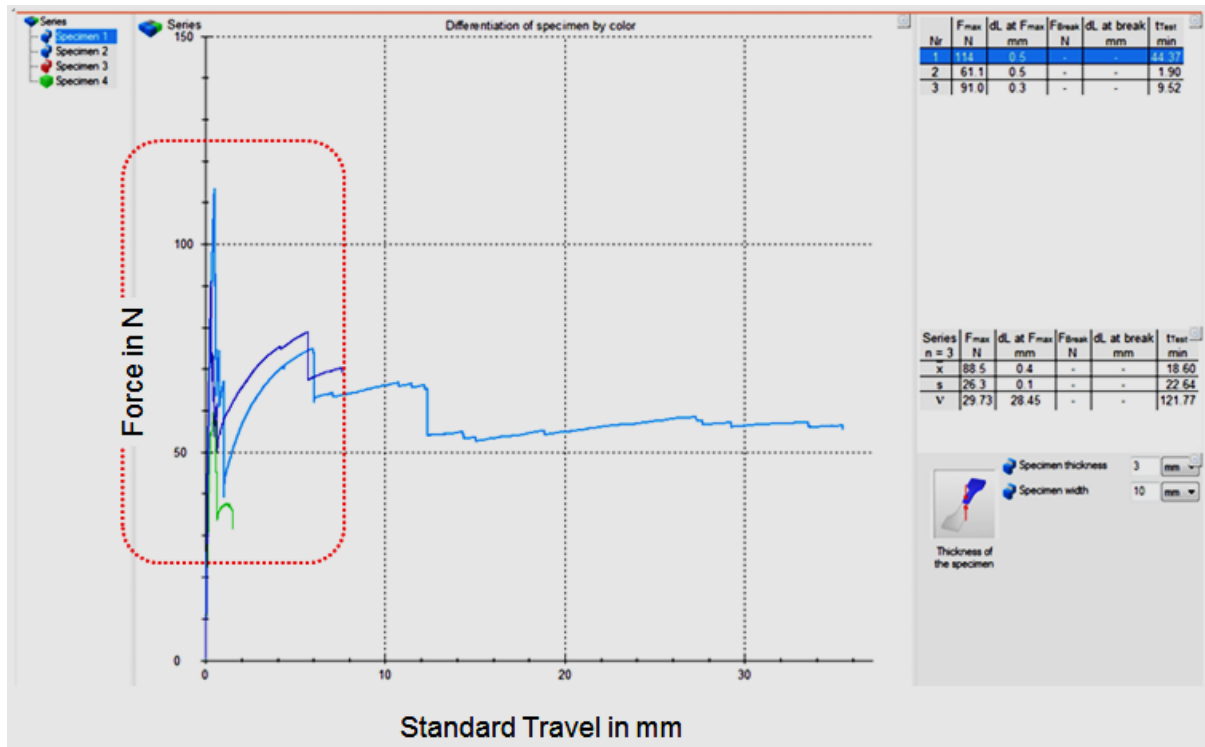


Figure 84: Test setup on the Zwick/Roell Z2.0 for UTS tests on specimen T1

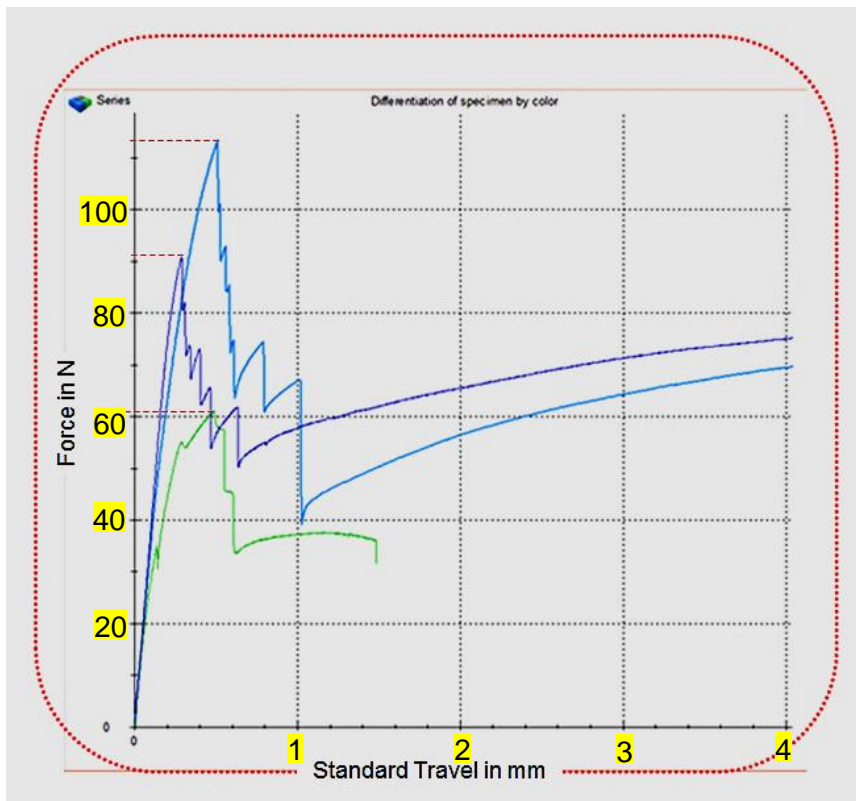
A gage length of 40mm was used between the holding grips on the specimen. A high load cell (2.5KN) was used due to the high tensile strength of the Teflon material and the anticipated high resistance of the tether to the pulling force. The test speed was set at 0.8mm/min.

3.8.5 Results

The UTS curve for the two specimens is given in figure 86 (“a” and “b”) below.



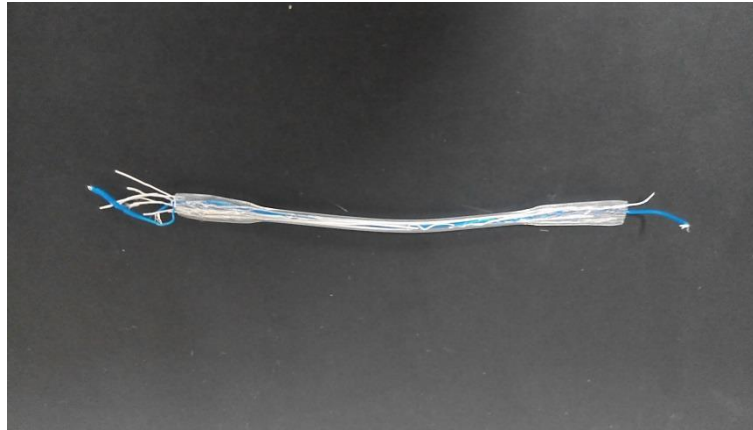
(a)



(b)

Figure 85: (a) UTS curves for T1 and T2 (T2A and T2B) (b) The enlarged portion of the graph showing the distinct positions of the maximum force attained by each specimen.

From the graph, it can be seen that there is a general sharp increase in the tension force at the beginning of the pulling to a maximum value which is then followed by an approximately equal rate of declining tension force. The deformed tether specimens after the UTS test are shown in figures 87, 88 and 89.



(a)



(b)

Figure 86: Deformation of specimens: (a) T1 and (b) T2 after the UTS test.

Table 20 below gives the results of the UTS test. The values for T2A were excluded in the “average” calculations for F_{max} , dL and UTS.

Specimen	Area ($m^2 \times 10^{-8}$)	F_{max} (N)	dL at F_{max} (mm)	UTS (MPa)	F_{max} Average (N)	dL Average (mm)	UTS Average (MPa)
T1	706.86	114.0	0.5	16.13	102.5	0.4	14.5
T2A	706.86	61.1	0.5	8.64			
T2B	706.86	91.0	0.3	12.87			

Table 20: UTS test results for T1, T2A and T2B

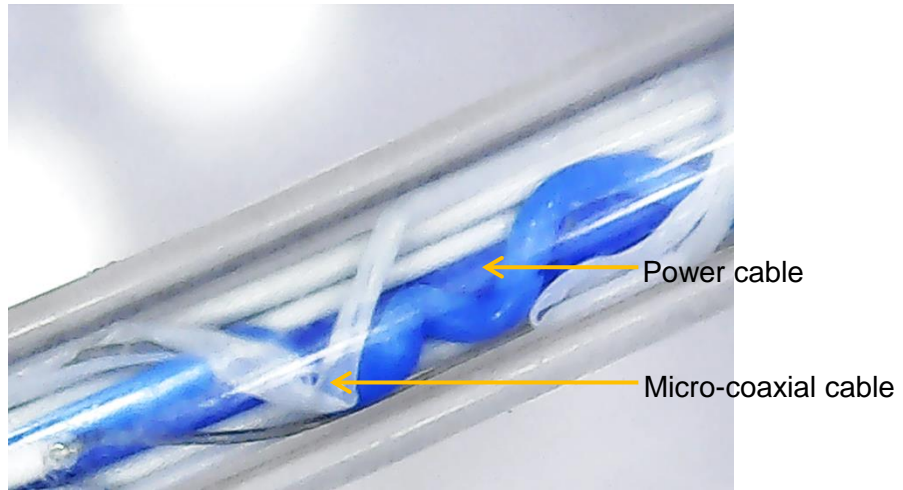


Figure 87: Deformation of micro-coaxial and power cables inside the Teflon tube

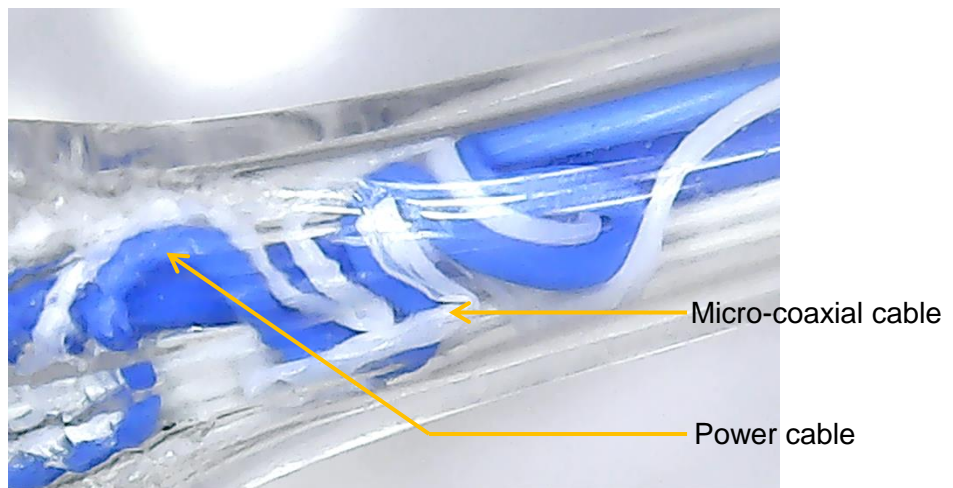


Figure 88: Deformation of specimens at the gripped area after the UTS test.

3.9 Adhesive Bonding and Bond Strength Test

An adhesive was used to bond the tether and the pills thereby giving mechanical strength to the tether-to-pill integration.

3.9.1 Materials

A silicone adhesive was selected for the bonding and the test procedure is shown pictorially in the method section.

3.9.2 Method

The pills were cleaned and placed neatly on a white sheet to ensure that they are not in contact with dirt as shown in figure 90 below. Dirt impurities such as grease stain have been known to cause poor bonding with adhesives [123]. A transparent plastic sheet was used as the glueing ground and placed on a wider black rubber sheet to give a colour contrast to the pills.

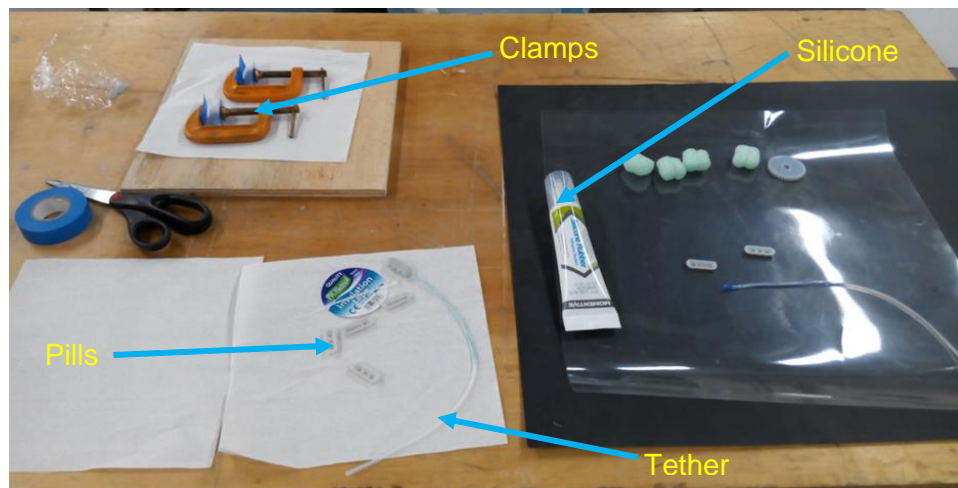


Figure 89: The setup for the adhesive bonding

The tether cables were protected in a plastic tape to avoid contact with the reinforcement pins on the pill. The end of the tether that was bound to the pill was bored to provide attachment for the reinforcement pins. The silicone adhesive was first applied around the pins of the cover cap to avoid it spilling into the tether and then around the thickness. The tether was pinned to the cover cap and covered with the base cap and the assembly was finally supported by a clamp fixed to the bond end of the pill. The bond was kept to cure for 72 hours. The bonding procedure is illustrated in figure 91.

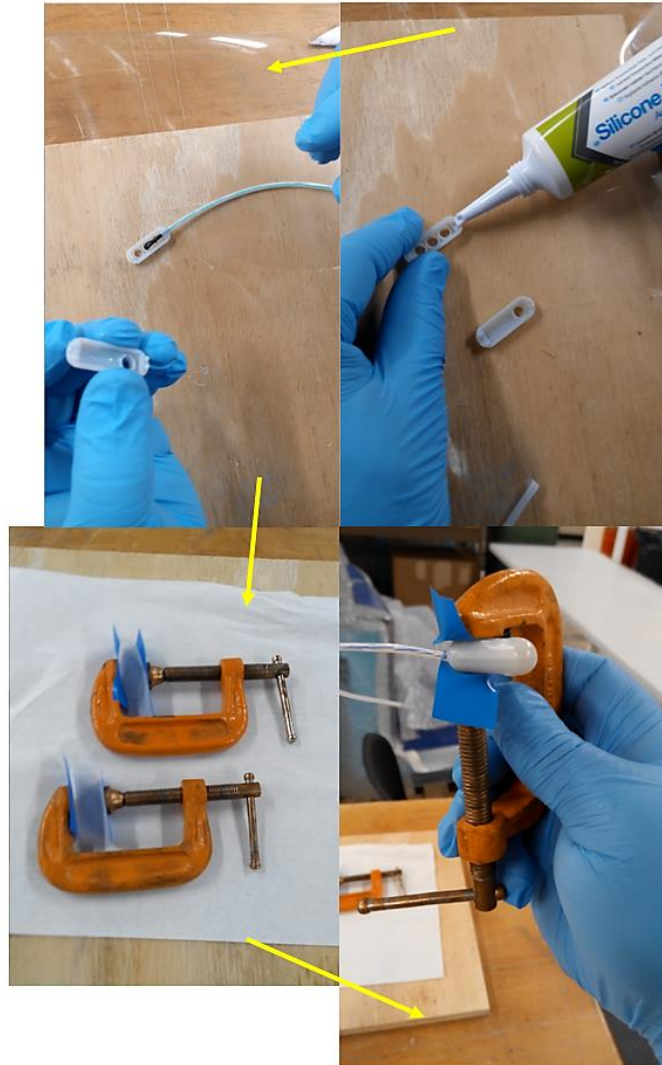


Figure 90: The adhesive bonding process

3.9.3 Adhesive Bonding Strength Test

A bond strength test was carried out to measure the maximum force that would cause a break in the tether-to-pill integration. The V 3-1 TUSCE design was used for this test.

Material test Machine

The Zwick/Roell Z2.0 was used for the bond strength test and the test setup is shown in figure 92. A load cell of 2.5KN was used in order to have a smooth graph plot and ensure that the holding grips provide firms support for the tether. The holding grip of the pill at the base has a clean and smooth surface. The gripping of the pill was made less tight to avoid damage to the pill and also mimic the slow movement of the pill during an endoscopy.

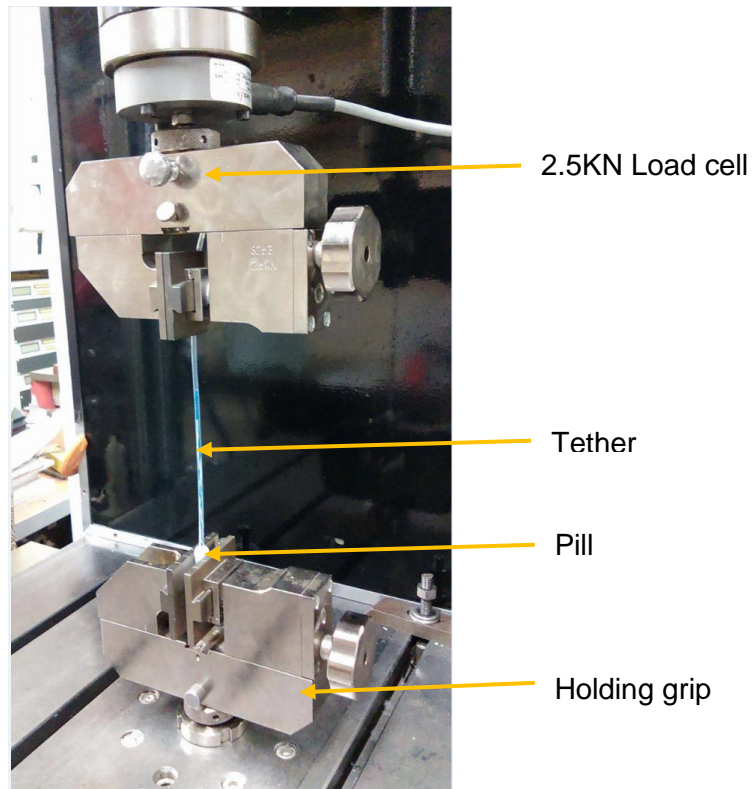


Figure 91: Setup for the bond strength test. The force of gripping the pill was made low to simulate the motion of the pill in the GI tract.

A gage length of 150mm was used between the holding grips and an elongation rate of 0.4mm/min was configured for the test. The result of the pulling force was plotted against the standard travel (elongation) of the tether as the crosshead moved up the test machine.

3.9.4 Result

The tether-to-pill bonding took approximately

The graph of the force of pulling against standard travel (elongation) along the tether is shown in figure 148 below.

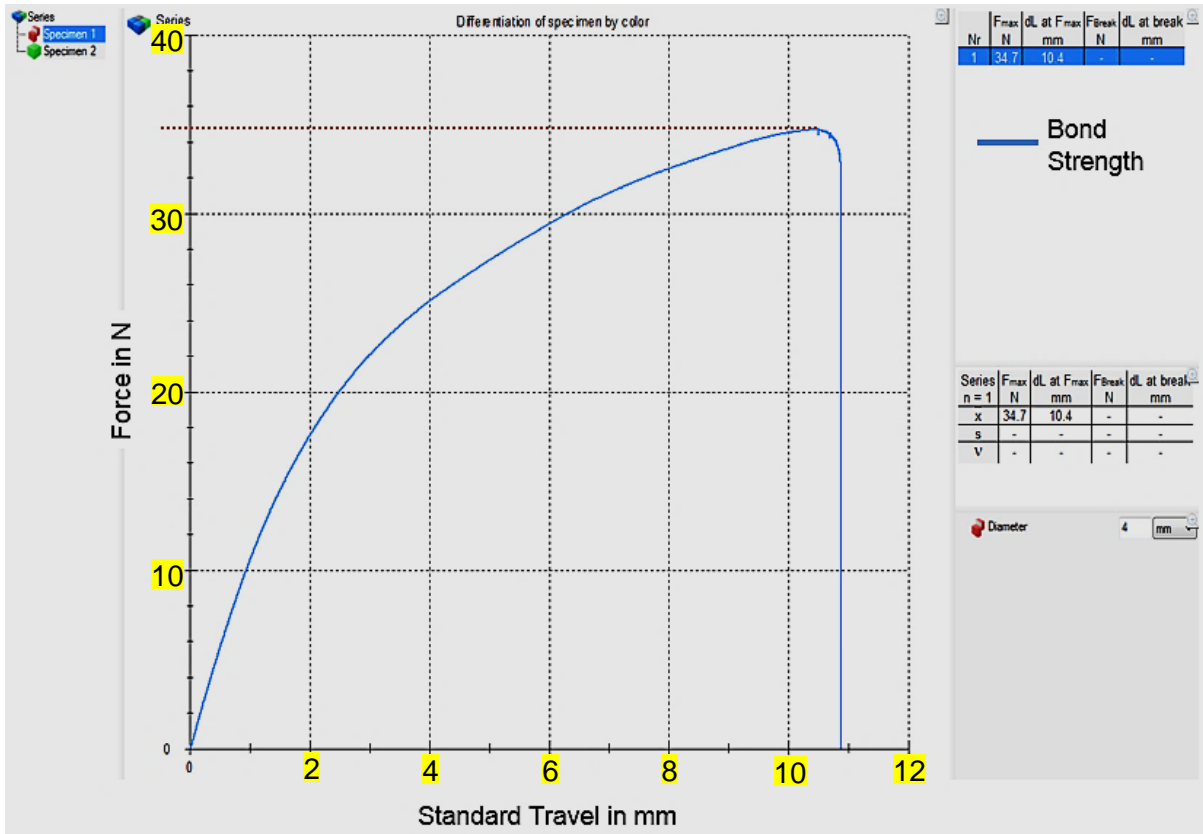


Figure 92: Bond strength curve for the tethered ultrasound capsule endoscope (TUSCE) using a silicone adhesive

From the plotted graph in figure 93 it can be observed that the maximum force needed to break the bond of the tether to the pill is 34.7N which occurred after the tether was stretched to 10.4mm of its original length (gage length). Using equation (4) the tensile strength of the bond is calculated as 4.91MPa. Table 21 below gives a summary of the test result.

Specimen	Outer Diameter	Area (m ² × 10 ⁻⁶)	F _{max} (N)	UTS (MPa)
V 3-1	3mm	7.069	34.7	4.91

Table 21: Tensile strength value for v 3-1

4.1 Biocompatibility

The biocompatibility test involved the assessment of the Teflon tubes and adhesives for medical standards according to ISO 10993-1:2009 and ISO 13485 and the biodegradability of the pill.

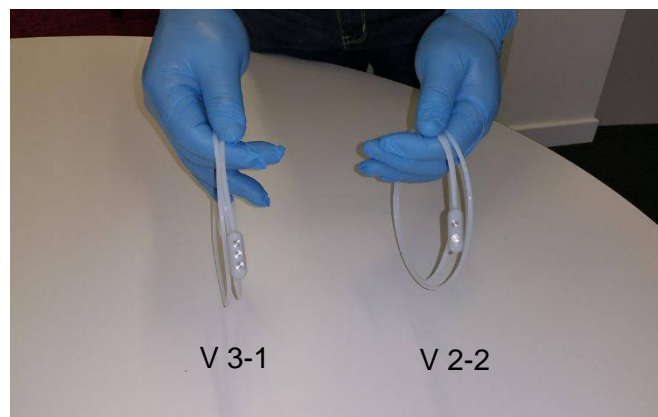
4.1.1 Results

The biocompatibility results are shown in table 22 below.

Material	Biocompatibility	Biodegradability	Reference
PTFE Teflons	No	Not applicable	FILE 5 in Appendix-CD
VeroWhite	No	No	[54]
Silicone Adhesive	Yes	Not applicable	FILE 4 in Appendix-CD

Table 22: Results of biocompatibility assessments

4.2 Final Products



(a)



Figure 93: Assembled TUSCE prototypes, V 2-2 and V 3-1

CHAPTER 5 DISCUSSION

5.1 Assembly of 3D Designed Pills

The assembly of the pill caps produced a capsule endoscope in the shape of a vitamin pill. This is essential because the ingestion of the capsule will give a prospective patient the feel of swallowing a vitamin supplement. The dimensions of the 3D CAD designed capsule endoscope before 3D printing indicate that the pill size is in consonance with the standard (30mm by 10mm) as specified by Lee et al [18].

5.1.1 Results of 3D Printing

The colour of the 3D-printed pills had the same colour (white) of the VeroWhite photopolymer material that was used in the Stratasys Objet30 printer. This indicates that the colour of the printed capsule endoscope is dependent on the colour of the photopolymer material used in the 3D printing process. The white colour was selected because it provided a good contrast to other components which aids visual inspection of the electronics and assembling of the pills. This is similar to the result of Endoscopic Submarine Capsule invented by Hoang et al [74].

The pills when viewed after the post-processing treatment had a rough texture on the body and in the shell section. This is due to the lack of a temporary support structure for the parts during the 3D printing process which agrees with the findings of Chia and Wu [41].

5.1.2 Microscopic Evaluation of Pills

The cured areas of the pills looked radiant under light from the microscope. This result exhibits the glossy feature of photopolymer materials. The partially cured area of the pill does not look glossy as there is no reflection of the incident light from the microscope. It can also be observed that the cured areas retained the features of the 3D CAD model such as the octagonal structure of the transducer holder in the V 3-1 TUSCE and pin holes in the V 2-2 TUSCE. The partially cured areas do not retain the exact 3D design of the pills. This indicates the disadvantage of stereolithography (SLA) rapid prototyping technique as it causes misshape in the 3D-printed parts [64] when 3D-parts are partially cured.

5.1.3 Conversion to STL File Format

The result of the converted part drawing (.SLDPRT) in the SolidWorks 3D CAD software to STL file format produced a tessellated 3D CAD model with layers of triangles that combined to form a geometry of polygons. This result agrees with the works of Hague R.J.M. and Reeves P.E. [65]. After making a comparison between the STL file format and the microscopic evaluation of the 3D capsule endoscopes it was observed that the surface of the pills has lines

running horizontally through the body of the pill. This helps to explain why the 3D printing process is called an additive manufacturing or layered manufacturing process as the structure of the printed pill is in the form of thinly sliced horizontal cross-sections [45, 52].

5.1.4 Comparison between mechanical measurements of the pills to the 3D CAD dimensions

Comparing the results of the pill size measurements using the vernier calliper and the SolidWorks 3D CAD software annotation it can be observed that there is a slight error in the diameter size of V 2-2 by 1.3% while the lengths of the pills were approximately equal for V 2-2 and exactly the same for V 3-1. These errors were easily corrected by adjusting the dimensions in the 3D CAD model. The difference in the measurements is due to the partially cured areas of the pill which are slightly thicker than the cured areas.

5.1.5 Comparison of the TUSCEs to Commercial WCEs and TCEs

In comparison to existing commercial wireless and tethered capsule endoscopes (Appendix B) V 2-2 and V 3-1 can compete favourably in terms of pill weight, size, and structure. V 2-2 and V 3-1 have smaller than the diameters of all the capsule endoscopes listed.

5.1.6 The pins and tether inlet

The positions of the pins allow for tight protection of the electronics and tether after assembly. This points that there should be a provision of adequate thickness on the pill caps to make the design of pins and pin holes possible. The thickness of the pill caps is also dependent on the tether size as the increase in the diameter of the Teflon tube requires a greater thickness for bond stability.

5.2 Tension tests

5.2.1 Variations in Test Time

In the tension tests of the micro-coaxial cable samples, the test time increased by 48 minutes between the UTS tests for coax1 to coax4 under the same load of 5N and speed of 0.4mm/min. This suggests that the test time increased with samples of larger diameter. But it was found that when coax5 was tensioned with a load of 2.5KN with the same speed of 0.4mm/min the recorded test time was approximately 14 minutes which is less than the test time for the tension test of coax1. This implies that using large load cells for tension testing of micro-coaxial samples cables reduces the test time by causing the samples to fail at a faster rate. The tension tests of the power cables followed the same trend as the micro-coaxial cables but with a marked difference in the tension test of sample PW2. It was observed that the test time for

specimens 2 and 3 for PW1 was less than that for specimen 1 by about 38 minutes after the test time for was increased from 0.4mm/min to 0.8mm/min under the same load of 1KN. This indicates that under the same load condition increasing the test speed of the tension test also reduces the test time.

5.2.2 Graphical Plotting

A smooth graph pattern was expected for the force-versus-elongation curves of coax1 to coax4 in contrast to the irregular distributions obtained. This can be attributed to the shape of the specimen. Specimens used in tensile tests are usually in the form of flat “dogbone” shapes as shown in figure 17. In order to restrict the deformation of the material within the narrow centre region and also to minimise the possibility of fracture occurring at the ends of the specimen. Since the cable specimens used were cylindrical and have microstructural dimensions the holding grips of the machine found it inconvenient to handle and consequently, the graph results have an edge-effect. [92, 93] This problem was solved by using wooden grips that have a smooth surface on the bigger Zwick/Roell Z250 test machine and also increasing the load cell value in order to exert a stronger gripping of the cable specimens. The smoother graphs generated can be seen in the results for coax 5, PW1 and PW2. However, this caused the failures to occur near the ends of the holding grips.

5.2.3 UTS test results of micro-coaxial cable samples

Coax1

The low force value of 1.75N for specimen 3 was obtained due to its weakness after undergoing the initial test. The low dL value for coax1 indicates that it is brittle.

Coax2

It was observed that the average F_{max} values for coax2 are slightly higher than that of coax1 and as a result, coax2 is less brittle than coax1.

Coax3

The long travel length as observed in the graph indicates that coax3 is more ductile than coax1 and coax2.

Coax4

The test time was longer than the other tests conducted because coax4 has a larger diameter and it exerted a greater resistance to the 500N load cell. The elongation values indicate that coax4 is more ductile than the previous micro-coaxial cable samples.

Coax5

The UTS curve for coax5 has a smooth and consistent pattern. This was achieved by using wooden holding grips and a greater load cell value. The elongation values of the specimens

after the UTS test were equal. This indicates that the coax5 UTS test had the highest precision and this was one of the features that prompted its selection for the tether design.

Power cables

The tensile test results for the power cables also indicate that PW2 is more tensile than PW1 by 65% and less brittle than PW1 by approximately 42%.

From the results, it was observed that Coax1 had the highest calculated value of tensile stress using equation (4). This does not mean that coax1 is more tensile than the other cable samples. This is due to the uneven distribution of the tension force in the specimens which affected the final value of the tensile strength. The true UTS value can be found by normalising the load-elongation curve of the UTS test to an engineering stress-versus-strain graph. The results of the calculated tensile strengths for coax1 show that coax1 experienced more stress than the other cable samples and was prone to failure in a short time than the other cable samples. This indicates that under the same load conditions a micro-coaxial cable with a smaller diameter will fail faster than other higher diameter samples.

5.2.4 Deformation in specimens

Results from the evaluation of deformed specimens show that the points of failure on the micro-coaxial and power cables occurred near the ends clamped to the tension load. This indicates the area that experienced the most stress application.

5.2.5 Trend in re-tested specimens

The results of the repeated tensile tests for specimen 3 of coax1 and specimen 3 of coax3 suggest that the micro-coaxial cable samples cannot exceed F_{max} values within the range of 1.72N to 1.75N once they have been subjected to a tensile load of 5N. This can be attributed to the weakening of the insulation material after the initial test.

5.2.6 Cable selection for tether design

Based on discussions with the Micro-engineering and Microsystems group of Sonopill the cables for tether design were selected according to the power and signal requirements for the sonocap and thermocap boards and the UT transducer which operates at a range of 30MHz. From the cable manufacturer's data sheet [126] it was observed that coax5 had the lowest signal attenuation (maximum dB/100ft) of 21.3 at 10MHz.

In [84], the level of extension before failure gives a measure of the ductility and brittle nature of a material. The elongation (dL) of the micro-coaxial sample cables increased in ascending order from coax1 to coax4 under the same load. The increase in UTS accompanied by an increase in dL means that coax5 has the highest stiffness and ductility. Similarly, PW1 was selected because of its high ductility.

5.3 Tether Design

5.3.1 Choice of Teflon

Perfluorotetraethylene (PTFE), Fluorinated Ethylene Propylene (FEP), and Perfluoroalkoxy (PFA) were utilised because they are biocompatible. PTFE is the most popular biocompatible fluoropolymer with a protracted history of in vivo medical applications but it lacks the transparency property of PFA and FEP. PFA Teflon was used in the UTS test and 3-point bend of the tether because of its transparency [112] and it combines the properties of PTFE and FEP. The use of PFA aided visual inspection of the tether specimens during the tether tensile strength test.

In the review of Arneson et al. [127] the size of the tether could cause gag reflex [127]. A 2mm inner diameter (ID) PFA Teflon was used because of the absence of a cable jetting service to pass the cables through a smaller diameter Teflon tube. A smaller Teflon tube with an outer diameter of 2mm is recommended. To pass the cables through the Teflon tube conveniently it is recommended that the cables and Teflon tube be of similar insulation materials. The cables and Teflon tubes used in this project are polymers of perfluorotetraethylene (PTFE). This helps to reduce friction between the cables and wall of the Teflon tube.

5.3.2 Bend test

By comparing the two results of the 3-point bend tests it can be deduced that the bending force increases as the bending radius decrease. The bending force curves for samples T1 and T2 followed the same design. The bending force is very high at the beginning and then it falls after attaining a peak value. In comparison to the bend tests carried out by Colloza [99] it was observed that at room temperature the change in bending force and bending radius increased swiftly at the beginning and then it dropped. Since the results of the tether 3-point bending test agree with Colloza's [99] bend tests at room temperature it is certain that the tether can be bent without causing failure. Though no literature was available for comparing the tether design. Since the average minimum bending radius for the tether at room temperature is 10mm, therefore the torque needed to reel and unreel the tether was calculated using equation (5) to give the value of 29.3Nm.

It should be noted that the sharp decline in the bending force to zero in T2 was due to a bending radius value of zero. At this point, the specimen could no longer change and the actuator pin does no work. The sudden rise in T1 approximately 29mm was due to the actuator making a slight contact with the wire support bracket.

5.3.3 UTS Test of the tether

The tether tensile strength test results show that the decline in the tension force is attributed to the deformation of the Teflon material after undergoing maximum stress. The curves for

both T1 and T2B have an intermittent rising and falling pattern which indicates that the shape of the tether specimen is not a “dogbone” as explained in [88]. The result also points that the failure of the specimen started from the Teflon tube (outer insulation) to one or more cables at a time. The deformation of cables in the tether samples was more intense near the ends attached to the holding grip. This suggests that the maximum stress on the tether will occur near the portion of the applied force.

5.4 Application

The results of the mechanical evaluation of the tether show that the tether has a high tensile strength and high flexibility which is applicable in a tethered capsule endoscopy (TCE) application but a smaller tether size is advised in order to avoid gag reflex.

5.5 Adhesive Bonding and Bonding Strength Test

A biocompatible silicone adhesive was used in the tether-to-pill bonding because of its elastomeric nature (flexibility) [117, 118], a minimum possibility of damaging the tissues [117, 123] of the GI tract. Additional mechanical strength was made to the bonding by attaching holes bored on the tether to the reinforcement pins on the pill caps.

Comparing the maximum force of the bond strength test (37.4N) to the maximum permissible actuation force (10N) in an endoscopy as researched by Shergill et al. [124] it is obvious that the bond strength exceeds this actuation threshold by 27.4N. This is desirable because it gives the clinician a better control over the endoscopy process as and eliminates the complication of a capsule retention.

The fixture time of 72 hours for silicone bond curing is very long. This can affect urgent applications in clinical research.

5.6 Final Product Description

5.6.1 V 2-2

V 2-2 is described as a TUSCE with 2 ultrasound (UT) transducers on each of the pill caps. The internal layout of V 2-2 is designed with a “box” design method as seen in figure 37, which allows for greater thickness of the pill caps as well as a rectangular shape to match the PCBs. The edges of the internal areas of the pill caps are well smoothed which gives it an attractive appearance. The edges on the body of the pill caps are also smoothed to ensure low friction between the pill and wall of the GI tract during capsule actuation. The assembly pins are positioned properly to provide a tight closure and protection of the electronic circuitry.

The design of the transducer holders allows for easy manipulation of the UT transducers during assembly as well as for retrieval of the transducers during troubleshooting operation. The spacing of the transducers permits the movement of electronic tools and positioning of surplus lengths of the micro-coaxial and power cables. However, it has an allowance of approximately 4mm for the PCBs when assembled meaning that the thickness of the UT transducer should not exceed 3mm in order to avoid sliding and pressure when it is in contact with the PCB.

5.6.2 V 3-1

V 3-1 is a TUSCE with 3 UT transducers on one the base cap and only one UT transducer on the cover cap. The “shell” design method of the internal layout allows for the low thickness of the pill caps and a shell structure similar to the internal structure of a vitamin pill. The edges on the body of the pill and in the shell are smoothed to give it a neat appearance and reduce the frictional force between the TUSCE and wall of the GI tract during the descent and withdrawal of the capsule pill. The shell layout of the pill provides enough space for the PCB and surplus lengths of cables. The assembly pins are well positioned to give a firm assembly of the pill caps and protection of the enclosed electronic circuitry.

The octagonal structure of the transducer holders offers high mechanical hardness to protect and keep the transducers firmly. This is essential for the “shell” design as it helps to protect other transducers in the base cap when assembling or retrieving one of the transducers. However, the use of 3 UT transducers on the base cap and one UT transducer on the cover cap indicates that the pill needs to be positioned adequately if the signal from the transducer in the cover cap is lost.

5.6.3 Comparison between V 2-2 and V 3-1

The “box” design of V 2-2 makes it heavier than “shelled” V 3-1 because the “box” design only takes of a non-uniform area of cross-section of the pill caps and this gives greater thickness to the pill. In contrast, the “shell” design method of V 3-1 chunked out a larger area of the cross-section from the pill and leaves it with a low thickness.

The lightness of V 3-1 indicates that it can be applied where the large weight of the TUSCE becomes a factor. Similarly, the V 2-2 TUSCE can be used where the increase in the speed of capsule motion due to low peristaltic action is needed.

5.6.4 The Tether

The power cables in the tether provide a steady electric power supply to the capsule endoscope; consequently, this will increase the time for efficient diagnosis and eliminating worries about the need for a battery change.

CHAPTER 7 CONCLUSIONS

This project was carried out with the aim of producing prototypes of capsule endoscopes with 3D printing technology for rapid testing of the GI tract and is part of the research objectives of the Sonopill project. The target design was a tethered ultrasound capsule endoscope (TUSCE) composed of 4 ultrasound (UT) transducers, one or two printed circuit boards and a tether for transmission of electric power and control signals and as the principle means of delivering and controlling the TUSCE into the GI tract.

The initial approach to the project involved making conceptual designs in line with the Sonopill-prescribed product specifications and two ideas were selected and realised in two TUSCE versions namely V 2-2 and V 3-1. The SolidWorks version 2015 3D CAD software was used to design 3D models of the TUSCE versions. The results of the designed TUSCEs show a “box extruded” design for V 2-2 and a “shell” design for V 3-1. The “fillet” tool was found to be a “power” tool in providing smoothed edges on the capsule design for low friction motion.

Stereolithography (SLA) 3D printing technique was used in a Stratasys Objet30 Pro printer to produce rapid prototypes of V 2-2 and V 3-1. This was achieved by converting the 3D CAD file (.SLDPRT) into an STL file format which the 3D printer can understand. The results of the 3D-printed capsules revealed the disadvantage of using the SLA rapid prototyping technique as it produced cured and partially cured parts due to the unavailability of a temporary support material.

The designed tether was composed of medical grade Teflon tubes and a combination of micro-coaxial cables and power cables. For quality control measures, mechanical evaluation tests were applied to qualify the designed tether and they include tensile tests, bend tests and a bond strength test. The results of the mechanical tests show that the materials used for the tether design were of the desired quality.

The bonding of the tether to the pill was implemented with a biocompatible silicone adhesive and an additional strength to the bond was provided mechanically by hooking the tether on reinforcement pins that were designed on the TUSCEs. The tether-to-pill bonding was qualified with a bond strength test which resulted in an efficient bonding for the TUSCE prototypes. The bond strength is high enough to avoid a capsule retention in the GI tract.

For an efficient design of a tethered ultrasound capsule endoscope (TUSCE) it is advised to start with the tether design to ensure that the capsule has the right parameters for a solid tether-to-pill integration design. Another 3D printing technique should also be explored if there are no temporary support materials available.

Finally, the overall results of this project show that 3D printing can be used to produce rapid prototypes of ultrasound capsule endoscopes which can be applied for clinical research in the diagnosis of GI diseases and this can also be achieved by using a tether which provides the means to actuate the prototypes through the GI tract. This will help the clinicians and the entire research team of Sonopill to understand the working modes of the prototypes and enhance ultrasound capsule endoscopy (USCE) as an expedient diagnostic process.

CHAPTER 8 FUTURE CONSIDERATIONS

3D printing is a viable tool in the production of biomedical devices. To meet the growing demand for treatment of gastrointestinal diseases it is important that capsule endoscopes are produced rapidly for prompt response to medical needs such as the early diagnosis of cancer.

- ❖ This project was limited to the design and fabrication of tethered ultrasound capsule endoscopes. It will be useful to explore the fabrication as well as ex vivo and in vivo clinical trials of the designs. This will enhance the design of the prototypes as valuable feedback from the clinical tests give invaluable information on the performance the design of the prototypes.
- ❖ Other 3D printing technologies such as the new Stratasys Polyjet 3D printing technology should be exploited for rapidly producing the capsules as this will provide a variety of material properties such as coloured printing, capsule transparency and flexibility.
- ❖ It was later discovered that the fixture time for the silicone adhesive bonding can be reduced by using ultraviolet light which gives it a fixture time of approximately minutes. Though silicone has better flexibility than other known adhesives, cyanoacrylates and epoxies can be applied for low fixture times and greater bond strength.
- ❖ The size of the tether can be reduced by using micro-coaxial and power cables and Teflon tubes with thinner diameters if a cable jetting service is used.
- ❖ The use of wireless capsule endoscopic ultrasound (WCEU) will eliminate the need for a tether system, consequently, this reduces the weight of the ultrasound capsule endoscope and introduce alternative capsule delivery or motion systems such as a robotic actuation and implementation of microelectromechanical systems (MEMS).

CHAPTER 9 REFERENCES

- [1] J. G. Williams, S. E. Roberts, M. F. Ali, W. Y. Cheung, D. r. Cohen, G. Demetry, A. Edwards, M. Greer, M. D. Hellier, H. A. Hutchings, B. Ip, M. F. Longo, I. T. Russell, H. A. Snooks and J. C. Williams, "Gastroenterology services in the UK. The burden of disease, and organisation and delivery of services for gastrointestinal and liver disorders: a review of the evidence," *Gut: An International Journal of Gastroenterology and Hepatology*, vol. 56, no. doi:10.1136/gut.2006.11759, pp. 1-2, 11 December 2006.
- [2] A. F. Peery et al, "Burden of Gastrointestinal Disease in the United States: 2012 Update," *International Journal of Cancer*, vol. 143, no. 5, p. 2, 2012.
- [3] Jacques et al., J. Ferlay, S. Hai-Rim, F. Bray and D. Form, "Estimates of worldwide burden of cancer in 2008: GLOBACON 2008," *International Journal of Cancer*, vol. 127, no. 12, p. 2894, 2010.
- [4] American Cancer Society, "Cancer in Africa," *American Cancer Society*, no. No. 861430, p. Introduction, 2011.
- [5] M. A. Siegel, J. J. Jacobson and R. J. Braun, "Diseases of the Gastrointestinal tract," in *Burket's Oral Medicine: Diagnosis and Treatment*, BC Decker Inc., 2003, pp. 389-406.
- [6] M. A. Khan and L. W. Solomon, *Gastrointestinal Tract Part 1: Basic Human Pathology II*, Massachusetts: Tufts University, 2008, pp. 1-28.
- [7] Apainter@bcssd.com, "Welcome to Mister Painter's Classroom Website! Advanced Biology," Google Sites, [Online]. Available: <https://sites.google.com/a/bcssd.com/painter/home>. [Accessed 08 August 2016].
- [8] G. Pan and L. Wang, "SwallowableWireless Capsule Endoscopy:," *Gastroenterology Research and Practice*, vol. 2012, no. doi:10.1155/2012/841691, pp. 1-9, 2011.
- [9] C. Mc Caffrey, O. Chevalerias, C. O'Mathuna and K. Twomey, "Swallowable-capsule Technology," *IEEE Pervasive Computing*, vol. 7, no. 1, pp. 23-29, 2008.
- [10] B. S. Lewis, "Small Intestinal Bleeding," *Gastroenterology Clinics of North America*, vol. 29, no. 1, pp. 67-95, 2000.
- [11] L. J. Silker and G. Ciuti, "Flexible and capsule endoscopy for screening, diagnosis and treatment," *Expert Review of Medical Devices*, vol. 11, no. 6, pp. 649-665, 2014.
- [12] G. Pan and L. Wang, "Swallowable Wireless Capsule Endoscopy: Progress and Technical Challenges," *Gastroenterology and Practice*, vol. 2012, no. DOI:10.1155/2012/841691, p. 3, 2012.
- [13] G. J. Michalina, J. S. Sauk, R. W. Carruth and K. A. Gallagher, "Tethered capsule endomicroscopy enables less-invasive imaging of gastrointestinal tract microstructure," *National Center for Biotechnology Information*, vol. 19, no. 2, pp. 1-2, 2013.

- [14] Macmillan Magazines Ltd, "Wireless Capsule Endoscopy: The discomfort of internal gastrointestinal examination may soon be a thing of the past," *NATURE*, pp. 417-418, 25 May 2000.
- [15] U. C. Goshal, "Capsule Endoscopy: A New Era of Gastrointestinal Endoscopy," in *Capsule Endoscopy: A New Era of Gastrointestinal Endoscopy, Endoscopy of GI Tract*, Lucknow, India, INTECH, 2013, p. 78.
- [16] D. Panescu, "Emerging technologies: An imaging pill for gastrointestinal Endoscopy," *IEEE Engineering in Medicine and Biology Magazine*, vol. 24, no. DOI:1109/MEMB.2005.1463383, pp. 12-14, 2005.
- [17] E. J. Siebel, R. E. Carrol, J. A. Dominitz, R. S. Johnston, D. C. Melville, C. M. Lee, S. M. Seitz and M. B. Kimmey, "Tethered Capsule Endoscopy, A Low-Cost and High Performance Alternative Technology for Screening of Esophageal Cancer and Barret's Esophagus," *IEEE Transactions on Biomedical Engineering*, vol. 55, no. 3, pp. 1032-1041, 2008.
- [18] J. Lee, G. S. Traverso, D. Blankschtein, R. Langer, K. E. Thomenius, S. B. Duane and B. W. Anthony, "Towards Wireless Endoscopic Ultrasound (WCEU)," in *IEEE International Ultrasonics Symposium Proceedings*, Chicago, IL, 2014.
- [19] H. T. Lutz and R. Soldner, "Basic Physics of Ultrasound," *Manual of Diagnostic Ultrasound*, vol. 1, no. 2nd Edition, pp. 3-5, 2011.
- [20] MdeicineNet.com, "Definition of Ultrasound/Ultrasonography," 13 May 2016. [Online]. Available: <http://www.medicinet.com>. [Accessed 11 August 2016].
- [21] A. Mongolia, A. Menciassi and P. Dario, "Recent Patents on Wireless Capsule Endoscopy," *Recent Patents on Biomedical Engineering*, vol. 1, no. No. 1, pp. 24-33, 2008.
- [22] J. Correia, "Final Report Summary-TROY(Endoscope Capsule using Ultrasound Technology)," Troy, 2009.
- [23] H. S. Lay, V. Seetohul, B. Cox, C. E. M. Demore and S. Cochran, "Design and Simulation of a High Frequency Ring-Shaped Linear Array for Capsule Ultrasound Endoscopy," in *IEEE Ultrasonics Symposium Proceedings*, 2014.
- [24] Technology, Institute for Medical Science and, "IMSat," 2010. [Online]. Available: <http://imsat.org/SandyCochran.htm>. [Accessed 09 August 2016].
- [25] P. S. Cochran, "Microultrasound: Applications Ahead," *RAD Magazine*, vol. 40, no. 474, pp. 11-12, 2014.
- [26] V. Seetohul, B. Cox and S. Cochran, "Robotic requirements for diagnosis and therapy with ultrasound capsule endoscopy," in *IEEE/RSI International Conference on Intelligent Robots and Systems*, 2015.
- [27] Sonopill, "Sonopill: The Future of Capsule Ultrasound," Sonopill, [Online]. Available: <http://sonopill.dundee.ac.uk>. [Accessed 08 May 2016].

- [28] www.3dprinting.com, "What is 3D Printing," 24 March 2016. [Online]. Available: <http://www.3dprinting.com>. [Accessed 2016 May 2016].
- [29] D. Rachlin, J. Van Dam and V. V. Gurukula, "Tethered Endoscope". USA Patent US 2015/0289752 A1, 15 October 2015.
- [30] L.-A. Topfer, "The Cytosponge: An Alternative to Endoscopy in Detecting Barret Esophagus," *CADTH ISSUES IN EMERGING HEALTH TECHNOLOGIES*, no. 144, pp. 3-7, October 2015.
- [31] S. R. Kadiri, P. Lao-Sirieix, M. O'Donovan, M. Das, J. M. Blazeby and e. al, "Acceptability and accuracy of a non-endoscopic screening test for Barrett's Oesophagus in primary care: Cohort Stusdy". Canada Patent CC-BY-NC-2.0, 10 September 2010.
- [32] M. Di Pietro, D. Chan, R. C. Fitzgerald and K. Wang , "Screening for barret's oesophagus," *Gastroentrology*, vol. 148, no. 5, pp. 912-923, 2015.
- [33] G. J. Micahlina , J. S. Sauk , R. W. Carruth and K. A. Gallagher, "Tethered Capsule Endomicroscopy Enables Less-invaisve Imaging of Gastrointestinal," *Digital Access to Scholarship at Harvard*, no. doi: 10.1038, pp. 238-240, 2015.
- [34] University of Glasgow, "Professor Sandy Cochran," 15 August 2016. [Online]. Available: <http://www.gla.ac.uk/schools/engineering/staff/sandycochran/>. [Accessed 15 August 2016].
- [35] The European Institute of Piezoelectric Materials and Devices, "Piezo Institute," 27 March 2015. [Online]. Available: <http://www.piezoinstitute.com/news/interview-sandy-cochran-principal-investigator-on-sonopill-programme>. [Accessed 12 August 2016].
- [36] J. D. Hardcastle and C. V. Mann, "Study of Large Bowel Persitalsis," *Gut*, vol. 9, no. doi:10.1136/gut.9.5.512, pp. 512-520, 1968.
- [37] J. Miscallef, *Beginning Design for 3D Printing*, New York: Springer Science+Business Media, 2015.
- [38] I. Gibson , D. Rosen and B. Stucker, *Additive Manufacturing Technologies*, New York: Springer Science+Business Media, 2015.
- [39] D. T. Pham and S. S. Dimov, "Rapid Prototyping and Rapid Tooling-The Key Enablers for Rapid Manufacturing," in *Institution of Mechanical Engineers, Part C: Journal of Mechanical Engineering Science*, Wales, 2003.
- [40] ASTM International, *Standard Terminology for Additive Manjufacturing Technologies*, West Conshohocken: ASTM International, 2013.
- [41] H. N. Chia and B. M. Wu, "Recent Advances in 3D Printing of Biomaterials," *Journal of Biological Engineering*, vol. 9:4, no. DOI:10.1186/s13036-015-0001-4, pp. 1-10, 2015.
- [42] D. L. Bourell, H. L. Marcus and J. W. Barlow, "Solid Freeform Fabrication An Advanced Manufacturing Approach," in *Solid Freeform Fabrication Symposium*, Austin, Texas, 1990.

- [43] J. J. Beaman, W. J. Barlow, D. L. Bourell and R. H. Crawford, *Solid Freeform Fabrication: A new Direction in Manufacturing (with Research and Applications in Thermal Laser Processing)*, New York: Springer Science+Business Media, 1997.
- [44] 3D PRINTING.COM, "What is 3D printing?," 2016. [Online]. Available: <http://www.3dprinting.com>. [Accessed 8 June 2016].
- [45] F. Rengier, A. Mehndiratta, H. v. Tengg-Kobligk, C. M. Zechmann, R. Unterhinninghofen, H. U. Kauczor and F. L. Giesel, "3D Printing Based on Imaging Data: Review of Medical Applications," *CARS*, vol. 5, no. DOI:10.1007/s11548-010-0476-x, pp. 335-341, 2010.
- [46] Dassault Systemes SolidWorks Corporation, "SolidWorks," 2016. [Online]. Available: <http://www.solidworks.com>. [Accessed 26 June 2016].
- [47] Dassault, Systemes, "Dassault Systemes," 2002-2016. [Online]. Available: <http://www.3ds.com>. [Accessed 26 June 2016].
- [48] C. Briand, "New in SolidWorks 2015!-The Split Feature can now Split Surface Bodies!," 26 September 2014. [Online]. Available: http://www.javelin-tech.com/blog/2014/09/split-surface-bodies/#.V7ltQ_krLcs. [Accessed 26 June 2016].
- [49] N.-D. Ciobata, "Standard Tessellation Language in Rapid Prototyping Technology," *The Scientific Bulletin of Valahia University-Materials and Mechanics*, pp. 1-84, 2012.
- [50] "What does STL mean in Language and Literature?," *Abbreviations*, 2016. [Online]. Available: www.abbreviations.com/term/1503512. [Accessed 26 June 2016].
- [51] Eric Miller, "A Guide to Creating Good STL Files," *PADT*, 12 December 2012. [Online]. Available: <http://www.padtinc.com/blog/additive-mfg/a-guide-to-creating-good-stl-files>. [Accessed 26 June 2016].
- [52] Wohlers, Terry T., "Wohlers Associates," 04 April 1992. [Online]. Available: <https://www.wohlerassociates.com/apr92cae.html>. [Accessed 26 June 2016].
- [53] R. J. M. Hague and P. E. Reeves, *Rapid Prototyping, Tooling and Manufacturing*, Shrewsbury: Rapra Technology Limited, 2000.
- [54] Stratasys Direct, Inc., *3D Printing Materials: Choosing the Right Material for your Application*, Stratasys Direct, Inc., 2015.
- [55] E. Reichmanis and J. Crivello, "Photopolymer Materials and Processes for Advanced Technologies," *ResearchGate*, vol. 26, no. DOI:10.1021/cm402262g, pp. 533-548, 2014.
- [56] R. Phillips, "Photopolymerization," *Journal of Photopolymerization*, vol. 25, no. DOI:10.1016/0047-2670(84)85016-9, pp. 79-82, 1984.
- [57] J. Burton, "A Primer on UV-Curable Inkjet Inks," *Specialty Graphic Imaging Association*, p. May, 2008.
- [58] Y. Yusuf, J. Steffen and N. J. Turro, *Photoinitiated Polymerization: Advances, Challenges, and Opportunities.*, New York: Istanbul, 2010.

- [59] Wikipedia, "Photopolymer," 30 June 2016. [Online]. [Accessed 30 June 2016].
- [60] D. T. Pham and R. S. Gault, "A Comparison of Rapid Prototyping Techniques," *International Journal of Machine Tools and Manufacture*, vol. 38, no. 0890-6955/98, pp. 1257-1287, 1998.
- [61] S. Hickey, "Chuck Hull: The Father of 3D Printing Who Shaped Technology," *The Guardian*, pp. <https://www.theguardian.com/business/2014/jun/22/chuck-hull-father-3d-printing-shaped-technology>, 22 June 2014.
- [62] 3D Systems, *Charles W. Hull Co-Founder and Chief Technology Officer*, 3D Systems, 2016, pp. <http://www.3dsystems.com/files/downloads/3D-Systems-Charles-W-Hull-Executive-Bio.pdf>.
- [63] F. P. Melchels, J. Feijen and D. W. Grijmpa, "A Review on Stereolithography and its Applications in Biomedical Engineering," *Biomaterials*, vol. 31, no. 24, pp. 6121-6130, 2010.
- [64] W. L. Wang, C. M. Cheah, J. Y. H. Fuh and L. Lu, "Influence of Process Parameters on Stereolithography Part Shrinkage," *Mater Design*, vol. 17, no. 4, pp. 2015-213, 1996.
- [65] TSI Solutions, "What is a Durometer?," [Online]. Available: <http://www.4tsi.com/wp-content/2012/10/What-is-a-Durometer.pdf>. [Accessed 06 July 2016].
- [66] X. Zhang, X. Jiang and C. Sun, "Micro-stereolithography of Polymeric and Ceramic Microstructures," *Sensors and Actuators A: Physical*, no. 77, pp. 149-156, 1999.
- [67] Wikipedia, "Stratasys," 11 June 2016. [Online]. Available: <https://en.wikipedia.org/wiki/Stratasys>. [Accessed 17 June 2016].
- [68] J. Boik, *Lessons from the Greatest Stock Traders of All Time*, McGraw-Hill Professional, 2004.
- [69] B. BusinessWeek, "Hot Growth Companies: Stratasys Profile," *BusinessWeek*, 31 October 2008.
- [70] Javelin Technologies Inc., "Javelin," 2016. [Online]. Available: <http://www.javelin-tech.com/3d-printer/materials/polyjet-photopolymer/stratasys-polyjet-technology/>. [Accessed 29 July 2016].
- [71] Stratasys Ltd., "Stratasys," Stratasys Ltd., 2016. [Online]. Available: <http://www.stratasys.com>. [Accessed 04 July 2016].
- [72] Stratasys Ltd., *Objet30 Prime: The World's Most Versatile Desktop 3D Printer*, Stratasys Ltd., 2016.
- [73] Stratasys Ltd., *Objet30 3D Printer Systems*, Stratasys Ltd., 2014.
- [74] N. T. Hoang, C. S. Bell and P. Valdastrì, "Utilisation of LEDs in a Communication Protocol for Endoscopic Submarine Capsules," *Young Scientist Journal*, vol. 5, no. May 2015 Issue, pp. 9-12, 2015.

- [75] *Creo Parametric: The Essential 3D Parametric CAD Solution*, PTC Inc. (PTC), 2016.
- [76] T. Weisel, "Just What the Doctor Ordered: 3D Printer Helps Arch Day Design Win More Business," Stratasys Ltd., California, 2013.
- [77] N. D. Thanh, T. E. T. Seah, K. Y. Ho and S. J. Phee, "Development and Testing of a Magnetically Actuated Capsule Endoscopy for Obesity Treatment," *PLoS ONE*, no. doi:10.1371/journal.pone.e014835, p. 11 (1):e014835, 2016.
- [78] B. C. Giardiello, E. Silvestri, V. Antognozzi, G. Iodice and M. Lorenzo, "Air-Filled vs Water-Filled Intra-gastric Balloon: A Prospective Randomized Study.," *OBES SURG*, vol. 22, no. DOI:10.1007/s11695-012-0786-x, pp. 1916-1919, 2012.
- [79] AlphaWire, *Micro Coaxial Cable*, New Jersey: Alpha Wire, 2016.
- [80] Micro-coax, *Coaxial Cable, Specification Control Drawing for Part Number: UT-141-95*, Micro-Coax Inc., 2016.
- [81] Wikipedia, "Wire," Wikimedia, 15 August 2016. [Online]. Available: <https://en.wikipedia.org/wiki/Wire>. [Accessed 15 August 2016].
- [82] Allied Wire and Cable, Inc., "Hook Up Wire and Lead Wire Frequently Asked Questions," 2016. [Online]. Available: <http://www.awcwire.com/faq-hook-up-wire.aspx>. [Accessed 07 July 2016].
- [83] RadioShack, "RadioShack UL Hookup Wire 22AWG," 2016. [Online]. Available: <https://www.radioshack.com/products/ul-hookup-wire-22awg-2?variant=5717682885>. [Accessed 07 July 2016].
- [84] W. J. Callister and D. G. Rethwisch, *Materials Science and Engineering*, 9th edition,, John Wiley and Sons, (Asia)Pte Ltd, 2015, pp. 210-227.
- [85] J. F. Shackelford, *Introduction to Material Science for Engineers*, 6th edition, Upper Saddle River, New Jersey: Pearson Education, Inc., Pearson Prentice Hall, 2005, pp. 190-213.
- [86] J. R. Davis, "Tensile specimen nomenclature," 26 September 2010. [Online]. Available: https://en.wikipedia.org/wiki/File:Tensile_specimen_nomenclature.svg. [Accessed 18 August 2016].
- [87] C. Mechanisms, "Tensile Testing For Plastic Prototype Development," 13 April 2016. [Online]. Available: <https://www.creativemechanisms.com/blog/tensile-testing-for-plastic-prototype-development>. [Accessed 15 July 2016].
- [88] Gedeon, Mike, "Tensile Testing," *Materion Brush Performance Alloys: Technical Tidbits*, p. Issue No.27, March 2011.
- [89] Nipun, "Main Difference – Yield Strength vs. Tensile Strength," 14 October 2015. [Online]. Available: <http://pediaa.com/difference-between-yield-strength-and-tensile-strength/>. [Accessed 15 July 2016].
- [90] V. John, *Introduction to Engineering Materials*, 4th edition, Hampshire and New York, N.Y: Palgrave Macmillan, 2003, pp. 515-516.

- [91] R. Higgins , *Properties of Engineering Materials*, 2nd edition, Oxford: Butterworth-Heinemann, Linacre House, Jordan Hill, Oxford OX2 8DP (A division of Reed Educational and Professional Publishing Ltd),, 2011.
- [92] S. Hazra, *Why are most tension specimens dog bone shaped?*, Quora, 2014.
- [93] StackExchange, *Why use a 'dogbone' shape for tensile testing specimens?*, Stack Exchange Inc., 2016, pp. <http://engineering.stackexchange.com/questions/7061/why-use-a-dogbone-shape-for-tensile-testing-specimens>.
- [94] DoITPoMS, *Teaching and Learning Packages*, “Yield strength and ductility,” University of Cambridge, Cambridge, 2015.
- [95] K. Serope and R. S. Stephen, *Manufacturing, Engineering & Technology*, 5th Edition, New Jersey: Pearson Education, 2006, p. 56.
- [96] W. F. Components, “WIRE BENDING RADIUS - WHAT IT IS AND HOW TO DETERMINE IT,” 2016. [Online]. Available: <https://www.westfloridacomponents.com/wire-bending-radius.html>. [Accessed 15 July 2016].
- [97] Anixter, “What is Minimum Bend Radius?,” 2016. [Online]. Available: https://www.anixter.com/en_uk/resources/literature/wire-wisdom/minimum-bend-radius.html. [Accessed 21 July 2016].
- [98] NASA, “National Aeronautics and Space Administration,” NASA, 13 February 2016. [Online]. Available: <https://www.nasa.gov/about/index.html>. [Accessed 19 August 2016].
- [99] A. Colloza, “Wire and Cable Cold Bending Test,” NASA Centre for Aerospace Information, Hanover, MD 21076-1320, 2010.
- [100] Wright Patterson Air Force Base;, *Applying Mechatronics to Promote Science*, New York City: Wright Patterson Air Force Base;, 2009, pp. http://engineering.nyu.edu/gk12/amps-cbri/pdf/Robotics%20in%20the%20Classroom-Wright-Patterson%20AFB/torque_robot.pdf.
- [101] Wikipedia, *Bend radius*, Wikipedia, 2016, p. https://en.wikipedia.org/wiki/Bend_radius.
- [102] D. F. Williams, “Progress in Biomedical Engineering,” *Definitions in Biomaterials*, vol. 4, no. 9, p. 72, 2008.
- [103] B. D. Ratner, “The Biocompatibility Manifesto: Biocompatibility for the Twenty-first Century,” *J. of Cardiovasc. Trans. Res.*, vol. 4, no. DOI:10.1007/s12265-011-9287-x, pp. 523-527, 2011.
- [104] L. Mertz, “What is Biocompatibility?,” *IEEE PULSE*, vol. 4, no. 4, pp. 14-15, 2013.
- [105] International Organization for Standardization (ISO), *ISO*, Geneva: ISO.
- [106] International Organisation for Standardisation (ISO), *ISO*, Geneva: ISO, 2016, pp. <http://www.iso.org/iso/home/standards/management-standards/iso13485.htm>.

- [107] International Organisation for Standardisation, *Biological evaluation of medical devices -- Part 1: Evaluation and testing within a risk management process*, Geneva: ISO, 2016.
- [108] Product Knowledge Network, *What is a Fluoropolymer*, <http://www.productknowledge.com/fluoropolymers-what-is-fluoropolymer.html>.
- [109] Wikipedia, "Teflon," 11 August 2016. [Online]. Available: [https://en.wikipedia.org/wiki/Teflon_\(nickname\)](https://en.wikipedia.org/wiki/Teflon_(nickname)). [Accessed 19 August 2016].
- [110] S. Ebnesajjad, *Introduction to Fluoropolymers*, FluoroConsultants Group, LLC, 2013.
- [111] Corrosion Resistant Products Ltd (CRP), *Fluoropolymers*, <http://www.crp.co.uk/technical.aspx?page=9>.
- [112] Zeus Industrial Products Inc., *The Polymer Minute*, p. <http://www.zeusinc.com>.
- [113] D. Trussell, "PTFE Tube," Donna Trussell, 26 March 2015. [Online]. Available: <http://donnatrussell.com/2015/03/26/ptfe-tube/>. [Accessed 19 August 2016].
- [114] FLUOROTHERM, "PFA Tubing," FLUOROTHERM, 2016. [Online]. Available: <http://www.fluorotherm.com/products/fluoropolymer-tubing/pfa-tubing/>. [Accessed 19 August 2016].
- [115] Saint-Gobain, "Saint-Gobain," 2016. [Online]. Available: <http://www.labpure.com/en/LabTubing.asp>. [Accessed 19 August 2016].
- [116] FLUOROTHERM, "FLUOROTHERM," 2016. [Online]. Available: <http://www.fluorotherm.com/products/fluoropolymer-tubing/fep-tubing/>. [Accessed 2016 August 2016].
- [117] G. Cummins and M. P. Y. Desmulliez, "Characterisation of adhesive bonds for ingestible biomedical applications," in *17th Electronics Packaging Technology Conference*, Suntec City, 2015.
- [118] Y. Qin, M. M. R. Howlader, J. M. Deen, Y. M. Haddara and R. P. Selvaganapathy, "Polymer Integration for Packaging of Implantable Sensors," *Sensors Actuators B Chem.*, vol. B, no. 202, pp. 754-778, 2014.
- [119] R. E. Baier, "Adhesion in the biologic environment," *Biomaterials Medical Devices and Artificial Organs*, vol. 12, pp. 133-159, 1985.
- [120] T. K. Shih, C. F. Chen, J. R. Ho and F. T. CHUANG, "Fabrication of PDMS (polydimethylsiloxane) microlens and diffuser using replica molding," *Microelectronics Engineering*, vol. 83, no. 11-12, p. 2499-2503, 2006.
- [121] R. Yoda, "Elastomers for biomedical applications," *Journal of Biomaterials Science, Polymer Edition*, vol. 9, no. 6, pp. 561-626, 2012.
- [122] A. Junkkins, "The Heart-Lung Machine Amanda," *Biomedical Engineering, University of Rhode Island BME 281*, no. Second Presentation, 12 November 2012.
- [123] FABRICO, *Advanced Adhesives for Medical Applications*, A division of EIS, 2016.

- [124] A. K. Shergill, K. R. Asundi, A. Barr, J. N. Shah, J. C. Ryan, M. R. Kenneth and D. Rempel, "Pinch Force and Fore-arm Muscle Load During Routine Colonoscopy: A Pilot Study," *Gastrintestinal Endoscopy*, vol. 69, no. 1, pp. 142-146, 2009.
- [125] R. Liska, M. Schster, C. Infuhr, C. Fritscher, B. Seidl, V. Schmidt, L. Kuna, A. Haase, F. Varga, H. Lichtenegger and J. Stampfl, "Photopolymers for Rapid Prototyping," *J. Coat. Technol. Res.*, vol. 4, no. DOI: 10.1007/s11998-007-9059-3, pp. 505-510, 2007.
- [126] Alpha Wire, "PART NO. 9442: Properties," 2016. [Online]. Available: <http://www.alphawire.com/en/Products/Cable/Alpha-Essentials/Coaxial-Cable/9442>. [Accessed 29 August 2016].
- [127] M. Arneson, W. Bandy and W. Shanks, "Ultrasound Scanning Capsule Endoscope". United States Patent US 2014/0323867 A1, 30 October 2014.
- [128] Stratasys Inc., *ABS*, Stratasys Inc., 2007.
- [129] "Chemical and Environmental Resistenace of Thermoplastics," 2016. [Online]. Available: <http://www.rtcompany.com>. [Accessed 04 June 2016].
- [130] Wikipedia, "Acrylonitrile Butadiene Styrene," 07 August 2016. [Online]. Available: http://ww.wikipedia.org/wiki/Acrylonitrile_butadiene_styrene. [Accessed 07 August 2016].
- [131] Matbase, "PLA monomere (Polylactic Acid)," 2016. [Online]. Available: <https://www.matbase.com/material-categories/natural-and-synthetic-polymers/agro-based-polymers/material-properties-of-polylactic-acid-monomere-pla-m.html#properties>. [Accessed 04 July 2016].
- [132] Wikipedia, "Polylactic Acid," 05 August 2016. [Online]. Available: https://ww.en.wikipedia.org/wiki/Polylactoc_acid. [Accessed 05 August 2016].
- [133] Ad van Wijk and Iris van Wijk, *3D Printing with Biomaterials: Towards a Sustainable and Circular Economy*, Delft: IOSM Press, 2013.
- [134] Bolck, Christiaan, Ravenstijn, Jan and Molenveld, S. L. Karin and U. R. Wageningen, *Biobased Plastics*, 2012.
- [135] Kappen and Frans, *Bioplastics and processing-Workshop 3D printing with Biomaterials*, Delft, 2013.
- [136] i.materialise, "i.materialise," 2016. [Online]. Available: <https://i.materialise.com/3d-printing-materials/high-detail-resin>. [Accessed 26 June 2016].
- [137] National Institute of Diabetes and Digestive and Kidney Diseases, "The Digestive System and How it Works," *National Digestive Diseases Information Clearing House*, pp. 1-4, September 2013.
- [138] M. R. Jacobson B., "A pH-endoradiosonde," *Lancet* 1957, no. 272:1224 [PMID: 13440011].

- [139] K. A. Karargyris A, "Capsule-odometer: A concept to improve accurate lesion localisation," *World J Gastroenterology*, no. DOI: 10.3748/wjg.v19.i35.5943], pp. 5943-5946, 2013.
- [140] K. A. Karargyris A, "OdoCapsule: next-generation wireless capsule endoscopy with accurate lesion localization and," *IEEE Trans Biomed Eng* 2015, no. PMID: 25167544, pp. 352-360, 2015.
- [141] Wikipedia, "Gavriel Iddan," Wikimedia Foundation, Inc., 15 February 2016. [Online]. Available: https://en.wikipedia.org/wiki/Gavriel_Iddan. [Accessed 09 August 2016].
- [142] G. I. Ltd, "Given Imaging," Given Imaging Ltd, 2001-2016. [Online]. Available: <http://www.givenimaging.com/en-us/Pages/default.aspx>. [Accessed 09 August 2016].
- [143] A. T. Tetsuya Nakamura, "Capsule Endoscopy: Past, Present, and Future," *World Journal of Gastroenterology*, no. DOI 10.1007/s00535-007-2153-6, pp. 93-99, 2008.
- [144] The Hillingdon Hospitals, NHS Foundation Trust, "What is Capsule Endoscopy?," October 2011. [Online]. Available: <https://www.thh.nhs.uk>. [Accessed July 2016].
- [145] A. G. Douglas and C.-s. L. Gostout, "Wireless Capsule Endoscopy," *Hospital Physician*, p. 14, 2003.
- [146] A.-R. A. Mohammed, J. Beeley and D. R. S. Cumming, "Wireless fluorescence capsule for endoscopy using single photon-based detection," www.nature.com/scientificreports, Glasgow, 2015.
- [147] Research Councils, UK, "Sonopill: Minimally invasive Gastrointestinal Diagnosis and Therapy," 27 July 2016. [Online]. Available: <http://gtr.rcuk/>. [Accessed July 2016].
- [148] G. R. Lockwood, D. H. Turnbull, D. A. Christopher and F. S. Foster, "Beyond 30MHz: Applications of High Frequency Imaging," *IEEE Engineering Med Biol*, no. 0739-5175/96/S5.00, pp. 60-71, 1996.
- [149] Fred Fischer, Stratasys, *Thermoplastics: The Strongest Choice for 3D Printing*, Stratasys Ltd, 2011.
- [150] 3D Printing for Beginners, "What Material Should I use for 3D Printing?," 2016. [Online]. Available: <http://www.3dprintingforbeginners.com>. [Accessed 08 June 2016].
- [151] Hewlett Packard, "hp," 2016. [Online]. Available: <http://www.hp.com>. [Accessed 26 June 2016].
- [152] R. J. Young, Chapman and Hall, *Introduction to Polymers*, 1987.
- [153] A. Bruce, A. Johnson, J. Lewis, O. Raff, R. Keith and W. Peter, *Molecular Biology of the Cell*, Garland Science, 2008.
- [154] K. Naka, *Monomers, Oligomers, Polymers and Macromolecules (Overview)*, Kyoto: Springer-Verlag Berlin Heidelberg, 2014.
- [155] Savia Associates, "Photopolymer," 2014. [Online]. Available: <http://www.photopolymer.com>. [Accessed 04 July 2016].

- [156] J. Yoo, M. J. Cima, S. Khanuja and E. M. Sachs, "Structural Ceramic Components by 3D Printing," *Advanced Research Projects Agency*.
- [157] 3D Printing Industry, "The Free Beginner's Guide to 3D Printing," 2016. [Online]. Available: <http://3dprintingindustry.com/>. [Accessed 06 July 2016].
- [158] D. Huson, "Materials and Process Innovation for 3D Printing of Ceramics," 2015, p. 13.
- [159] ABS Plastic.eu, "3D Printing Materials, 3D Printing News, ABS Plastic," ABS Plastic.eu, [Online]. Available: <http://www.absplastic.eu/abs-plastic-explained/#more-988>. [Accessed 04 July 2016].
- [160] CustomPartNet, "Fused Deposition Modelling (FDM)," 2009. [Online]. Available: <http://www.custompartnet.com/wu/fused-deposition-modelling>. [Accessed 06 July 2016].
- [161] R. van Noort, "The Future of Dental Services is Digital," *Dental materials*, vol. 28, no. 1, pp. 3-12, 2012.
- [162] C. Ancey, *Notebook Introduction to Fluid Rheology*, Lausanne: Laboratoire Hydraulique Environnementale (LHE), 2005.
- [163] S. J. Kalita, S. Bose, H. L. Hosick and A. Bandyopadhyah, "Development of Controlled Porosity Polymer-Ceramic Composite Scaffolds Via FDM," *Material Science and Engineering: C*, vol. 23, no. 5, pp. 613-614, 2003.
- [164] University of Texas:News, "Selective Laser Sintering, Birth of an Industry," 06 December 2012. [Online]. Available: <http://www.me.utexas.edu/news/news/selective-laser-sintering-birth-of-an-industry>. [Accessed 06 July 2016].
- [165] L. C. Ventola, "Medical Applications for 3D Printing: Current and Projected Uses," *P&T*, vol. 39, no. 10, pp. 704-711, 2014.
- [166] Massachusetts Institute of Technology, "MIT," Massachusetts Institute of Technology, 17 August 2016. [Online]. Available: <http://web.mit.edu/>. [Accessed 17 August 2016].
- [167] M. J. Cima, E. Sachs, L. G. Cima, J. Yoo, S. Khanuja, S. W. Borland and et al., "Computer Derived Microstructures by 3D Printing: Bio and Structural Materials," in *Solid Freeform Fabrication Symposium Proceedings: DTIC Document*, Austin, 1994.
- [168] L. G. Griffith, B. Wu, M. J. Cima, M. J. Powers, B. Chaignaud and J. P. Vacanti, "In vitro Organogenesis of Liver Tissues," *Annals of the New York Academy of Sciences*, vol. 831, no. DOI: 10.1111/j.1749-6632.1997.tb52212.x, pp. 382-397, 1997.
- [169] B. M. Wu, S. W. Borland, R. A. Giordano, L. G. Cima, E. M. Sachs and M. J. Cima, "Solid Free-form Fabrication of Drug Delivery Devices," *J. Control Release*, vol. 40, no. 1-2, pp. 77-87, 1996.
- [170] H. Seitz, W. Reider, S. Irsen, B. Leukers and C. Tille, "3-Dimensional Printing of Porous Cermaic Scaffolds for Bone Tissue Engineering," *Journal of Biomedical Materials Research*, vol. 74B, no. 2, pp. 782-788, 2005.

- [171] S. S. Kim, H. Utsunomiya, J. A. Koski, B. M. Wu, M. J. Cima, J. Sohn and et al., "Survival and Function of Hepatocytes on a Novel Three-dimensional Synthetic Biodegradable Polymer Scaffold with an Intrinsic Network of Channels," *Annals of Surgery*, vol. 228, no. 1, p. 8, 1998.
- [172] J. Zeltinger, J. K. Sherwood, D. A. Graham, R. Mueller and L. G. Griffith, "Effect of Pore Size and Void Fraction on Cellular Adhesion, proliferation, and Matrix Deposition," *Tissue Engineering*, vol. 7, no. 5, pp. 557-572, 2004.
- [173] M. S. Kim, A. R. Hangsen, O. Wink, R. A. Quaipe and J. D. Carrol, "Prototyping: A New Tool in Understanding and Treating Strutural Heart Disease," *Circulation*, vol. 2394, no. <http://dx.doi.org/10.1161/CIRCULATIONAHA.107.740977>, p. 2388, 2008.
- [174] H. Hiramatsu, H. Yamaguchi, S. Nimi and H. Ono, "Rapid prototyping of the larynx for laryngeal frame work surgery," *Nippon Jibiinkoka Gakkai Kaiho*, vol. 107, no. 10, pp. 949-955, 2004.
- [175] J. Hart, *An Introduction to Additive Manufacturing*, Massachussets: <http://web.mit.edu>, 2015.
- [176] E. Palermo, "What is Laminated Object Manufacturing?," 09 October 2013. [Online]. Available: <http://www.livescience.com/40310-laminated-object-manufacturing.html>. [Accessed 29 June J2016].
- [177] K. Sungwan, "Manoeuvrable Capsule Endoscope Based on Gimbaled Ducred-Fan Sysytem," in *Create for the Future Design Contest 2016*, Seoul, 2016.
- [178] D. Mikhailov, "Lily," in *Endoscopic Complex of New Generation*, 2014.
- [179] 3. Systems, "MEPhI harnesses 3D printing Technology to Quickly Prototype much-needed Engineering Solutions," 3D Systems Corporation, 2014.
- [180] R. J. Plunkett, "The History of Pertetrafluoroethylene: Discovery and Development," in *Symposium on the History of High Performance Polymers at the American Chemical Society Meeting*, New York, 1986.
- [181] DuPont, "DU PONT," 2016. [Online]. Available: <http://www.dupont.com>. [Accessed 2016 August 2016].
- [182] K. Graffte, "Fluoropolymers: Fitting the Bill for Medical Applications," *Medical Device and Diagonistic Industry (MDDI)*, 2005.
- [183] J. Cooler, *Advanced Adhesives for Medical Applications*, Medical Design Technology, 2011, pp. <https://www.mdtmag.com/article/2011/08/advanced-adhesives-medical-applications>.
- [184] International Affairs and Best Practice Guidelines, "Ostimy Care and Management," *Clinical Best Practice Guideline*, pp. 17-25, August 2009.
- [185] Loctite, *Loctite: Design Guide for Bonding Plastics LT-2197*, 2011.

- [186] John Morris Group, "John Morris Group," John Morris Group, 2016. [Online]. Available: <https://www.johnmorrisingroup.com/About-Us/Company-History>. [Accessed 19 August 2016].
- [187] R. G. McGregor, *Testing Bond Strength of Glue for Optimal Packaging*, Brookfield Ametek, Packaging Materials.
- [188] Stratasys Ltd., *Objet30 Pro Datasheet*, Stratasys Ltd, 2015.
- [189] Kim Nylund et al., "Sonography of the Small Intestine," *World Journal of Gastroenterology*, vol. 15, no. 11, pp. 1319-1330, 2009.
- [190] WebMD Medical Reference, "WebMD," WebMD, LLC., 2005-2016. [Online]. Available: <http://www.webmd.com>. [Accessed May 2016].
- [191] Awesome Inc. template, "Borland Groover Clinic from Sihanok Hospital," 03 January 2014. [Online]. Available: <http://borlandgroovercambodia.blogspot.co.uk>. [Accessed August 2016].
- [192] E. D. Cambridge University , *Materials Data Book*, Cambridge: Cambridge University Engineering Department, 2003.
- [193] L. J. Sliker and G. Ciuti, "Flexible and Capsule Endoscopy for Screening, Diagnosis and Treatment," *Expert Review of Medical Devices*, vol. 11, no. 6, pp. 649-665, 2014.
- [194] L. Zhao-Shen, L. Zhuan and M. McAlindon, *Handbook of Capsule Endoscopy*, Springer Science+Buisness Media D, 2014.
- [195] A. Bernassau, D. Hutson, C. E. M. Demore, D. Flynn, F. Amalou, J. Parry , J. McAneny, T. W. Button, M. P. Y. Desmuliez and S. Cochran, "Progress Towards Wafer-scale Fabrication of Ultrasound Arrays for Real-time High Resolution Biomedical Imaging.," *Sensor Review*, vol. 29, no. 4, pp. 333-338, 2009.
- [196] S. Odegaard, L. B. Nesje, O. D. Laerum and M. B. Kimmey, "High Frequency Ultrasonographic Imaging of the Gastrointestinal Wall," *Expert Review of Medical Devices*, vol. 9:3, no. DOI:10.1586/erd.12.6, pp. 263-273, 2012.
- [197] Y. M. Bhat, S. Banerjee, B. A. Barth, S. S. Chauchan, K. T. Gottlieb, V. Konda, J. T. Maple, F. M. Murad, P. R. Pfau, D. K. Pleskow, U. D. Siddigui, J. L. Tokar, A. Wang and S. A. Rodriguez, "Tissue Adhesives: Cyanoacrylate Glue and Fibrin Sealant," *Gastrointestinal Endoscopy*, vol. 78, no. 2, pp. 209-215, 2013.
- [198] A. Koulaouzidis, D. K. Lakovidis, A. Karagyris and E. Rondonotti, "Wireless endoscopy in 2020: Will it still be a capsule?," *World Journal of Gastroenterology*, vol. 21, no. 17, pp. 5119-5128, 2015.
- [199] C. Lam, X. Mo , S. H. Teoh and D. W. Hutmacher, "Scaffold Development Using 3D Printing with a Starch-based Polymer," *Material Science Engineering*, vol. 20, no. 1-2, pp. 49-56, 2002.

CHAPTER 10 APPENDIX

10.1 Appendix A

The tables below shows the technical specifications for various 3D printing materials.

Feature	Specification	Reference
Melting temperature	Not applicable	[128]
Density	Range: 0.5 to 11g/cm ³	[129]
Glass transition temperature	Approximately 104°C	[128]
Wall thickness	1mm to 2.5mm	[44]
Chemical formula	(C ₈ H ₈ ·C ₄ H ₆ ·C ₃ H ₃ N) _n	[130]

Table 23: Technical specification for ABS thermoplastic 3D printing material

Feature	Specification	Reference
Melting temperature	150°C to 165°C	[131]
Density	Range: 1.210–1.430 g/cm ³	[131]
Glass transition temperature	45°C to 65°C	[131]
Wall thickness	1mm to 2mm	[44]
Chemical formula	(C ₃ H ₄ O ₂) _n	[132]

Table 24: Technical specifications for PLA printing material [2]

The table below illustrates the comparison between the ABS and PLA thermoplastics.

Characteristics	ABS	PLA
Hardness	Very hard	Less hard and can warp when dropped
Colour appearance	Less attractive colour	Lustrous appearance
Reaction with moisture (during printing)	Sprays out droplets that can easily be dried	Sprays out droplets that are difficult to dry and depolymerizes at high temperatures
Durability of products	Durable	Less durable
Effect of heating	Less warping	Can warp or deform
Toxicity of fumes	Very toxic	Non-toxic fumes below 200°C
Biodegradability and Biocompatibility	Non-biodegradable and less biocompatible	Biodegradable and biocompatible
Printing speed[38]	Lower printing speed and difficult to print	High printing speed

Table 25: Comparison between ABS and PLA thermoplastics [133, 134, 135]

Feature	Specification
Accuracy	±0.1% (with a lower limit of ±0.2mm)
Clearance	0.4mm
Maximum Size	100 x 100 x 100 mm
Minimum Details	0.2mm to 0.3mm
Minimum Wall Thickness	1mm
Interlocking or Enclosed Parts	Yes

Table 26: Technical specification for high detail resin [136]

Feature	Specification
Accuracy	±1%
Clearance	0.6mm
Maximum Size	260 x 160 x 193 mm
Minimum Details	0.3mm
Minimum Wall Thickness	0.4mm
Interlocking or Enclosed Parts	No

Table 27: Technical specification for smooth detail resin [136]

Feature	Specification
Layer thickness (thinnest)	40 microns
Size (minimum)	0.012In
Biocompatibility	Yes: Titanium (Ti64)

Table 28: Technical specification for smooth detail resin [54]

10.2 Appendix B

Figure 94 shows a comparison in the size between different capsule endoscopes available in the capsule endoscopy market.

Table 1. Passive capsule endoscopes.




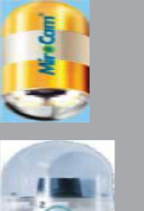







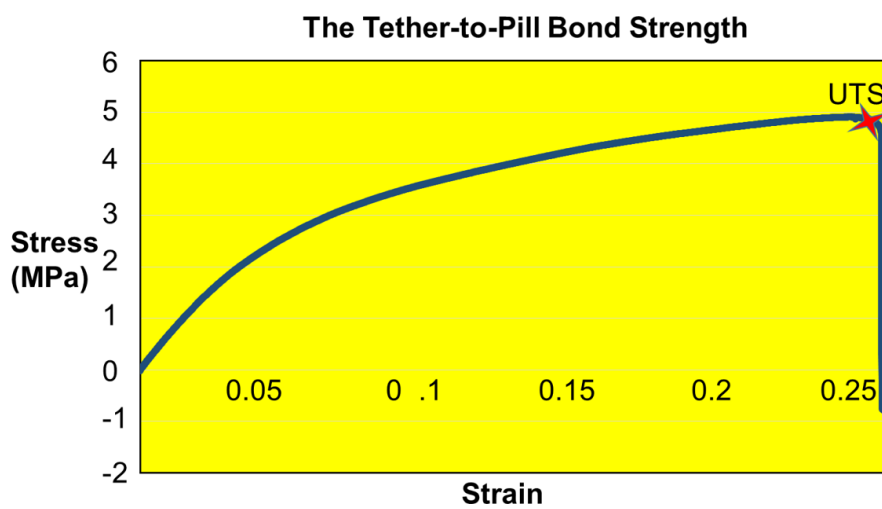
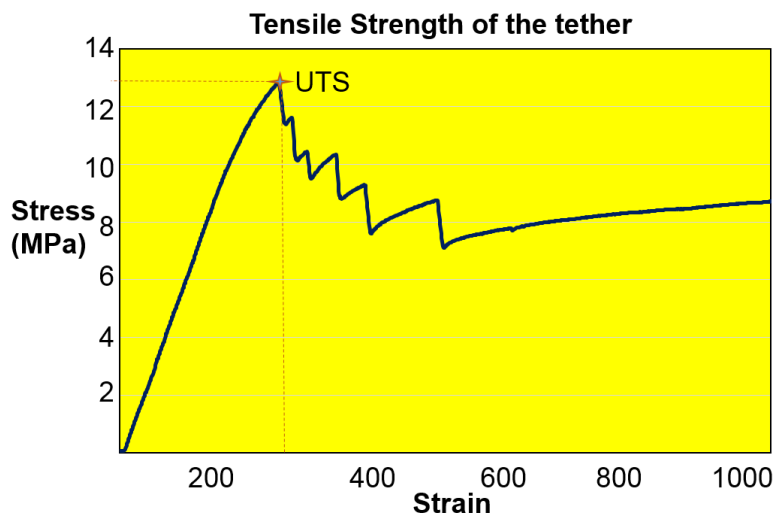
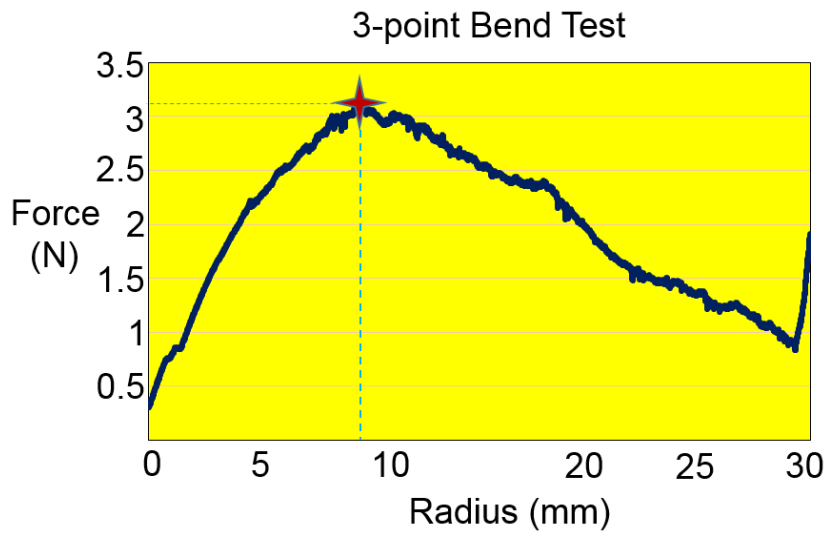
Model											
	PillCam SB (MZA)	PillCam SB 3	PillCam ESO	PillCam ESO 2	PillCam ESO 3	PillCam Colon	PillCam Colon 2	MiroCam® MC1000-W	EndoCapsule 10	OMOM®	CapsoCam SV1
Manufacturer (location)	PillCam Given Imaging Ltd. (Yokneam, Israel)			PillCam Given Imaging Ltd. (Yokneam, Israel)			PillCam Given Imaging Ltd. (Yokneam, Israel)			JinShan Science and Technology Co. (Chongqing, China)	CapsoVision, Inc. (Saratoga, CA, USA)
Operative region	SB	SB	ESO	ESO	ESO	Colon	Colon	SB	SB	SB	SB
Mass (g)	3.3	2.9	3.0	3.7	2.9	2.9	2.9	3.25	3.8	3.3	N/A
Dimensions (mm)	11 × 26	11 × 26	11 × 26	11 × 26	11 × 26	11 × 31	11 × 31	10.8 × 24.5	11 × 26	13 × 27.9	11 × 31

Figure 94: Comparison between the sizes of different commercial capsule endoscopes [193]

10.3 Appendix C

This section shows the normalized graphs of the mechanical evaluation of the tether.



10.4 Appendix-CD

This CD contains the following.

FOLDER	DOCUMENT
FILE 1	Stratasys 3D Printers and materials datasheets
FILE 2	AlphaWire datasheets
FILE 3	Mechanical evaluation data
FILE 4	Techsil silicone adhesive datasheet
FILE 5	Adtech fluoropolymer datasheets
FILE 6	SolidWorks 3D CAD capsule designs